Interactions of microplastic particles with iron oxyhydroxides in aqueous phase:

The role of surface properties on aggregation and sedimentation

DISSERTATION

zur Erlangung des akademischen Grades einer Doktorin der Naturwissenschaften (Dr. rer. nat.)

In der Bayreuther Graduiertenschule für Mathematik und Naturwissenschaften (BayNAT) der Universität Bayreuth

Vorgelegt von

Johanna Schmidtmann

geboren in Mettingen

Bayreuth, 2024

Die vorliegende Arbeit wurde in der Zeit von Januar 2020 bis Mai 2024 in Bayreuth am Lehrstuhl für Hydrologie unter Betreuung von Herrn Professor Dr. Stefan Peiffer angefertigt.

Vollständiger Abdruck der von der Bayreuther Graduiertenschule für Mathematik und Naturwissenschaften (BayNAT) der Universität Bayreuth genehmigten Dissertation zur Erlangung des akademischen Grades einer Doktorin der Naturwissenschaften (Dr. rer. nat.).

Form der Dissertation:	Kumulative Dissertation
Dissertation eingereicht am:	28. Mai 2024
Zulassung durch das Leitungsgremium:	12. Juni 2024
Wissenschaftliches Kolloquium:	7. Oktober 2024

Amtierender Direktor: Prof. Dr. Jürgen Köhler

Prüfungsausschuss:

Prof. Dr. Stefan Peiffer	(Gutachter)
Prof. Dr. Eva Lehndorff	(Gutachterin)
Prof. Dr. Martin Obst	(Vorsitz)
JProf. Dr. Anke Nölscher	

Acknowledgements

First, I would like to thank Stefan Peiffer for his supervision and guidance throughout the last four years. I thank him for his support, his encouragement and motivation and our shared discussions – of course the scientific ones, but also those about politics, hiking or cross-country skiing.

I would also like to thank the Hydrology Department. Thanks to all the technicians, especially Jutta Eckert, Martina Rohr, and Isolde Baumann, for finding creative solutions in the lab, helping with experimental work, or simply ensuring coffee during coffee break every day! Thanks to Barbara Jakob for always taking care of the administrative work and generally for always supporting us PhD students. And of course, thanks to all other Hydro-members, especially the fellow PhD students and *Young Hydros*: Katharina Blaurock, Laura Wegner, Jan-Pascal Boos, Hassan Elagami, Xingyu Liu, Karel As, Joscha Opitz, Marco La Capra, Usman Munir, Natasha Gariremo, Alexey Kuleshov, Xiaoqiao Tang and Bouchra Marouane. Besides, I would like to thank my HiWis and Master students who have worked with me in the past years.

Further, I would like to thank the *SFB Mikroplastik* and all members. The SFB did not only provide me with funding but also supported me throughout the PhD. I would like to express my gratitude to Melanie Pöhlmann, who has always been there to help me with any SFB or research related questions or to simply encourage and motivate us PhD students.

Thank you for proof-reading and commenting the first draft of this dissertation, Nora Meides, Katharina Blaurock, and Andreas Cramer.

A special thanks to my PhD colleagues who have become close friends over the last few years: Nora, Teresa, Matze, Basti, Dimi, Moritz, Daniel, and Johanna. Without our lunch at Mensa, coffee breaks at Glashaus or after-work Aperol at Leons, my time at university would not have been the same!

Many thanks to my flat mates and friends in Bayreuth who always supported and motivated me: Chris, Miri, José, Mare, Tanu, Lena, Linus, Kathy, Laura, and Rina.

And finally, I want to thank my family, especially my Mum and sister. Thank you, Mama and Alina, for all your love, your support and motivation, or care packages with snacks for surviving the last weeks of writing this thesis.

Contents

Summary

The pollution of the environment with microplastics (MP) is ubiquitous. Therefore, it is essential to understand how MP behaves in the environment, how it interacts with widely distributed environmental colloids, and how these interactions affect the fate and transport of MP. This dissertation investigated how interactions of MP with naturally occurring iron oxyhydroxides influence the surface properties of MP particles, the heteroaggregation and the sedimentation in water.

In Study 1, the heteroaggregation of 1 µm polystyrene (PS) and ferrihydrite, a naturally occurring iron oxyhydroxide, was investigated in dependency of the pH. Interactions between the particles strongly depended on electrostatic interactions. At acidic pH values, the negatively charged PS particles were coated with positively charged ferrihydrite particles, leading to charge reversal. At alkaline pH, no aggregation occurred since both particle types were negatively charged and repelled each other. At neutral pH values, PS was also coated with ferrihydrite particles. However, the low charge of ferrihydrite in this pH range, contrary to the acidic range, caused charge neutralization of coated PS particles leading to strong heteroaggregation, resulting in rapid sedimentation. After just one day, PS particles had almost completely sedimented. In the acidic and alkaline pH range, only slight sedimentation occurred because repulsion forces prevented the formation of larger aggregates. Concluding, interactions with natural colloids influence not only the surface properties of MP in aquatic environments but also drive sedimentation and therefore influence MP transport in water.

In Study 2, aggregation and sedimentation were examined for UV-weathered PS particles, in addition to pristine particles. UV-irradiation led to a decrease in particle size, roughening and "shrinking" of the surfaces, reduction of negative surface charge and the formation of dissolved and particulate weathering products. These altered properties of the PS particles also affected the heteroaggregation with ferrihydrite. With increasing UV-weathering, the isoelectric point shifted from neutral to acidic. Remarkably, maximum heteroaggregation and sedimentation for weathered PS with ferrihydrite were observed not only at the isoelectric point but over a wider pH range, presumably due to the increased surface reactivity of the UV-weathered particles. The formation of functional groups on the surface due to UV-weathering might have allowed not only electrostatic interactions between the particles to take place but also additional interactions such as hydrogen bonding. It is furthermore likely that PS weathering products, such as oligomers, additionally influenced the aggregation behavior through interactions with PS and ferrihydrite. In summary, UV-induced changes of the PS surface increased the interactions with ferrihydrite and the subsequent sedimentation of PS. Additionally, with increasing UV-weathering the formation of dissolved weathering products was observed and eventually 90% of the PS escaped from the suspension, most likely as gas.

Since strong interactions between PS and ferrihydrite were observed in the first two studies, Study 3 examined how MP coating with ferrihydrite affects the initial hydrophobic properties of MP in soil. For this purpose, MP hotspots (PS and polyethylene terephthalate (PET), 20-75 µm) were introduced into sand, and the capillary rise of water was imaged using time-series neutron radiography. Uncoated MP hotspots were non-wettable. For coated MP hotspots, differences were observed depending on polymer type: while coated PS remained non-wettable, water was attracted into the coated PET hotspots. Our results suggest that the ferrihydrite coating of MP alters surface wetting properties depending on the polymer type and thus counteracts the hydrophobic properties of pristine MP. The dynamics of MP coating and wettability are key factors for biotic and abiotic degradation processes.

Study 4 developed an analytical method for quantifying PS particles with diameters in the lower micrometer range from aqueous solution. For laboratory experiments with MP (e.g. sedimentation experiments from Study 1 and 2) a fast and simple quantification method is essential and often associated with lower requirements than for environmental samples. Here it was shown that a Total Organic Carbon (TOC) analyzer is suitable for quantifying PS in the lower micrometer range. For successful oxidation of PS to CO_2 in the instrument, the addition of iron or aluminum hydroxides as an additional catalyst was necessary. This increased the recovery from 52.9% to 89.7%. Thus, the presented TOC method offers a simple and fast alternative for quantifying MP samples in the lower micrometer range when no other organic substances are present in the sample.

In summary, this dissertation shows that the surface properties of MP particles in the environment and their sedimentation strongly depend on interactions with natural particles and colloids. In the aqueous phase, strong heteroaggregation with iron oxyhydroxides caused MP sedimentation. In soil, MP coating with iron oxyhydroxides rendered the initial hydrophobic surface of MP more wettable. Therefore, the consideration of interactions with environmental colloids is essential to draw predictions about MP behavior and its fate in the environment.

Zusammenfassung

Die Verschmutzung der Umwelt mit Mikroplastik (MP) ist allgegenwärtig. Daher ist es wichtig zu verstehen, wie sich MP in der Umwelt verhält, wie es mit weit verbreiteten Umweltpartikeln interagiert und wie sich diese Wechselwirkungen auf den Verbleib sowie den Transport von MP in der Umwelt auswirken. Diese Dissertation untersucht, inwieweit Wechselwirkungen von MP mit natürlich vorkommenden Eisenoxyhydroxiden die Oberflächeneigenschaften von MP-Partikeln und deren Sedimentation im Wasser beeinflusst.

In Studie 1 wurde die Heteroaggregation von 1 µm Polystyrol (PS) und Ferrihydrit, einem natürlichem vorkommenden Eisenoxyhydroxid, unter Einfluss des pH-Wertes untersucht. Die Interaktionen zwischen den Partikeln waren stark von den elektrostatischen Wechselwirkungen abhängig. Bei sauren und neutralen pH-Werten wurden die negativ geladenen PS-Partikel mit positiv geladenen Ferrihydrit-Partikeln beschichtet. Im sauren Bereich führte dies zu einer Ladungsumkehr von negativ zu positiv. Im neutralen Bereich hingegen sorgte die Ferrihydrit-Beschichtung für eine Ladungsneutralisierung, welche zu starker Heteroaggregation führte. Diese starke Heteroaggregation führte zu rascher Sedimentation des MP. Bereits nach einem Tag waren die PS-Partikel fast vollständig sedimentiert. Im sauren und alkalischen pH-Bereich blieb die Sedimentation aus, da die beschichteten Partikel im sauren Bereich eine hohe positive Ladung annahmen, welche weitere Aggregation verhinderte. Im alkalischen Bereich fand keine Aggregation statt, da PS und Ferrihydrit beide negativ geladen waren und sich somit weitestgehend voneinander abstießen. Abschließend lässt sich feststellen, dass Wechselwirkungen mit natürlichen Partikeln nicht nur die Oberflächeneigenschaften von MP beeinflussen, sondern auch zu verstärkter Sedimentation führt, welche den Transport von MP im Wasser beeinflusst.

In Studie 2 wurde die Aggregation und Sedimentation statt mit fabrikneuen PS-Partikeln mit UV-bestrahlten Partikeln untersucht. Durch UV-Bestrahlung nahm die Partikelgröße ab, die Oberflächen wurden rauer und „schrumpeliger“, die negative Oberflächenladung nahm ab und gelöste und partikuläre Verwitterungsprodukte entstanden. Die veränderten Eigenschaften der PS-Partikel führten zu veränderter Heteroaggregation mit Ferrihydrit. Mit zunehmender Bewitterung wurde der Ladungsnullpunkt vom neutralen in den sauren Bereich verschoben. Auffällig war, dass maximale Heteroaggregation und Sedimentation von gealtertem PS mit Ferrihydrit nicht nur am Ladungsnullpunkt zu beobachten war, sondern über einen größeren pH-Bereich, vermutlich durch die erhöhte Oberflächenreaktivität der bestrahlten Partikel. Durch die Entstehung von funktionellen Gruppen auf der Oberfläche konnten sich nicht nur elektrostatische Wechselwirkungen zwischen den Partikeln, sondern auch andere Interaktionen wie z.B. Wasserstoffbrückenbindungen ausbilden. Ein weiterer Aspekt, der

Einfluss auf das Aggregationsverhalten hatte, waren durch die Alterung entstandene Verwitterungsprodukte, die ebenfalls mit PS und Ferrihydrit wechselwirkten. Zusammenfassend erhöhten UV-induzierte Veränderungen der PS-Oberfläche die Wechselwirkungen mit Ferrihydrit und dadurch die Sedimentation von PS. Darüber hinaus wurde mit zunehmender UV-Verwitterung die Bildung gelöster Verwitterungsprodukte beobachtet, und letztendlich entwichen etwa 90% des PS aus der Suspension als Gas.

Nachdem in den ersten beiden Studien starke Wechselwirkungen zwischen PS und Ferrihydrit festgestellt wurden, wurde in Studie 3 untersucht, inwieweit eine Beschichtung von MP mit Ferrihydrit die initial hydrophoben Eigenschaften von MP im Boden verändert. Dafür wurden MP Hotspots (PS und Polyethylenterephthalat (PET), 20-75 µm) in Sand eingebracht und der Kapillaraufstieg von Wasser mittels Neutronenradiographie abgebildet. Unbeschichtete, fabrikneue MP Hotspots waren nicht mit Wasser benetzbar. Für beschichtete MP Hotspots wurden Unterschiede je nach Polymertyp beobachtet: beschichtetes PS war weiterhin wasserabweisend, beschichtetes PET hingegen sog Wasser in den Hotspot auf. Unsere Ergebnisse zeigen, dass eine Ferrihydrit-Beschichtung die Oberflächenbenetzbarkeit von MP je nach Polymerart verändert und somit den hydrophoben Eigenschaften von fabrikneuem MP entgegenwirkt. Die Dynamik der MP-Beschichtung und die zunehmende Benetzbarkeit sind Schlüsselfaktoren für biotische und abiotische Abbauprozesse im Boden.

In Studie 4 wurde eine analytische Methode zur Quantifizierung von PS-Partikeln, mit Durchmessern in den unteren Mikrometern, aus wässriger Phase erarbeitet. Für Laborexperimente mit MP (z.B. Sedimentationsversuche aus Studie 1 und 2) ist eine schnelle und einfache Quantifizierungsmethode nicht nur essenziell, sie ist oft auch mit geringeren Anforderungen als bei Umweltproben verbunden. Hier wurde gezeigt, dass sich ein Total Organic Carbon (TOC) Analysator zur Quantifizierung von PS im unteren Mikrometerbereich eignet. Für eine erfolgreiche Oxidation von PS zu CO_2 in dem Instrument ist die Zugabe von Eisen- oder Aluminiumhydroxiden als zusätzlicher Katalysator notwendig. Dadurch kann die Wiederfindung von 52,9% auf 89,7% erhöht werden. Die TOC-Methode bietet somit eine einfache und schnelle Alternative für die Quantifizierung von MP in dem unteren Mikrometer-bereich für Proben, in denen keine weiteren organische Substanzen vorhanden sind.

Zusammenfassend wurde in dieser Arbeit gezeigt, dass die Oberflächeneigenschaften von MP in der Umwelt sowie deren Sedimentation stark von den Wechselwirkungen mit natürlichen Partikeln und Kolloiden abhängen. In der wässrigen Phase führt starke Heteroaggregation mit Ferrihydrit zu Sedimentation von MP und im Boden verändert eine Beschichtung von MP mit Ferrihydrit die initial hydrophoben Eigenschaften der MP-Partikel. Somit ist es essenziell, die Wechselwirkungen mit natürlichen Substanzen zu berücksichtigen, wenn Vorhersagen über das Verhalten oder den Verbleib von MP in der Umwelt getroffen werden.

1 Introduction

1.1 Plastic - an emerging environmental pollutant

Nowadays, plastics are present in almost every part of our lives. Plastic products dominate packaging and are widely used for clothing, transportation, electronic devices, household items, agriculture and medical equipment (Geyer, 2020; PlasticsEurope, 2022). Advantageous properties such as low density, low costs and high durability make plastic products a powerful material for many applications. The total global plastic production grew from around 2 million tons (Mt) in 1950 to 390.7 Mt in 2021 (Geyer, 2020; PlasticsEurope, 2022). The largest contribution was packaging materials with 44%, followed by the building and construction sector with 18% (PlasticsEurope, 2022). The lifetime of plastic products varies from a few seconds or minutes (e.g., packaging or medical products) to several years. However, the increasing amount of plastic produced is accompanied by an enormous quantity of plastic waste. Geyer (2020) estimated the global recycling, incineration and discard rates for non-fiber plastic waste: Since 1980, the recycling and incineration rate increased from zero to 18% and 26%, respectively, in 2017, while the discard rate decreased from 100% to 56% (Geyer, 2020). However, the absolute amount of discarded waste increased, as the global plastic production was increasing. In 2017 around 210 Mt were discarded (Geyer, 2020). The calculated discard includes disposal in landfills, dumps and the natural environment.

In the environment, initially advantageous properties such as the high resistance and durability of plastics are causing a major environmental challenge: the accumulation of plastic waste in the environment. Today, nearly every environmental compartment is contaminated with plastics. It has been detected in the marine and coastal environment (Browne et al., 2011; Cózar et al., 2014), freshwater (Eerkes-Medrano et al., 2015; Horton et al., 2017), soils (Scheurer and Bigalke, 2018; Zubris and Richards, 2005), air (Cai et al., 2017; Dris et al., 2016), and even at remote places like Antarctica (Kelly et al., 2020).

1.2 Microplastic in the environment

In the environment, plastic products or fragments are exposed to a variety of environmental stressors - biotic and abiotic - leading to degradation (Gewert et al., 2015; Shah et al., 2008; Singh and Sharma, 2008; Zhang et al., 2021). Plastic particles smaller 5 mm are defined as microplastic (European Chemicals Agency, 2019; SAPEA, 2019) (MP) and are further classified as primary or secondary material. Even though most researchers use 5 mm as cut-off, the size classification of MP differs, and no uniform definition has been reached in the

microplastic community. The classification of MP into primary or secondary material depends on whether the particles are produced in the size of MP (primary) or whether they originate from the fragmentation of larger items (secondary) (GESAMP, 2015).

In the early 1970s, first reports on the presence of MP in North Atlantic surface waters (Austin and Stoops-Glas, 1977; Carpenter and Smith, 1972; Colton et al., 1974) and on New Zealand beaches (Gregory, 1977) were published. Later, particularly in the last 10-15 years, the number of scientific publications on MP increased rapidly (**Figure 1**), accompanied by a growing concern about potential environmental threats caused by MP.

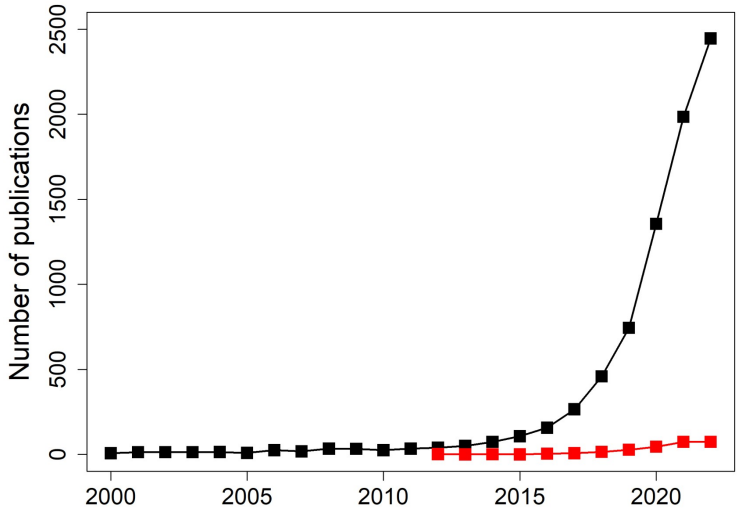

Figure 1. *Annual number of publications related to microplastic from 2000 - 2022. Data from Web of Science (accessed on 07.12.2023) searching for "microplastic", "micro-plastic", "nanoplastic", or "nano-plastic" (black) and in combination with "aggregation" (red).*

The United Nations Environmental Programme (UNEP) identified MP as one of six emerging issues of environmental concern (UN Environment, 2017). Not only the widespread presence of MP particles in the environment is emerging but also the potential threat to ecosystems and their habitants. It has been shown that MP can induce chemical and physical toxicity and negatively influence feeding, growth, reproduction and survival on biota (Bergmann et al., 2015; Foley et al., 2018; SAPEA, 2019; Wagner and Lambert, 2018).

To understand the risk MP is posing to the environment and its habitants, it is essential to study its transport and fate to then evaluate which environmental compartments might be most affected. For MP particles in the micron and submicron range, surface characteristics play a greater role compared to larger material due to the increased surface-to-volume ratio. Interactions with other naturally occurring substances, e.g. aggregation (the process of two particles colliding, followed by attachment (Alimi et al., 2018)), control the environmental fate and transport of MP and must therefore be included in modelling transport processes.

However, in comparison to the total number of publications in the field of MP research, aggregation processes have not yet received much attention (**Figure 1**) and therefore require further investigation.

In the following, background information on colloidal science and environmental colloids is presented that is necessary to evaluate the interactions of MP with environmental colloids and the resulting impact on MP aggregation and mobility.

1.3 Basics of colloidal science

Colloids are historically defined as particles with a size range between 1 nm and 1 µm that remain stable in aqueous phase over a specific time period and therefore exhibit potential for mobility and transport (Goodwin, 2009; Lead et al., 1997; Spielman-Sun et al., 2024). However, Spielman-Sun et al. (2024) recently suggested that the definition of a colloid, especially the size range, should be more flexible: it would be preferable to use a wider size range or a size range that is adapted to the substance of interest. Another challenge is that in many studies, the *particulate* phase is differentiated from the *dissolved* phase by filtration, e.g. aquatic chemists usually use 0.2 or 0.45 µm pore sizes to distinguish between particulate and dissolved phase (Lead and Wilkinson, 2006). Not only do the filter sizes vary depending on the discipline, but the group of colloids is often completely neglected when only differentiating between particulate and dissolved phases by filtration (Bao et al., 2023; Lead and Wilkinson, 2006). In this thesis, the definition of a colloid is not strictly based on the size range between 1 nm and 1 µm but rather on the traditional characteristics of colloidal chemistry: any organic or inorganic entity with a size large enough to have a supramolecular structure and exhibit properties distinctly different from those of the surrounding aqueous phase (Lead and Wilkinson, 2006). On the other side, the upper size limit is reached when interfacial phenomena become qualitatively less important due to the smaller relative surface-to-volume ratio of the colloid/particle (Lead and Wilkinson, 2006). In other words, colloids are generally small enough that, when no aggregation is taking place, Brownian motion is sufficient to keep them suspended in the water column for periods longer than hours to days (Lead and Wilkinson, 2006).

Most colloids are charged. The surface charge can arise from (i) chemical reactions at the surface (i.e. iron oxyhydroxides, silica), (ii) isomorphous replacement within the lattice (aluminosilicates) or (iii) ion adsorption (Filella, 2006; Stumm and Morgan, 2012). Close to the electrically charged surface, a countercharge is established in the solution (Stumm and Morgan, 2012). Different models explain this electric double layer, e.g. the diffusive double-layer by Gouy-Chapman (Stumm and Morgan, 2012). In this model, electrostatic and thermal

forces are considered to explain the distribution of counter ions close to the charged surface. The surface charge is compensated by an unequal distribution of co- and counter-ions that extend to a certain distance from the surface (Tadros, 2015). In the first layer, the direct surrounding of the surface, more counter-ions are located and strongly bound to the surface, while the second layer is almost diffusively distributed in the liquid and ions are less strongly bound (Stumm and Morgan, 2012). Within this diffusive layer, a theoretic boundary exists, in which ions and particles form a stable entity. If the charged particle moves in a liquid, the ions within this boundary (also called shear or slipping plane) move with it. The electric potential at the slipping plane is called zeta potential (Stumm and Morgan, 2012). The magnitude of the zeta potential indicates the potential stability of a colloidal system. It is calculated from the experimentally determined electrophoretic mobility, the velocity of charged particles within an electric field between anode and cathode (Stumm and Morgan, 2012). The zeta potential states whether a surface charge is positive or negative and indicates the isoelectric point (pH_{IEP}). The pH_{IEP} is defined by "the condition where particles do not move in an applied electric field" (Stumm and Morgan, 2012), hence the net surface charge of a particle is zero. Furthermore, the zeta potential is strongly affected by pH and ionic strength of the surrounding liquid. Generally, if the zeta potential has a large negative or positive value, the particles are likely to repel each other and stay separated. However, if the zeta potential values are rather low (< 30 mV), the tendency of particle aggregation is enhanced, as the repulsion forces between the particles are smaller. Aggregation can occur between identical particles (homoaggregation) or between different particle types (heteroaggregation) and often leads to subsequent sedimentation (Praetorius et al., 2014; Velzeboer et al., 2014).

1.4 Environmental colloids

Colloids and suspended particles are ubiquitous in natural waters. They are present in fresh surface waters, groundwaters, oceans and soil waters in high concentrations (> 10^6 cm^{-3}) (Stumm and Morgan, 2012). Particles and colloids in natural waters are extremely diverse and range from organisms, biological debris and organic macromolecules to various minerals, clays and oxides (Stumm and Morgan, 2012). They are highly dynamic and continuously generated, e.g. by precipitation and nucleation from oversaturated solutions or by physical fragmentation and erosion (Stumm and Morgan, 2012). Furthermore, they undergo changes in composition and can be removed from the water by dissolution or aggregation and subsequent settling (Stumm and Morgan, 2012).

We only have limited knowledge of the actual size distribution of naturally occurring colloids, whether they exist as isolated entities or as aggregates (Lead and Wilkinson, 2006). The sizes of one colloid type often spread over orders of magnitude (**Figure 2**). Furthermore, in natural

waters, colloids are typically present as components of heteroaggregates and only rarely found in purified forms (Lead and Wilkinson, 2006).

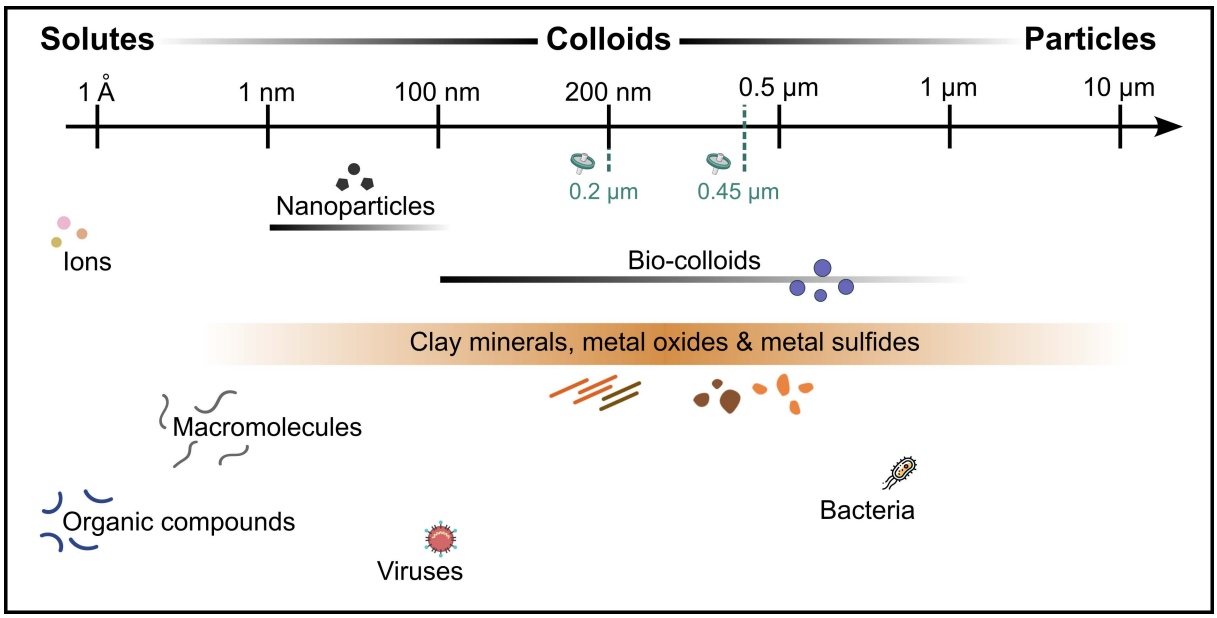

Figure 2. *Size distributions of several environmental colloids, particles and solutes. Based on Lead and Wilkinson (2006) and Spielman-Sun et al. (2024).*

One group of environmental colloids is the one of iron oxides, hydroxides, and oxyhydroxides (from here on collectively referred to as “iron oxyhydroxides”). They are common minerals which are widespread in the environment (Joshi and Kappler, 2020; Schwertmann and Cornell, 2000). They consist of ferrous (Fe(II)) or ferric (Fe(III)) iron, oxygen (O) and/or hydroxyl (OH) groups (**Table 1**) and can be found in the hydrosphere, pedosphere, atmosphere, biosphere and lithosphere (Cornell and Schwertmann, 2003; Joshi and Kappler, 2020). Iron oxyhydroxides typically occur as small crystals with dimensions in the micro- or nanometer scale (Cornell and Schwertmann, 2003). Due to their high surface-to-volume ratio and high reactivity, they participate in various interactions between the above mentioned environmental compartments (Cornell and Schwertmann, 2003). The dissolved concentrations of iron can range from several nanomoles to millimoles per liter in aqueous phases and from microgram to high milligram per gram in solids (Kappler et al., 2021).

Initially, iron oxyhydroxides are introduced into the environment during the weathering of rocks (i.e., oxidation and hydrolysis of iron-containing silicates, sulfides or carbonates) (Schwertmann and Cornell, 2000). Under anaerobic conditions, re-mobilization of iron oxyhydroxides may occur by microbial reduction (Schwertmann and Cornell, 2000). Generally, the precipitation, dissolution and reprecipitation of iron oxyhydroxides is controlled by pH, redox potential (Eh), temperature and water activity (Schwertmann and Cornell, 2000).

Since iron oxyhydroxides are not only widely distributed in the environment but also strongly interact with other particles and colloids, the fate of various substances, e.g. heavy metals, natural organic matter (NOM) or eutrophication compounds, is affected by the iron cycle (Cornell and Schwertmann, 2003). For example, when iron oxyhydroxides precipitate in aqueous systems, they may bind toxic heavy metals or NOM, which then co-precipitate with the iron oxyhydroxide (Cornell and Schwertmann, 2003; Curtinrich et al., 2022; Nierop et al., 2002; Peiffer et al., 1999). However, under anaerobic conditions, dissolution of the iron oxyhydroxide and consequently re-mobilization of the bound substances may take place (Cornell and Schwertmann, 2003). Hence, iron oxyhydroxides play a crucial role on mobilization and transport of substances within aquatic environments, particularly in understanding the mechanisms of heteroaggregation. When MP particles enter the environment, they are likely to interact with iron oxyhydroxides. These interactions, such as heteroaggregation, will in turn influence the fate of MP in the environment.

***Table 1**: The iron oxyhydroxides (Cornell and Schwertmann, 2003).*

Oxyhydroxides and hydroxides	**Oxides**
Goethite α-FeOOH	Hematite α-Fe_2O_3
Akageneite β-FeOOH	Maghemite γ-Fe_2O_3
Lepidocrocite γ-FeOOH	Magnetite Fe_3O_4
Schwertmannite $Fe_{16}O_{16}(OH)_y(SO_4)_z$ * n H_2O	β-Fe_2O_3
Ferrihydrite Fe_5HO_8 * 4 H_2O	ε-Fe_2O_3
Feroxyhyte δ'-FeOOH	Wüstite FeO
High pressure FeOOH	
δ-FeOOH	
Bernalite $Fe(OH)_3$	
$Fe(OH)_2$	
Green Rusts $Fe_x^{III}Fe_y^{II}(OH)_{3x+2y-z}(A^-)_z$, A^-=Cl^-, $^1/_2$ SO_4^{2-}	

To study how MP properties and the fate of MP are affected by interactions with environmental particles, we chose **ferrihydrite** as a representative for iron oxyhydroxides in the environment. Ferrihydrite is a poorly crystalline iron oxyhydroxide that is widespread in the environment and due to its very small particle size (primary particle diameter in the low nanometer range) an important vector for mobilization and transport of various substances in the environment (Jambor and Dutrizac, 1998; Kappler et al., 2021; Schwertmann and Cornell, 2000). Ferrihydrite often occurs “in, at, or near aerated surfaces of soils, rivers, lakes and both hydrothermal and cold springs” (Guo and Barnard, 2013). Its composition is not yet fully understood and seems to be variable. However, the formula Fe_5HO_8 * 4 H_2O is often used

(Schwertmann and Cornell, 2000). Due to the high surface area of ferrihydrite (> 200 m^2/g) (Schwertmann and Cornell, 2000) it is an important sorbent in various processes in the natural environment.

1.5 Interactions of microplastic with environmental colloids

As previously mentioned, various naturally occurring particles and colloids exist in the environment. MP particles entering the environment will inevitably get into contact with those substances. Interactions between MP and naturally occurring colloids, such as heteroaggregation, are likely to influence the surface and transport properties of MP.

To date, several studies have investigated the homoaggregation of MP particles in dependency of pH or ionic strength (Liu et al., 2021; Oncsik et al., 2014; Sun et al., 2020). However, theses studies were typically conducted under the absence of environmental substances. Since the number of natural particles and colloids surpasses that of MP particles in the environment, homoaggregation of MP is less relevant than heteroaggregation of MP with those natural substances. Consequently, homoaggregation of MP particles will not be discussed in detail.

Interactions of MP with environmental colloids are influenced by several factors. On the one hand the environmental conditions such as pH, ionic strength, type of electrolytes and coexisting particles and colloids. On the other hand the MP properties themselves, such as composition, surface charge and particle size (Wang et al., 2021). Alterations of some of these factors might influence other parameters. The surface charge of particles for example is highly dependent on pH or ionic strength.

The aggregation of MP with organic material has been widely reported in the past few years. The effect of dissolved organic matter (DOM) on the stability of MP particles cannot be generalized as it varies strongly among the studies (Sharma et al., 2021). The main explanation for this might be the influence of surface charge on the aggregation. As different studies use different model MP particles with different charges, the observed effects of DOM on MP stability vary. DOM was found to stabilize MP particles in the aqueous phase by enhancing electrostatic and steric repulsion and to destabilize MP by bridging or reversing surface charge (Cai et al., 2018; Li et al., 2018; Pradel et al., 2021). Furthermore, heteroaggregation between MP and biogenic particles, such as microalgae or phytoplankton, has been shown to increase the sedimentation rate of MP (Lagarde et al., 2016; Long et al., 2015; Michels et al., 2018). It can be concluded that electrostatic interactions are one of the most important factors determining if aggregation occurs or whether MP is stabilized by environmental colloids. This has not only been observed for organic material but also for

inorganic particles. Similarly charged minerals and MP particles were found to repel each other and thus stabilize MP in suspension (Sharma et al., 2021; Zhang et al., 2020). However, opposingly charged minerals or iron oxyhydroxides and MP have been found to interact and adsorb to one another (M. Li et al., 2019; Oriekhova and Stoll, 2018). Li et al. (2019) demonstrated that, depending on particle size, iron oxyhydroxides adsorbed onto the MP surface or vice versa if the particle size of iron oxyhydroxides clearly exceeds that of MP particles. Such coating of MP particles by environmental substances can largely modify the surface properties of MP. The surface charge can be reversed by the coating which further influences interactions with other particles and may also promote the uptake of MP by organisms and cells (Ramsperger et al., 2022; Wieland et al., 2024).

Further studies demonstrated that polystyrene (PS) and iron oxyhydroxides form heteroaggregates depending on pH and particle concentration (Oriekhova and Stoll, 2018; Vu et al., 2022). At conditions where charge neutralization was achieved, a strong increase in aggregate size was observed. Heteroaggregation of engineered nanoparticles (ENPs) with natural colloids and suspended solids was reported to strongly affect the aquatic transport and sedimentation of ENPs (Praetorius et al., 2014; Velzeboer et al., 2014). Furthermore, first studies investigating the effect of MP heteroaggregation on its sedimentation in water were conducted. They revealed that heteroaggregation between MP and biogenic particles or organisms increased the sedimentation of MP (Lagarde et al., 2016; Long et al., 2015; Michels et al., 2018). Even though iron oxyhydroxides are highly abundant in aquatic systems (Cornell and Schwertmann, 2003) and strongly interact with other water constituents and influence their transport (Lalonde et al., 2012; Lo and Waite, 2000; Nierop et al., 2002; Peiffer et al., 1999), no systematic study on MP heteroaggregation and subsequent sedimentation of MP with iron oxyhydroxides has been performed.

1.5.1 Effect of UV-weathering on MP and its interactions

In the environment, plastic particles are exposed to various weathering processes that induce changes in their polymer properties due to abiotic and/or biotic processes (Zhang et al., 2021). Biotic degradation refers to the degradation of plastics caused by organisms and abiotic degradation includes chemical or physical degradation mechanisms, e.g. light, temperature, water or mechanical stress (Zhang et al., 2021). The exposure of plastic particles to sunlight is one of most important processes initiating plastic degradation in the environment and has gained more and more attention in recent years. UV-weathering does not only trigger the formation of MP from larger plastic debris but also cause changes in chemical composition, surface charge, and mechanical properties of particles (Meides et al., 2021; Zhang et al., 2021,

2022). All these changes might influence the interactions of MP with natural particles and colloids.

Previous studies report increased negative surface charge of MP due to UV-weathering (Jin Liu et al., 2019; Y. Liu et al., 2019; Wang et al., 2023; Zhang et al., 2022). Hence, electrostatic attraction or repulsion forces between particles might be altered by UV-weathering. The increase in negative charge is attributed to the formation of oxygen-containing functional groups (OFGs) on the MP surface (Y. Liu et al., 2019; Wang et al., 2023; Zhang et al., 2022). This might not only impact the surface charge of MP but also enable other interaction forces to take place. In case of PS for example (a polymer consisting of a long hydrocarbon chain with attached phenyl groups), the formation of OFGs, such as carboxyl or carbonyl groups renders the polymer surface more polar and might allow interactions forces like hydrogen bonding or ligand exchange to take place (Duan et al., 2021; Zhang et al., 2022). Furthermore, UV-weathering increases surface roughness of MP, which offers more active surface sites for interactions with environmental compounds (Duan et al., 2021). First results reported that UV-weathered PS nanoparticles interacted with clay minerals even though the pristine PS particles and clay minerals repelled each other (Zhang et al., 2022). Moreover, the adsorption of PS nanoparticles onto iron minerals was found to be enhanced after UV-weathering of PS (Zhang et al., 2022). Hence, changes on the MP surface caused by UV-weathering are expected to intensify interactions with natural particles and must be considered when studying the aggregation and sedimentation behavior of MP particles in the environment.

Even though UV-induced changes on the MP surface affect interactions with environmental colloids, to our knowledge, no study on the effect of UV-weathering on heteroaggregation and subsequent sedimentation of MP has been performed yet. In this thesis, we will look at the combined effect of UV-weathering and heteroaggregation of MP with iron oxyhydroxides on sedimentation to gain a more comprehensive understanding of these processes.

1.5.2 Impact of MP interactions on MP wettability in soil

As highlighted in the previous chapters, research on MP particles in aqueous phase showed that interactions with environmental particles affect the surface properties of MP. These processes do not exclusively happen in aquatic environments. Terrestrial ecosystems are also confronted with increasing amounts of MP pollution. Once MP are incorporated in soil, they are exposed to several soil water constituents that might alter MP surfaces through adsorption and aggregation. Hence, interactions with potential binding agents such as minerals, metal hydroxides and organic matter have the potential to alter MP properties in soils (Lu et al., 2021; Ren et al., 2021; Yan et al., 2020).

In terrestrial ecosystems, MP contamination often occurs locally by deposition of larger plastic fragments with hotspots of high MP content (Cramer et al., 2022). As MP particles are typically hydrophobic, they are likely to increase the soil water repellency, when they are deposited at the soil surface or incorporated in the bulk soil (Cramer et al., 2022). Consequently, locally reduced soil water content and air entrapment may occur, affecting soil functions such as capillary water flow and MP degradation (Cramer et al., 2022). Previous experiments have shown that soil water repellency increased due to polyethylene terephthalate (PET) deposition in soil with the effect of inhibiting capillary rise (Cramer et al., 2022). The areas with high MP content were bypassed by water leading to locally reduced soil water contents. These observations imply that MP in soil is not easily wetted by soil water which might affect MP degradation as water accelerates biotic and abiotic degradation processes (Ali et al., 2021).

As shown in aquatic systems, interactions of MP with environmental particles influence their surface properties (Li et al., 2018; Oriekhova and Stoll, 2018; Schefer et al., 2023; Vu et al., 2022). A coating of MP with more hydrophilic particles might further increase the MP wettability (Lu et al., 2021; Ren et al., 2021; Yan et al., 2020) and hence decrease the effect of soil water repellency that was found for pristine particles (Cramer et al., 2022). As the presence of water accelerates biotic and abiotic degradation processes, it is highly relevant to understand the wetting kinetics of MP in order to predict MP degradation. However, studies on interactions of MP with soil water components and the resulting changes of MP surface properties are scarce, as most studies focused on interactions in aquatic systems. Therefore, this thesis will not only focus on the interactions of MP in water but will also shed a light on the influence of MP interactions with environmental substances on MP wettability in porous media.

1.6 Analytical challenges in quantifying sub-micrometer MP

Quantification of MP particles remains a challenge, especially for particles in the colloidal size range. For environmental samples, several identification methods are used, such as Fourier-transform infrared spectroscopy (FTIR), Raman spectroscopy, and gas chromatography-mass spectroscopy (GC-MS) (Prata et al., 2019). All of these techniques have limitations, e.g. detection limit, lower-size limit of detection, complex samples preparation, analysis time, accuracy, costs or availability of equipment (Prata et al., 2019).

For laboratory studies, e.g. sedimentation studies of colloidal PS in the presence of environmental colloids, the requirements differ compared to real environmental samples. On the one hand, the type and size of MP particles as well as the sample matrix is known compared to environmental samples, on the other hand, the small size of colloidal MP faces new challenges like lower-size limits of detection. For studying the sedimentation of MP in the

presence of inorganic particles, new possible analysis methods come into play, as MP particles present the only organic compound in the sample. In environmental science, Total Organic Carbon (TOC) analyzers are well established for quantifying dissolved and particulate organic carbon in aquatic samples (Aiken et al., 2002; Blaurock et al., 2022, 2021; Knorr, 2013; Volk et al., 2002). For MP analysis however, the application of a TOC analyzer is rare, even though it allows quantification of sub micrometer MP particles as no lower-size limit exist. Hong et al. (2021) used a TOC method with solid sample combustion to quantify MP from sewage samples after removing other organic material by digestion with Fenton's reagent. The recovery ranged between 76% and 98% for six different types of plastics (Hong et al., 2021). Contrary to those relatively high recoveries, Aiken et al. (2002) found only unsatisfactory recoveries for 1 µm PS beads with an average of 43.3%.

Hence, it remains unsolved whether TOC analysis serves as a reliable, fast and cost-effective alternative for quantifying MPs in well-defined MP samples from laboratory experiments. In this work, we will test the applicability of a TOC analyzer for micrometer-sized MP analysis in aqueous systems for samples without other organic material.

2 Objectives and Structure

The presented thesis was conducted as part of the *Collaborative Research Center (CRC) 1357 Microplastic* at the University of Bayreuth. The CRC investigates the formation, migration and effects of MP in the environment. This work was carried out in the subproject B01 that aimed to investigate the mechanisms of interaction on and with MP particles in water. As part of this subproject, my focus was set on the interactions between MP particles with ferrihydrite, as representative for iron oxyhydroxides in the environment.

The overall goal of this dissertation was to understand the interactions and aggregation between MP and ferrihydrite. Because many MP particles are exposed to UV-weathering in the environment, rendering their size, shape, surface properties and composition, we investigated not only pristine MP particles, but also UV-weathered particles to obtain a comprehensive understanding of the effects of weathering on aggregation. Furthermore, we aimed to understand how aggregation processes affect the surface properties, the sedimentation, and the environmental behavior of MP. Since the adsorption of environmental colloids onto the initially hydrophobic surfaces of MP might change their wettability, a further objective was to investigate if ferrihydrite coating reduces the soil water repellency induced by hydrophobic properties of MP.

This thesis comprises four studies. While Study 1 and 2 investigated the heteroaggregation and subsequent sedimentation of pristine and UV-weathered MP particles in water, Study 3 shed a light on the effect of ferrihydrite coating on the wettability of MP hotspots in porous media during capillary rise. Study 4 tested the applicability of TOC measurements for the quantification of micrometer-sized PS particles from laboratory-based experiments. In the following, I will formulate the research questions and hypotheses of all four studies in detail:

Study 1: Heteroaggregation of PS microplastic with ferrihydrite leads to rapid removal of microplastic particles from the water column

This study aimed to investigate under which pH conditions heteroaggregation between PS and ferrihydrite occurs and how this affects the sedimentation of PS in aquatic systems.

Research questions of Study 1:

- Do PS particles interact with ferrihydrite and how do pH variations influence the interactions?
- How is the sedimentation of PS affected by heteroaggregation with ferrihydrite?

We hypothesize that interactions between PS and ferrihydrite occur based on electrostatic attraction forces. Hence, if the particles are oppositely charged, we assume interactions to take place. At pH values at which charge neutralization occurs, we expect the formation of heteroaggregates, which will presumably lead to enhanced sedimentation of the aggregates.

Study 2: UV-weathering affects heteroaggregation and subsequent sedimentation of polystyrene microplastic particles with ferrihydrite

In Study 2 we first investigate how UV-weathering influences PS surface properties and secondly how these changes influence the heteroaggregation and sedimentation of PS particles with ferrihydrite.

Research questions of Study 2:

- How does UV-weathering of 1 µm PS influence the surface properties of the particles, e.g. zeta potential, surface roughness and size?
- How do these changes influence the heteroaggregation and sedimentation of PS with ferrihydrite?

We hypothesize that UV-weathering will reduce particle size, increase surface roughness and lead to the formation of oxygen-containing functional groups on the MP surface. These groups are likely to reduce surface charge of weathered MP and enhance surface reactivity as further interactions might take place, e.g. hydrogen bonding. This would intensify the interactions between weathered PS and ferrihydrite, likely leading to aggregation and sedimentation taking place over a wider range of conditions.

Study 3: Ferrihydrite coating reduces microplastic induced soil water repellency

In this study, we investigate how pre-coating or *in-situ* coating of MP with ferrihydrite affects the water repellency of MP in porous media during capillary rise.

Research questions of Study 3:

- How does a pre-coating of MP with ferrihydrite change the wettability of MP in porous media?
- Can a coating also be formed *in-situ* when a pristine MP hotspot is embedded in porous media and capillary rise with ferrihydrite suspension is performed?
- Are there differences in wettability and coating between different polymer types (PS and PET)?

We hypothesize that a pre-coating of MP with ferrihydrite increases the wettability of MP. Furthermore, we expect that capillary rise with ferrihydrite suspension leads to an *in-situ* coating of MP and hence to increased wettability. Lastly, we assume that the wettability of pristine MP as well as the coating differs between the polymer types, as they have different compositions and thus different surface groups that influence these processes.

Study 4: A rapid method to quantify sub-micrometer polystyrene particles in aqueous model systems by TOC analysis

In this study, we investigate if the quantification of MP from samples with a simple matrix (no other organic substances except for MP) can be done by TOC analysis.

Research questions of Study 4:

- Can the concentration of micrometer-sized MP particles in aqueous samples be successfully determined using a TOC analyzer?
- Does the particle size have an influence on the recovery of the TOC measurements?

We hypothesize that the quantification of MP in the lower micrometer range is feasible using TOC analysis. However, with increasing particles size, the catalytic combustion in the instrument might not be sufficient to convert the complete particle to CO_2, reducing the recovery of the samples. Hence, an additional catalyst might be necessary to improve the recovery.

3 Material and Methods

3.1 Selection of particles

3.1.1 Microplastic particles

For Study 1 and 2, spherical PS particles with a diameter of 1 µm were used (Microparticles). According to the manufacturer, sulfate groups remained on the particle surface due to the manufacturing process. The particles density was 1.05 g/cm^3. In Study 3, we used irregular shaped PS and PET particles with a size range of 20-75 µm. The original material (Veolia Deutschland GmbH) was milled by a centrifugal mill (ZM200, Retsch GmbH) and sieved into the required size fraction. In Study 4, we used spherical PS particles with diameters of 0.5, 1, 2 and 6 µm (Polyscience).

To investigate the different wettability of pristine MP particles compared to coated MP particles (Study 3), we coated 20-75 µm PS and PET with ferrihydrite. For this, we shook 2 g of PS or PET for 2 h in ferrihydrite suspension at 16 rpm in an overhead shaker and then filtered the suspension to separate the coated MP from the remaining ferrihydrite colloids in the suspension. The filter was dried overnight at 40 °C. To calculate the amount of iron adsorbed to the PS or PET surface, the specific surface area was determined by the Brunauer–Emmett–Teller (BET) method. The amount of iron adsorbed onto the MP surfaces, was determined photometrically after dissolving and reducing the adsorbed ferric particles to ferrous iron.

3.1.2 Metal hydroxides

In all four studies, we used the poorly crystalline iron oxyhydroxides ferrihydrite. We synthesized 6-line ferrihydrite according to Cornell and Schwertmann (2003). By XRD analysis, we confirmed that the synthesized product was 6-line ferrihydrite (from here on referred to as “ferrihydrite”). In addition to ferrihydrite, in Study 4, we used aluminum (Al) hydroxide. The details regarding the synthesis can be found in the Method section of Study 4.

3.2 UV-weathering of microplastic

In Study 2, we investigated the aggregation and sedimentation of laboratory-controlled UV-weathered 1 µm PS particles. To obtain UV-weathered MP, we used a UVACUBE 400 irradiation chamber for solar simulation, equipped with a SOL500 lamp (both Dr. Hönle AG). The acceleration factor of the weathering chamber compared to average German irradiation is 10 (calculated based on data provided by the supplier). PS suspensions with a concentration of 100 mg/L were irradiated in quartz beakers for various periods between 0 and 1000 h. However, for aggregation and sedimentation studies we only used the periods of 0, 48 and

96 h, because for longer UV-irradiation, almost all PS particles were found in the size fraction < 0.45 µm and approx. half of the carbon/PS was removed from the sample as gas.

From all irradiated samples, the amount of total organic carbon (TOC) in the samples was determined to investigate how much carbon has left the sample as gas. Furthermore, we determined the dissolved organic carbon (DOC) fraction. Therefore, the suspensions were filtered through 0.45 µm. Please note that even though we use the term 'DOC', carbon found in this size fraction might be either dissolved or present as particles smaller than 0.45 µm.

3.3 Sedimentation experiment

Sedimentation experiments in Study 1 and 2 were conducted in narrow glass vessels. The tested pH range of samples containing pristine or weathered PS (10 mg/L) and ferrihydrite (10 mg/L) was 3 to 11. In Study 1, the reaction time was set to one day and one week. For Study 2 (weathered particles) we only looked at a reaction time of one day, as the results of Study 1 showed that the relevant sedimentation patterns were already observed after one day. After the reaction and sedimentation time of one day or one week, we carefully removed the upper 8 mL of the samples with a pipette. This part was stored in an additional vial and is referred to as 'solution'. The lower 2 mL of the sample are referred to as 'sediment' (**Figure 3**). The concentration of PS in solution and sediment was determined by TOC analysis.

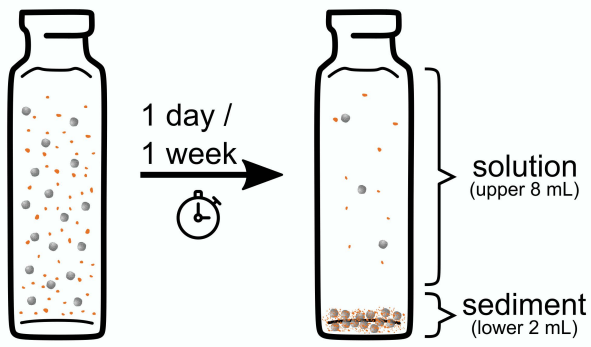

Figure 3. *Simplified illustration of the experimental setup of sedimentation experiments with PS and ferrihydrite (10 mg/L each).*

3.4 Determination of zeta potential and hydrodynamic diameter

To study the aggregation of PS and ferrihydrite, we used a ZetaSizer Nano ZS (Malvern Panalytical) for Study 1 and 2. With the zeta potential we gained information of the surface charge of PS and ferrihydrite as well as those samples in which both particles were present. By Dynamic Light Scattering (DLS) we determined the z-average hydrodynamic diameter of the samples to see at which pH conditions aggregation took place. The tested pH range was 3 to 11. In all samples, the concentrations of PS and ferrihydrite were 10 mg/L each.

Additionally, in Study 2 we determined the zeta potential of UV-weathered particles to investigate how the surface charge is influenced by UV-weathering.

In Study 3, the zeta potential values of 20-75 µm PS and PET particles were derived from streaming potential measurements. They were conducted with the electrokinetic analyzer SurPASS 3 (Anton Paar GmbH) and a cylindrical cell.

3.5 TOC analysis

In Study 4 we tested the applicability of a TOC analyzer (TOC-L-Analyzer, Shimadzu) for quantification of sub-micrometer PS particles. Therefore 0.5, 1, 2 and 6 µm PS suspensions of various concentrations were measured using the TOC analyzer in the presence and absence of Fe and Al hydroxides. The metal hydroxides were added to the samples to test their catalytic effect on the oxidation of PS to CO_2.

Furthermore, the TOC analyzer was used to (i) measure the amount of PS that sedimented after interaction with ferrihydrite and (ii) to determine the amount of TOC and DOC in PS samples after UV-weathering. Detailed description of the measurement protocols can be found in the corresponding publications.

3.6 Scanning electron microscopy and energy-dispersive X-ray spectroscopy

Scanning electron microscopy (SEM) was performed for Study 1-3. In Study 3, the dried (pristine or ferrihydrite-coated) PS and PET was placed on a standard sample holder and coated with a thin layer of platinum (Cressington 208 HR sputter coater). SEM images were recorded with a Zeiss ULTRA PLUS (Carl Zeiss Microscopy) and used to identify if a successful coating of PS and PET with ferrihydrite was done. In Study 1 and 2, the sample preparation slightly differed. Instead of dried material, the suspensions containing PS, ferrihydrite, or PS and ferrihydrite was investigated and analyzed regarding the aggregation. 4 µL of one sample was dropped onto a glow-discharged carbon-supported TEM copper grip (S160 Plano) and dried under ambient conditions. Analogous to Study 3, the samples were coated with platinum, and SEM images were recorded.

Additionally, energy-dispersive X-ray spectroscopy (EDS) was done for a subset of samples using a Zeiss LEO 1530 (Carl Zeiss Microscopy) operating at 2 kV and equipped with an UltraDry EDS detector using Pathfinder software (Thermo Fisher Scientific). EDS resolution was enhanced by use of a thin layer of carbon as specimen support and low acceleration voltage.

3.7 Neutron imaging

In Study 3, we used neutron imaging to quantify the water saturation of MP hotspots in porous media during capillary rise. Time-series neutron radiography was conducted at the NEUTRA beamline at the Paul Scherrer Institute in Villigen, Switzerland. We filled aluminum containers halfway with pre-treated and washed quartz sand (700-1200 µm, Raneem, Sand-Schultz GmbH). Then, a MP hotspot (0.02 g) was added with a funnel and afterwards the other half was filled with sand (**Figure 4**).

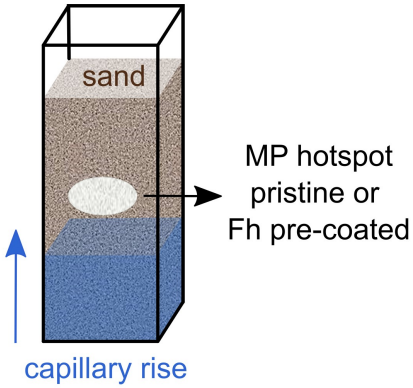

Figure 4. *Schematic setup of a sample container filled with sand and MP hotspot during capillary rise.*

The hotspots consisted of pristine or with ferrihydrite coated PS or PET. Capillary rise was imaged to estimate the water saturation of the hotspot. The filled sample container was placed in an open container with in and out flow, providing a constant water table for capillary rise. A peristaltic pump at constant flow rate supplied the respective liquid. The imbibition of three different liquids was recorded for ten or six replicates of different MP hotspots (**Table 2**). As liquids for capillary rise, we used (i) deionized water with 10 mM NaCl (water), (ii) 10 mg/L ferrihydrite suspension with 10 mM NaCl (Fh10) and (iii) 100 mg/L ferrihydrite suspension with 10 mM NaCl (Fh100). We performed two wetting-drying cycles for the experiments with Fh10 and Fh100 and one cycle for experiments with water.

Table 2*. Capillary rise experiments for neutron imaging.*

MP	Liquid	Repetitions
Pristine PET	Water, Fh10, Fh100	10
Coated PET	Water	6
Pristine PS	Water, Fh10, Fh100	10
Coated PS	Water	6

4 Summary of Results and Discussion

4.1 Study 1: Heteroaggregation of PS microplastic with ferrihydrite leads to rapid removal of microplastic particles from the water column

In this study we investigated the interactions between 1 µm PS particles and ferrihydrite. Over a pH range between 3 and 11 we analyzed if aggregation between the particles took place. Since particle aggregation strongly influences the settling of particles in water, we additionally investigated the sedimentation of PS in presence and absence of ferrihydrite.

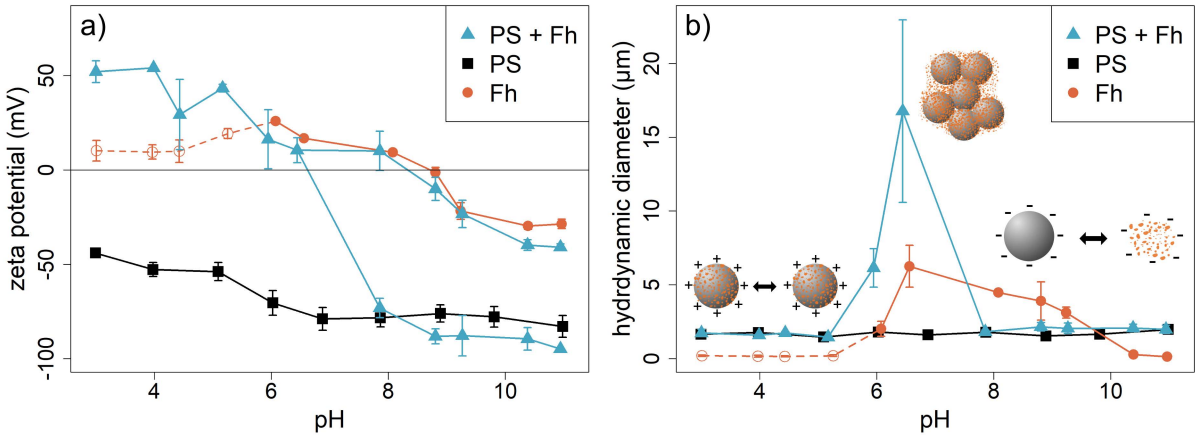

Figure 5. a) *Zeta potential and* ***b)*** *z-average hydrodynamic diameter of PS, ferrihydrite (Fh), and samples with PS and ferrihydrite (PS+Fh). For ferrihydrite samples with pH < 6, the count rates were not sufficient for reliable light scattering measurements and therefore should be regarded with caution (dashed line). In* ***b)*** *simplified illustrations of interactions between PS and ferrihydrite are embedded: At acidic pH, negatively charged PS particles are coated with positively charged ferrihydrite leading to charge reversal. At neutral pH, coating of PS with ferrihydrite results in charge neutralization allowing strong heteroaggregation. At alkaline pH, both particle types are negatively charged, thus repulsive forces prevent aggregation.*

PS particles were highly negatively charged over the tested pH range with zeta potentials ranging between -44 mV (pH 3) and -82.9 mV (pH 11) (**Figure 5a**, black data points). Strong electrostatic repulsion between the particles prevented major homoaggregation. However, with a mean hydrodynamic diameter of 1.7 µm, we assume some homoaggregates must have formed despite strong repulsion (**Figure 5b**). After one day of settling (in the absence of ferrihydrite), the PS concentration in the sediment was only slightly increased compared to the solution. However, after one week of settling time, the PS concentration in the sediment increased. Between 30.4% and 47.8% of the PS in the sample was found in the sediment. Please consider that due to the experimental setup (**Figure 3a**), 20% of the PS should already be found in the sediment if no sedimentation occurs. As no pH dependence for the

sedimentation has been observed and high zeta potential values suggest strong repulsion between the particles, we attribute the sedimentation primarily to long-term storage effects.

For ferrihydrite particles, we found positive zeta potential values at acidic and neutral pH values, the isoelectric point at pH ≈ 8.7 and negative zeta potential values for pH > pH_{IEP} (**Figure 5a**, orange data points). At pH 6-9, electrostatic repulsion between ferrihydrite particles was low which allowed homoaggregation. This was confirmed by low zeta potential values suggesting low repulsion and by increased hydrodynamic diameter values (**Figure 5b**), indicating the formation of homoaggregates.

The results of zeta potential and hydrodynamic diameter of PS differed greatly after the particles reacted with ferrihydrite for one week. Instead of a high negative surface charge, we found positive charges for acidic and neutral pH values (**Figure 5a**, blue data points). Another striking observation is the sharp increase in aggregate size at circumneutral pH (**Figure 5b**). This can only be explained by strong aggregation between the particles. Heteroaggregation took place at this pH range because the negative PS particles were coated by ferrihydrite particles. Since ferrihydrite particles had only a very low positive charge at circumneutral pH, charge neutralization was almost achieved. Therefore, electrostatic repulsion between the ferrihydrite coated PS particles was minimal and allowed further aggregation of the coated particles. On SEM images we can clearly see such heteroaggregates in which ferrihydrite serves as a bridging agent between the PS particles (**Figure 6**).

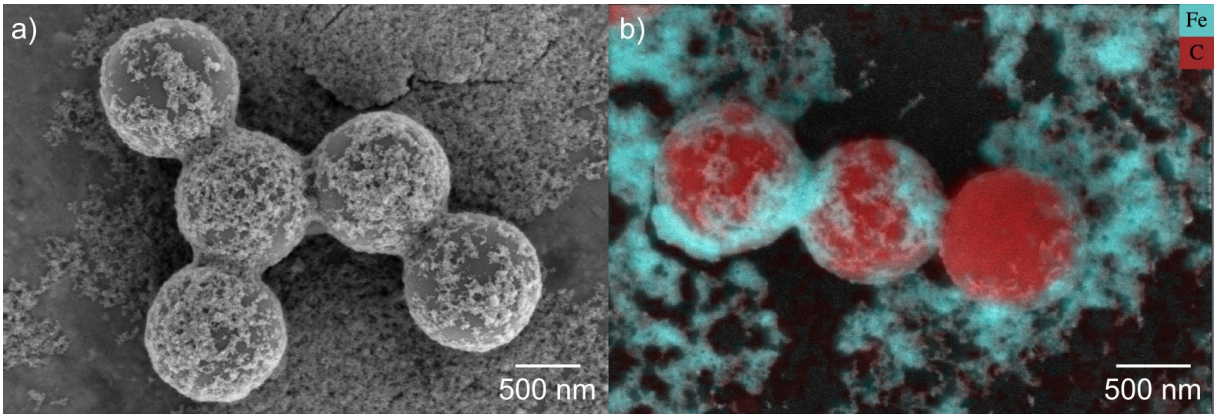

***Figure 6**. **a)** SEM image of a formed heteroaggregate of PS and ferrihydrite at pH 6.5. Ferrihydrite is found on the surface of PS and as linkage between the PS particles. **b)** EDS analysis confirms that the aggregated material is ferrihydrite.*

In the acidic pH range, the negatively charged PS particles were also coated with ferrihydrite. However, no increase in aggregate size was observed (**Figure 5b**). At this pH range, ferrihydrite particles contained a stronger positive surface charge compared to neutral pH values. Thereby, a coating of PS with nano-sized ferrihydrite particles led to charge reversal

but any further aggregation of the coated PS particles was prevented by the strong positively rendered charge (**Figure 5a**).

At alkaline pH values, both types of particles were negatively charged, and electrostatic repulsion inhibited major interactions. The detection of two different zeta potential peaks per measurement suggest the presence of two differently charged species. As one measurement point aligns well with the zeta potential of ferrihydrite and the other one with that of PS, the assumption of those particles staying separated in suspension is strengthened. Simplified illustrations of interactions between PS and ferrihydrite particles at different pH ranges are embedded in **Figure 5b**.

Looking at the sedimentation of PS in presence of ferrihydrite, clear correlations with aggregation results are observed. Maximal sedimentation (after one day and one week) was found at circumneutral pH values, where maximal heteroaggregation of PS and ferrihydrite was observed. With 90-93% of PS found in the sediment at pH 6-6.5, almost all PS particles were removed from the water column already after one day of settling. Furthermore, compared to blank samples (without ferrihydrite) the sedimentation of PS was (at least slightly) enhanced to approx. 50% at all pH conditions in presence of ferrihydrite, for a sedimentation time of one week. After only one day of sedimentation however, the sedimentation in presence of ferrihydrite did not increase compared to the absence of ferrihydrite at pH values where no heteroaggregation took place.

In conclusion, Study 1 showed that interactions of PS particles and ferrihydrite are strongly pH-dependent as they are driven by electrostatic interaction forces and the surface charge of ferrihydrite varies over the pH-range. At circumneutral pH, charge neutralization of suspensions with PS and ferrihydrite resulted in the formation of heteroaggregates which subsequently sedimented. Overall, our findings suggest that MP particles tend to form environmental corona at their surface. This might consist of iron oxyhydroxides but also of other environmental colloids. Once MP particles enter the aquatic environment, their surface properties are strongly controlled by the interactions with natural constituents and heteroaggregation is likely to reduce their residence time in the water column since it results in fast sedimentation.

4.2 Study 2: UV-weathering affects heteroaggregation and subsequent sedimentation of polystyrene microplastic particles with ferrihydrite

In Study 2, we first investigated the influence of laboratory-controlled UV-weathering on surface properties of PS particles. Subsequently we studied the impact of UV-weathering on pH-dependent heteroaggregation and sedimentation of PS with ferrihydrite.

UV-weathering of PS strongly impacted the size, shape, surface characteristics and composition of particles. With increasing weathering, the particle sizes decreased, the shapes became more irregular, surface roughness increased and for some particles the formation of cavities was observed. Furthermore, opposing to our hypothesis, the initial strong negative zeta potentials of PS rendered less negative after UV-weathering. We attribute this to UV-induced cleavage of negatively charged sulfate groups from the PS surface, which are remnants from the manufacturing process. However, the surface charge remained within a negative range. We ascribe this to the formation of oxygen-containing functional groups on the PS surface, induced by UV-irradiation (Y. Liu et al., 2019; Wang et al., 2023; Zhang et al., 2022). Interestingly, the TOC mass of PS samples decreased strongly, especially between 48 and 240 h of UV-irradiation. The fraction of DOC (< 0.45 µm) peaked after 144 h of weathering. For longer weathering (> 144 h), DOC and TOC concentrations were similar, suggesting that most particles were smaller than 0.45 µm, some might even be present as dissolved weathering products. After 300 h, only approx. 10% of the initial carbon (and thus PS) remained in the samples. Hence, a substantial proportion of carbon must have been released from the samples, likely in gaseous form. These results confirm previous work showing the formation of DOC and/or gases like CO_2 during the UV-weathering of plastic particles (Juanjuan Liu et al., 2019; Pfohl et al., 2022; Ward et al., 2019). Our observations of a temporary increase in DOC accompanied by a continuous PS mass loss match well with a previously established three-stage chemical-reaction for UV-induced degradation (Duan et al., 2021): (i) *Initiation*: chain scission of bonds within the polymer structure, formation of radicals (e.g. $R^{\cdot}$, $RO^{\cdot}$, $ROO^{\cdot}$) and reactive oxygen species, such as hydroxyl or superoxide radicals takes place (Duan et al., 2021). (ii) *Propagation*: highly active radicals promote self-catalyzed reactions (Duan et al., 2021). The analyzed PS particles degrade further into smaller particles, dissolved species and gaseous components. (iii) *Termination*: total mineralization of the particles (Duan et al., 2021). For the analyzed PS particles however, 10% of the initial carbon mass remained in the samples and was therefore not transformed into gas.

The interactions between pristine PS and ferrihydrite after one day of reaction aligned well with those of one week reaction time (Study 1): charge neutralization allows strong

heteroaggregation at circumneutral pH with subsequent sedimentation. PS weathering of 48 h did not affect the heteroaggregation and sedimentation substantially. However, strongly weathered PS particles (PS_{96h}), showed a very different behavior of heteroaggregation and sedimentation with ferrihydrite compared to pristine PS (**Figure 7**). The pH_{IEP} of PS_{96h} and ferrihydrite samples was shifted to an acidic pH value of approx. 4. This also changed the pH range where heteroaggregation and sedimentation occurred (**Figure 7**). Furthermore, the maximum aggregate size decreased compared to pristine particles (**Figure 7a**). The pattern that heteroaggregation takes place at the pH_{IEP} and results in sedimentation also applied for UV-weathered particles. However, aggregation and especially sedimentation were not only observed at the pH_{IEP}, but over a broader pH range between 3 and 7 (**Figure 7b**). We conclude that interactions between PS and ferrihydrite causing heteroaggregation and sedimentation, were intensified after 96 h of PS weathering.

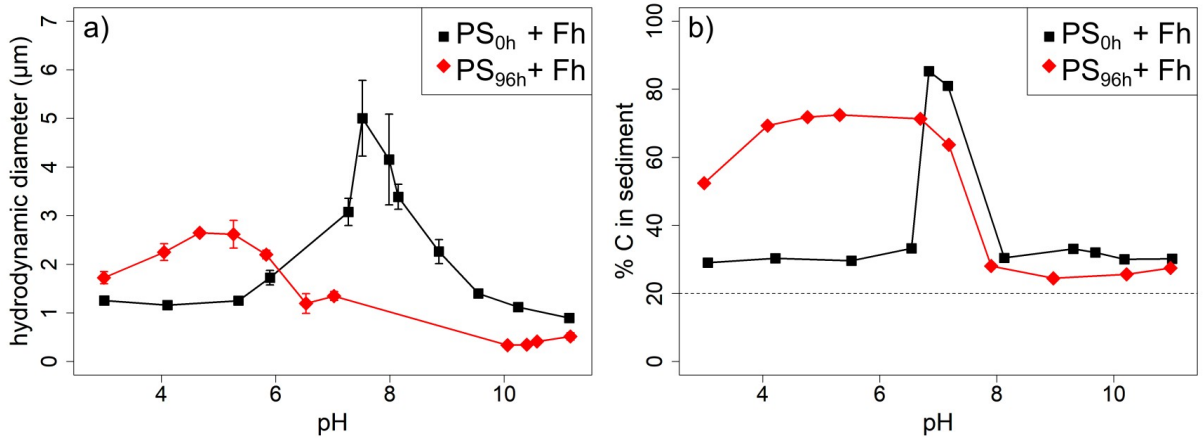

Figure 7. a) *z-average hydrodynamic diameter and* ***b)*** *sedimentation of pristine PS (PS_{0h}) and PS exposed to UV-irradiation for 96 h (PS_{96h}) after reaction with ferrihydrite for one day.*

Our results suggest that aside of electrostatic interactions, further interactions must have taken place between PS_{96h} and ferrihydrite particles. The electrostatic interactions should not change substantially as the surface charge of weathered PS remained in a similar range compared to pristine PS (even though it became less negative). Therefore, we attribute the interactions being expanded over a broader pH-range to two factors: (i) the formation of oxygen-containing functional groups on the MP surface increased the surface reactivity and likely enabled other interaction forces to take place: e.g. hydrogen bonding or ligand exchange (Duan et al., 2021; Zhang et al., 2022). (ii) Small particle fragments or dissolved substances formed during weathering were likely to be involved in the interactions between PS_{96h} and ferrihydrite (**Figure 8**).

In summary, in Study 2 we showed that UV-weathering strongly influences the surface properties and reactivity of PS and therefore also impacts the interactions with ferrihydrite (and

likely other particles and colloids present in a natural setting) resulting in a wider pH range where aggregation-facilitated sedimentation occurs.

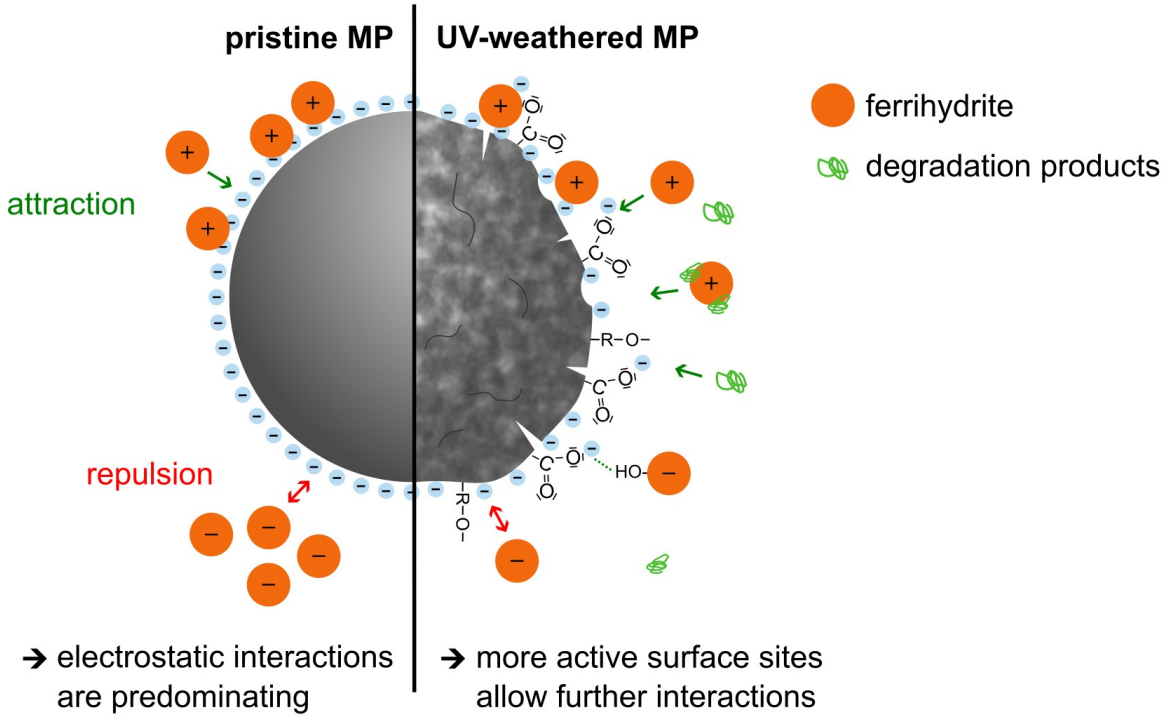

Figure 8. *Conceptual model representing the different interactions of pristine and UV-weathered PS particles with ferrihydrite. For pristine MP particles, the interactions with ferrihydrite are predominated by electrostatic interactions. With increasing UV-weathering, not only the more active surface sites are formed on the MP surface that allow further interactions (e.g. hydrogen bonding) with ferrihydrite. Additionally formed degradations products might also interact with ferrihydrite or the MP particles.*

4.3 Study 3: Ferrihydrite coating reduces microplastic induced soil water repellency

In Study 3 we tested the influence of ferrihydrite coating on the wettability of MP in porous media. Therefore, we investigated if pristine and coated (pre or *in-situ* coated) MP hotspots embedded in quartz sand show differences in their wettability during capillary rise with water or ferrihydrite suspension.

The analysis of water saturation from neutron imaging showed low water saturations for pristine MP hotspots during capillary rise with water (**Figure 9a**). Even though the water saturation of PET was slightly higher compared to PS, both pristine MP types were considered non-wettable, and the rising water bypassed the hotspots (**Figure 9b+c**). Pre-coating of PET with ferrihydrite clearly changed the water saturation. The coated PET hotspots were rendered

wettable (**Figure 9a**), and we observed water flow into the hotspot during capillary rise (**Figure 9e**). For PS, only minor differences in water saturation between pristine and coated PS particles were visible. The water saturation of coated PS increased slightly compared to pristine PS, but the hotspots were still non-wettable (**Figure 9d**).

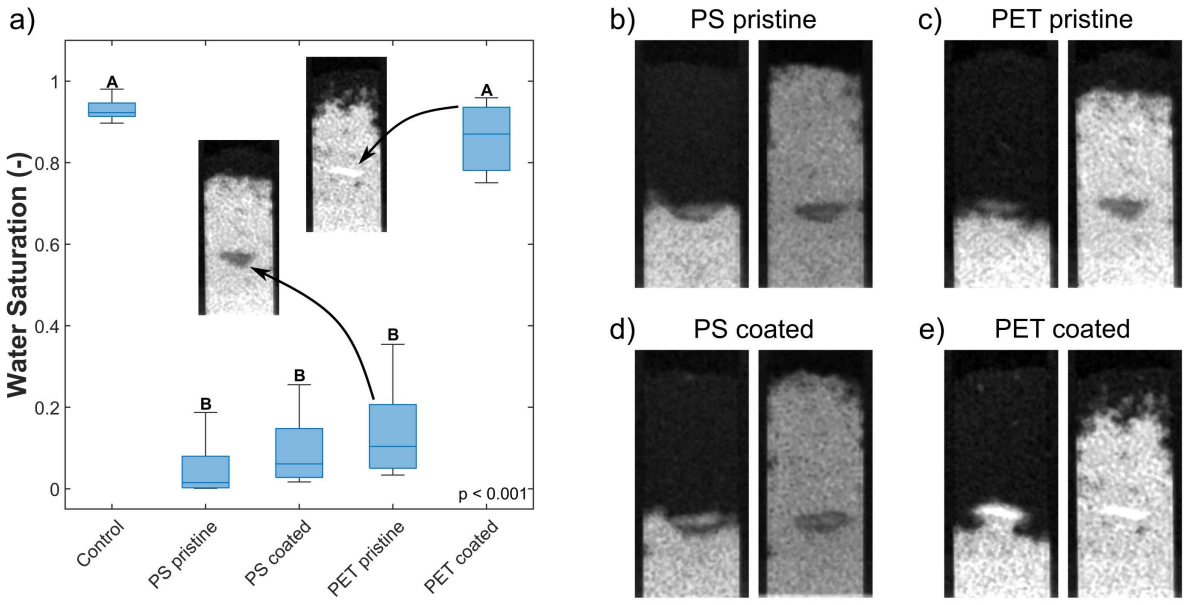

Figure 9. a) *Water saturation of MP hotspots after capillary rise with water (control = without MP hotspot).* ***b)-e)*** *Neutron images during and at the end of capillary rise of water. The hotspots consist of* ***b)*** *pristine PS,* ***c)*** *pristine PET,* ***d)*** *ferrihydrite-coated PS and* ***e)*** *ferrihydrite-coated PET. For each set, the left image is taken at a time step at which the rising water reaches the hotspot. For coated PET, water flow into the hotspot is observed whereas for the other variants, water bypasses the hotspot. The right image of each set is taken at the end of capillary rise.*

The increase in wettability of coated PET compared to coated PS can be explained by the effectiveness of the ferrihydrite coating. The amount of ferrihydrite adsorbed onto the PET surface was approx. four times higher compared to PS. As zeta potential values of pristine PS and PET were similar, we attributed this disparity not to effects of surface charge but to the presence of functional groups in the polymer backbone of PET which enhanced ferrihydrite adsorption compared to PS.

Table 3*. Mean static contact angles of pristine and coated MP (°), n = 11.*

Pristine PS	Pristine PET	Coated PS	Coated PET
143.7 ± 3.3	123.8 ± 3.9	127.1 ± 3.7	101.7 ± 4.4

Static contact angle (CA) measurements of pristine and coated MP align with the effectiveness of ferrihydrite coating but do not fully explain the different water saturation of MP hotspots during capillary rise. Particles with CA below 90° are typically considered to allow for good wettability, whereas those with higher CA are regarded as hydrophobic (Bachmann et al.,

2003, 2000). Pristine PET showed lower static CA than pristine PS (**Table 3**). Ferrihydrite coating decreased the CA for both polymer types, indicating a change in polarity. Coated PET exhibited the lowest CA whereas the value for coated PS was in the range of pristine PET (**Table 3**). Even though all particles exceeded the threshold of 90° and theoretically needed to be considered as hydrophobic, the lower CA of pristine and coated PET compared to pristine and coated PS indicated higher surface polarity and therefore a higher wettability. Hence, this explains the higher water saturation of pristine PET compared to PS and the more effective coating with ferrihydrite. However, the wettability of coated PET observed during capillary rise seems to contradict the result of static CA measurements. Even though the value of coated PET was the lowest along the other MP variants, it still indicated non-polarity. Such discrepancy arises from methodological differences between static CA measurements (quasi-two-dimensional system) and capillary rise that adheres to effective, dynamic CA of water in a three-dimensional pore space.

In a second experiment we investigated if coating of MP with ferrihydrite can also be established *in-situ*. But regardless of the ferrihydrite concentration in the imbibing liquid (10 or 100 mg/L ferrihydrite), contrary to our hypothesis, no effective *in-situ* coating of pristine MP with ferrihydrite was observed after two wetting-drying cycles and the MP hotspots remained non-wettable. However, the water saturation of the MP hotspots increased slightly but not significantly. In line with results of pre-coated MP, the water saturation of PET increased stronger compared to PS, presumably due to the presence of more functional groups in the PET polymer backbone. Generally, the slight increased water saturation suggests that ferrihydrite coating occurred locally, likely at the edges of the hotspot. As the suspension bypassed the hotspots, we assumed that only the MP particles at the hotspot boundaries had contact with the imbibing ferrihydrite suspension. Therefore, an increased number of wetting-drying cycles might allow the ferrihydrite suspension to propagate deeper into the MP hotspot, and thus allow stronger *in-situ* coating of MP.

In conclusion, depending on polymer type, capillary driven imbibition of water into MP hotspots was facilitated by ferrihydrite pre-coating of MP. Contrary, *in-situ* coating of pristine MP hotspots with ferrihydrite suspension (regardless of ferrihydrite concentration) did not establish a coating that increased the wettability and thus did not allow imbibition of water in two wetting cycles. As the presence of water accelerates biotic and abiotic degradation processes, the understanding of wetting kinetics is important to predict MP degradation (Ali et al., 2021). Our results indicate that natural particles like iron oxyhydroxides can increase the wettability of MP in porous media. This might counteract previously observed limitation of capillary flow and reduced local water contents due to MP particles in soil (Cramer et al., 2022).

4.4 Study 4: A rapid method to quantify sub-micrometer polystyrene particles in aqueous model systems by TOC analysis

In Study 4, we propose a quantification method for MP particles in model systems based on the determination of the carbon content. For several laboratory experiments with MP, e.g. sedimentation experiments from Study 1 and 2, a fast quantification method is required. At the same time, the requirements of MP detection from laboratory samples are often lower compared to environmental samples. In cases where no other organic substances are present in the samples, the quantification can be done by determining the carbon concentration. In environmental science, TOC analyzers are traditionally used for quantifying DOC or particulate organic carbon (POC) in aquatic samples. In this study we proved its applicability for commercially available PS particles in the lower micrometer range (0.5, 1, 2, 6 µm).

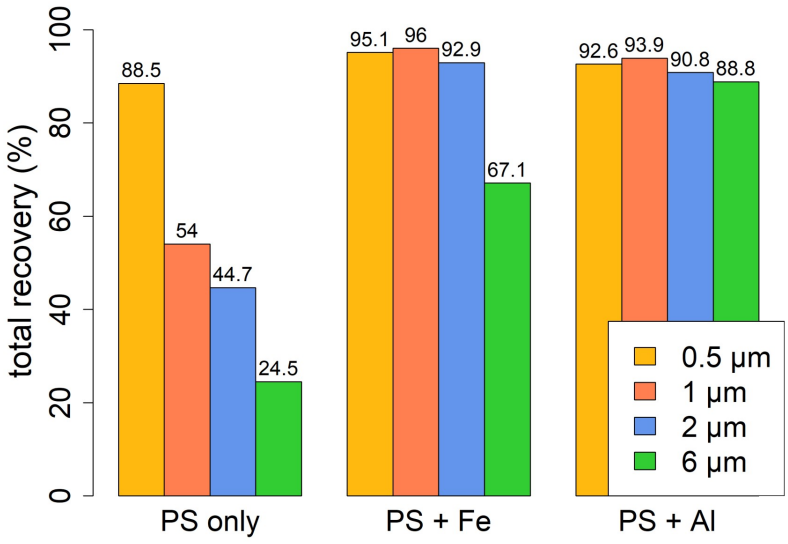

Figure 10. *Total recovery in percent for each particle size in presence and absence of Fe or Al hydroxide in the PS samples.*

The recovery of PS varied depending on particle size. We found lower recoveries with increasing particle size from 88.5% (0.5 µm) to 24.5% (6 µm) (**Figure 10**). Based on the low recovery for larger particles, we assumed that PS particles were not completely oxidized to CO_2 during the high-temperature catalytic oxidation in the instrument. The particle size (but not the concentration) seemed to be the limiting factor for a complete oxidation to CO_2, as smaller particles (with a higher surface-to-volume ratio) offer a larger surface area for chemical attacks during the high-temperature catalytic oxidation.

With addition of Fe or Al hydroxides to samples prior measurement, the unsatisfactory recoveries were improved strongly. For 0.5-2 µm PS, the recoveries were enhanced to over

90% and the precision increased. For the largest tested particles (6 µm), recoveries of 67.1% and 88.8% were found in presence of Fe or Al hydroxides, respectively.

Hence, our findings suggest that the Pt-catalyst used in the instrument was not sufficient for complete oxidation of PS particles to CO_2. The addition of metal hydroxides increased the catalytic activity and allowed for complete oxidation of particles and their subsequent TOC measurement. This agrees well with previous literature reporting an enhanced catalytic activity of Pt/Al_2O_3 to oxidize CO at room temperature by deposition of iron oxide on the Pt/Al_2O_3 catalyst (Cha et al., 2021). However, an upper limit in PS particle size seemed to exist as indicated by the relatively low recoveries and high standard deviations found for 6 µm PS particles despite the addition of metal hydroxides.

Concluding, with the addition of Fe or Al hydroxides, TOC measurements present a fast, simple, and cheap alternative to commonly used methods for MP quantification in experiments studying the environmental behavior of MP in the sub-micrometer and nanometer range. We recommend the application for this method for samples in which no other organic particles (except MP) are present.

5 Conclusions

The pollution of the environment with plastic and MP has received tremendous attention in recent years, and the number of scientific studies has rapidly increased (**Figure 1**). Despite the scientific effort to understand the (transport) behavior of MP in environmental compartments and its interactions with other particles and colloids, the details have not yet been fully understood. This dissertation addresses different MP-types (weathered and non-weathered, PS and PET), combined with two different environmental settings (water and soil) in the presence of naturally occurring colloids (ferrihydrite). This combination enabled us to further understand the interactions of MP with environmental colloids and to evaluate the consequences of interactions of MP with iron oxyhydroxides for (i) MP sedimentation in water and (ii) the effect on MP wettability in soil. Details will be discussed in the following chapters.

5.1 Environmental implications of MP aggregation and sedimentation

Study 1 and 2 clearly demonstrate that the presence of ferrihydrite is not only a driving factor for heteroaggregation but also promotes the sedimentation of PS. The interactions between MP and ferrihydrite are strongly pH-dependent, mainly because the surface charge of iron oxyhydroxides varies strongly over the pH-range. Hence, for pristine MP particles, electrostatic interactions between MP and ferrihydrite determine whether the particles aggregate or not. At pH conditions, where charge neutralization is achieved, heteroaggregation takes place. The formation of large aggregates of PS and the much denser ferrihydrite leads to rapid sedimentation. Hence, through this process of heteroaggregation and subsequent sedimentation of the aggregates, MP particles are likely to be removed from the water column and transported to deeper water layers or the sediment (Lagarde et al., 2016; Leiser et al., 2021a, 2021b, 2020; Y. Li et al., 2019; Long et al., 2015; Michels et al., 2018).

Increased sedimentation of MP facilitated by heteroaggregation impacts the residence time in water, and thus influences the exposure time of aquatic organisms to MP. The transport of MP particles to the sediment implies that exposure times of aquatic organisms might be reduced and concurrently the risk for organisms living in the benthic zone might be increased as sediments of rivers, lakes and the sea may act as a sink for MP particles (Leiser et al., 2021b; Näkki et al., 2019; Turner et al., 2019; van Emmerik et al., 2022). Hence, future studies examining the risks of MP on organisms, should not primarily focus on organisms in the water column but also on organisms in the sediment.

Through interactions of MP with environmental colloids, the behavior of MP particles is not only impacted by heteroaggregation that is driving sedimentation. Also coating processes of MP with natural substances, affecting surface properties (even though not sedimentation) might

influence the environmental behavior of MP. Within this thesis we showed that ferrihydrite coating can reverse the surface charge of MP and increase the hydrophilicity of the particles. These changes in physicochemical properties in turn have the potential to impact uptake mechanisms of organisms and cells (Ramsperger et al., 2022; Wieland et al., 2024).

In Study 2, we set our focus on more environmentally relevant MP, considering particles previously exposed to UV-irradiation, to mimic the process of natural weathering of MP. Exposure to UV-irradiation modified surface properties, sizes and shapes of PS particles, and led to the formation of dissolved and particulate weathering products. This, in turn, increased the reactivity of the particles, likely due to the formation of hydrophilic functional groups on the surface, allowing interactions via hydrogen bonding (Duan et al., 2021; Zhang et al., 2022). These results indicate that with increasing weathering and subsequently increasing number of reactive functional groups on the surface, the importance of electrostatic attraction forces on aggregation may decrease, as for those particles also additional specific interactions are possible. Hence, the impact of surface charge, which played the major role on interactions of pristine particles, might be reduced for weathered particles.

The interactions between weathered PS and ferrihydrite were not only influenced by the altered surface properties due to UV-weathering but also by the presence of UV-induced degradation products. In natural environments, it is questionable if these products would have such a strong impact on MP aggregation as they probably distribute quickly in larger water bodies. Furthermore, the amount of natural particles in the environment surpasses that of MP particles by far (Koelmans et al., 2022). This makes it more likely that MP particles or their degradation products interact with naturally occurring colloids rather than with each other. The degradation products (in this work measured as DOC fraction) might become part of the natural DOC fraction that is known to adsorb on iron oxyhydroxides (Gu et al., 1996; Sharp et al., 2006) and form iron-DOC flocs (Droppo et al., 1997; Sharp et al., 2006) which might be transported as environmental colloids. Hence, not only the interactions of MP particles with iron oxyhydroxides but also those of their degradation products may affect the overall fate of MP in the environment.

Furthermore, in the environment, not only UV-weathering of MP might increase the reactivity and thus the heteroaggregation and sedimentation of MP particles. A formation of biofilms on MP will change the physicochemical properties of MP particles and is likely to enhance their adhesiveness, thus making them more “sticky” (He et al., 2022; Michels et al., 2018; Rummel et al., 2017). This will subsequently increase the aggregation with other natural colloids and thereby the potential of sedimentation.

To understand the fate of MP in water bodies, it is certainly not enough to study under which conditions they sediment; it is also necessary to consider whether the settled particles are re-mobilized under certain conditions – especially when redox-active iron species are involved. The mobility and reactivity of iron in the environment is redox-dependent (Kappler et al., 2021). For example, microbial iron reduction might result in the dissolution of iron oxyhydroxides. Consequently, the mobility of substances and particles bound to iron oxyhydroxides is strongly dependent on the precipitation and dissolution of iron minerals (Kappler et al., 2021). One could therefore assume that MP particles, which have previously sedimented after heteroaggregation with iron oxyhydroxides, might be re-mobilized and therefore released from the sediment under iron-reducing conditions. However, a recent study has shown otherwise: Leiser et al. (2021b) investigated not only the sedimentation of polyethylene (PE) particles facilitated by iron-organo aggregates, they also studied the re-mobilization from the sediment under oxic and anoxic conditions. Surprisingly, no significant remobilization of MP particles was observed, not even under anoxic conditions and iron reduction (Leiser et al., 2021b). These results were explained by the transport of the aggregates from the sediment surface deeper into the sediments (Leiser et al., 2021b). Such deeper penetration of MP particles into the sediment might not only explain recent findings of MP particles being found in sediments deposited before the start of the industrial production of polymers (Dimante-Deimantovica et al., 2024) but also indicate that deposition of MP particles in sediments might be stable over a longer time period (Leiser et al., 2021b).

Even though the experiments in this thesis were conducted under laboratory conditions, we are confident that the process of aggregation and subsequent sedimentation is highly relevant in natural environments. Besides ferrihydrite a variety of additional inorganic, organic or biogenic particles is present in the environment, representing potential aggregation “partners” with diverse properties (Lagarde et al., 2016; Leiser et al., 2021a, 2020; Y. Li et al., 2019; Long et al., 2015; Michels et al., 2018). Therefore, it is likely that also MP particles with properties other than the strongly negatively charged MP particles studied here, will interact with certain environmental particles.

5.2 Environmental implications of interactions on MP wettability

Within this thesis we could not only show that the sedimentation of MP particles is enhanced by heteroaggregation with ferrihydrite. We further investigated how interactions of MP particles with ferrihydrite affect surface properties and wettability of MP incorporated in porous media. We showed that environmental relevant substances, such as ferrihydrite, can render the wettability of MP in porous media: the initial hydrophobicity of pristine MP particles was

reduced by ferrihydrite coating. The change in wettability depends on a successful coating of the hydrophobic MP surface by ferrihydrite.

The results of Study 3 are of high environmental relevance, because pristine MP was previously found to increase soil water repellency and limit capillary flow which can lead to a reduced local water content (Cramer et al., 2022). Here, we could show that the wettability of MP hotspots increased by coating with ferrihydrite, however depending on polymer type. For PET particles, the ferrihydrite coating allowed the water to enter the MP hotspot during capillary rise and render it completely wettable. This implies that contrary to the pristine PET hotspot, water was allowed to the enter the hotspot of coated PET. Transferred to the environment, this finding indicates that also microorganisms and their enzymes, which migrate with water flow, will get into contact with MP, which in turn can facilitate biotic degradation of MP particles.

Connecting the results of Study 2 and 3, we can assume that UV-weathering of MP will increase the wettability of MP particles. Photooxidation due to UV-weathering forms carboxy, peroxyl and keto groups on the MP surface (Meides et al., 2021). The increased number of (hydrophilic) functional groups on the surface itself will already increase the wettability of MP but it will furthermore increase the reactivity of MP. This, in turn, allows coating of the surface with environmental colloids, such as ferrihydrite, that will further enhance the wettability. Weathering of MP could also decrease the differences in wettability and coating among different types of polymers as it generally increases the hydrophilicity of all polymer types.

5.3 Limitations and Outlook

As in any study, our laboratory experiments face several limitations and cannot fully mimic the complexity of the real environment. The choice of spherical PS particles (Study 1, 2, 4) does not represent the variety of shapes of MP particles in the environment (e.g. angular, fibers etc.). However, our goal was to gain a first understanding of interactions of MP particles with environmentally relevant substances and therefore well-defined model particles are of advantage, especially for measuring colloidal properties such as zeta potential. The spherical PS particles used in Study 1, 2 and 4 face further limitations: firstly, we only analyzed PS particles and no other polymer types in these studies. However, the availability of polymers (other than PS) in the colloidal size range was very limited and we therefore could not investigate either the aggregation and sedimentation behavior nor the applicability of the TOC method for other polymer types. Secondly, the surface charge of PS particles in Study 1 and 2 was strongly negative due to the manufacturing process. However, the milled, irregularly shaped PS and PET particles used in Study 3 showed similar interactions with ferrihydrite even

though their surface charge was significantly lower (zeta potential of approx. -40 mV at neutral pH).

In future studies, the focus should be on secondary MP particles with diverse properties (shape, size, surface charge, polymer type, weathering). The accumulated knowledge of the past years regarding research on interactions of spherical, colloidal MP with environmental particles however can serve as a basis to be expanded upon with more complex systems. This also applies for the sample matrix. For our experiments, we chose a rather simple sample matrix (ionic strength of 10 mM). In aquatic environments, the variety of other dissolved substances and other particles is by far larger and should be considered in future work. The presence of other particles in the environmental systems might offer even more potential interaction partners for MP heteroaggregation.

Another aspect of high interest is the reversibility of aggregation and sedimentation. In this thesis it was shown that heteroaggregation promotes in sedimentation of MP. Thus, sediments might act as a sink for MP particles. But the question remains, if such aggregates might be re-mobilized under specific environmental conditions, e.g. anoxic conditions which will result in the reduction of Fe(III) and the dissolution of the iron minerals. Leiser et al. (2021b) did not observe re-mobilization of MP in iron-organo flocs during anoxic conditions due to entrapment of MP in the sediment. However, it remains unclear how aggregates consisting of MP and iron minerals behave after iron reduction and dissolution. Especially for aggregates that have not penetrated deeper into the sediments (as it was observed from Leiser et al. (2021b)), we assume that re-mobilization of MP particles takes place after iron reduction. Furthermore, if MP-heteroaggregates disintegrate after reduction of iron, it is still unknown whether those MP particles remain in or on the sediments or get re-mobilize to the water column.

One aspect that has – to the best of my knowledge - not yet received much attention, is to investigate the role of aggregation and subsequent sedimentation of MP in rivers or water with strong currents or turbulences. Rivers are considered as the main transport pathway of MP particles from land to sea (Meijer et al., 2021). Hence, understanding the mechanisms of MP retention in rivers is crucial to gain insights into the load of MP that is transported into the sea and the amount of MP being stored in the riverbeds or estuaries. Previous research found that a considerable amount of MP is stored in the riverbeds (van Emmerik et al., 2022). However, it is unknown whether aggregation-facilitated sedimentation of MP is a main driver for this or if these processes do not play such a big role in rivers due to higher turbulence and flow compared to stagnant water bodies.

Furthermore, our results on UV-weathering of PS beads have revealed some interesting aspects that should be further investigated but do not fall within the main research focus of this

thesis. (i) Generally, accelerated UV-weathering was done for 1 µm MP particles designed for research. For the future, it is necessary to investigate if differences between the weathering processes of such particles in comparison to more environmentally relevant secondary MP particles exist. The observation of PS particles becoming hollow during UV-weathering might indicate different weathering processes of MP beads compared to larger material, e.g. MP that was milled from lager debris (Meides et al., 2021). This could be caused by different manufacturing processes of PS (emulsion polymerization vs. seeded growth). (ii) For the analyzed 1 µm PS, 90% of the carbon mass was transferred into gas after only 12 days of accelerated weathering. This seems rather fast. Future research should investigate the effect of particle size on total mineralization as well as the impact of the irradiation intensity of the weathering chamber. The continuous accelerated irradiation in the weathering chamber compared to the discontinuous irradiation in the environmental (day-night cycle) might have led to additional acceleration of the weathering process (beyond the factor calculated solely based on radiation intensity) and thus to the fast conversion of PS to gaseous compounds.

For capillary rise experiments (Study 3), an *in-situ* coating of MP hotspots with ferrihydrite was not achieved during two wetting-drying cycles. Therefore, in upcoming experiments, the number of wetting-drying cycles of capillary rise experiments with ferrihydrite containing soil solution should be enhanced. These cycles were supposed to mimic fluctuating moisture conditions in the vadose zone, a process that is expected to happen numerous times in the environment. The initial hydrophobicity of MP prevented the ferrihydrite containing soil solution to enter the MP hotspot and thus to get into contact with the MP particles. An increased number of wetting and drying might allow the ferrihydrite suspension to propagate further into the MP hotspots in each wetting cycle and eventually render the particles wettable. Another interesting aspect for capillary rise experiments would be the analysis of UV-weathered particles. As UV-weathering increases the hydrophilicity of MP, the water repellency of MP during capillary rise should be reduced compared to pristine particles.

Lastly, even though our experiments were designed to gain a better understanding of MP behavior in the environment, our results of rapid sedimentation after aggregation with iron oxyhydroxides might be valuable for industrial applications, e.g. wastewater treatment plants (WWTP). The removal of MP in WWTP is of great relevance as they play an important role in releasing MP to the environment (Browne et al., 2011). A common step in the treatment of wastewater is the elimination of phosphate. This is often achieved by the precipitation of iron or aluminum salts. As our results show that MP forms heteroaggregates with iron oxyhydroxides, the precipitation step might already be an efficient way of MP removal from wastewater in WWTP. Therefore, it should be investigated to what extent WWTPs already remove MP particles from the wastewater by precipitation of iron or aluminum salts, whether

there are differences between different particle sizes, polymer types, particle shapes etc. and how the removal rate can generally be increased.

In conclusion, the research findings of this thesis have demonstrated that interactions of MP with environmental colloids significantly impact the properties of MP. Through adsorption and surface coating, both the charge and wettability can be altered, which in turn affects further interactions of MP in water, or conversely, increases its wettability in porous media. Furthermore, heteroaggregation between the particles facilitates strong sedimentation of MP and therefore influences its fate and transport in the environment.

References

Aiken, G., A. Kaplan, L., Weishaar, J., 2002. Assessment of relative accuracy in the determination of organic matter concentrations in aquatic systems. Journal of Environmental Monitoring 4, 70–74. https://doi.org/10.1039/B107322M

Ali, S.S., Elsamahy, T., Al-Tohamy, R., Zhu, D., Mahmoud, Y.A.-G., Koutra, E., Metwally, M.A., Kornaros, M., Sun, J., 2021. Plastic wastes biodegradation: Mechanisms, challenges and future prospects. Science of The Total Environment 780, 146590. https://doi.org/10.1016/j.scitotenv.2021.146590

Alimi, O.S., Farner Budarz, J., Hernandez, L.M., Tufenkji, N., 2018. Microplastics and nanoplastics in aquatic environments: aggregation, deposition, and enhanced contaminant transport. Environ. Sci. Technol. 52, 1704–1724. https://doi.org/10.1021/acs.est.7b05559

Austin, H.M., Stoops-Glas, P.M., 1977. The distribution of polystyrene spheres and nibs in Block Island Sound during 1972–1973. Chesapeake Science 18, 89–92. https://doi.org/10.2307/1350372

Bachmann, J., Horton, R., van der Ploeg, R.R., Woche, S., 2000. Modified sessile drop method for assessing initial soil–water contact angle of sandy soil. Soil Science Society of America Journal 64, 564–567. https://doi.org/10.2136/sssaj2000.642564x

Bachmann, J., Woche, S.K., Goebel, M.-O., Kirkham, M.B., Horton, R., 2003. Extended methodology for determining wetting properties of porous media. Water Resources Research 39. https://doi.org/10.1029/2003WR002143

Bao, T., Wang, P., Hu, B., Wang, X., Qian, J., 2023. Mobilization of colloids during sediment resuspension and its effect on the release of heavy metals and dissolved organic matter. Science of The Total Environment 861, 160678. https://doi.org/10.1016/j.scitotenv.2022.160678

Bergmann, M., Gutow, L., Klages, M. (Eds.), 2015. Marine Anthropogenic Litter. Springer International Publishing, Cham. https://doi.org/10.1007/978-3-319-16510-3

Blaurock, K., Beudert, B., Gilfedder, B.S., Fleckenstein, J.H., Peiffer, S., Hopp, L., 2021. Low hydrological connectivity after summer drought inhibits DOC export in a forested headwater catchment. Hydrol. Earth Syst. Sci. 25, 5133–5151. https://doi.org/10.5194/hess-25-5133-2021

Blaurock, K., Garthen, P., da Silva, M.P., Beudert, B., Gilfedder, B.S., Fleckenstein, J.H., Peiffer, S., Lechtenfeld, O.J., Hopp, L., 2022. Riparian Microtopography Affects Event-Driven Stream DOC Concentrations and DOM Quality in a Forested Headwater Catchment. Journal of Geophysical Research: Biogeosciences 127, e2022JG006831. https://doi.org/10.1029/2022JG006831

Browne, M.A., Crump, P., Niven, S.J., Teuten, E., Tonkin, A., Galloway, T., Thompson, R., 2011. Accumulation of microplastic on shorelines woldwide: sources and sinks. Environmental science & technology 45, 9175–9179.

Cai, L., Hu, L., Shi, H., Ye, J., Zhang, Y., Kim, H., 2018. Effects of inorganic ions and natural organic matter on the aggregation of nanoplastics. Chemosphere 197, 142–151. https://doi.org/10.1016/j.chemosphere.2018.01.052

Cai, L., Wang, J., Peng, J., Tan, Z., Zhan, Z., Tan, X., Chen, Q., 2017. Characteristic of microplastics in the atmospheric fallout from Dongguan city, China: preliminary research and first evidence. Environ Sci Pollut Res 24, 24928–24935. https://doi.org/10.1007/s11356-017-0116-x

Carpenter, E.J., Smith, K.L., 1972. Plastics on the Sargasso Sea Surface. Science 175, 1240–1241. https://doi.org/10.1126/science.175.4027.1240

Cha, B.J., Kim, S.Y., Choi, C.M., Sung, J.Y., Choi, M.C., Seo, H.O., Kim, Y.D., 2021. Ultra-low loading of iron oxide on Pt/Al2O3 for enhanced catalytic activity of CO oxidation at room temperature:

A simple method for applications. Chemical Engineering Journal 404, 126560. https://doi.org/10.1016/j.cej.2020.126560

Colton, J.B., Burns, B.R., Knapp, F.D., 1974. Plastic Particles in Surface Waters of the Northwestern Atlantic. Science 185, 491–497. https://doi.org/10.1126/science.185.4150.491

Cornell, R.M., Schwertmann, U., 2003. The Iron Oxides: Structure, Properties, Reactions, Occurrences and Uses. John Wiley & Sons.

Cózar, A., Echevarría, F., González-Gordillo, J.I., Irigoien, X., Úbeda, B., Hernández-León, S., Palma, Á.T., Navarro, S., García-de-Lomas, J., Ruiz, A., Fernández-de-Puelles, M.L., Duarte, C.M., 2014. Plastic debris in the open ocean. Proceedings of the National Academy of Sciences 111, 10239–10244. https://doi.org/10.1073/pnas.1314705111

Cramer, A., Benard, P., Zarebanadkouki, M., Kaestner, A., Carminati, A., 2022. Microplastic induces soil water repellency and limits capillary flow. Vadose Zone Journal 22, e20215. https://doi.org/10.1002/vzj2.20215

Curtinrich, H.J., Sebestyen, S.D., Griffiths, N.A., Hall, S.J., 2022. Warming Stimulates Iron-Mediated Carbon and Nutrient Cycling in Mineral-Poor Peatlands. Ecosystems 25, 44–60. https://doi.org/10.1007/s10021-021-00639-3

Dimante-Deimantovica, I., Saarni, S., Barone, M., Buhhalko, N., Stivrins, N., Suhareva, N., Tylmann, W., Vianello, A., Vollertsen, J., 2024. Downward migrating microplastics in lake sediments are a tricky indicator for the onset of the Anthropocene. Science Advances 10, eadi8136. https://doi.org/10.1126/sciadv.adi8136

Dris, R., Gasperi, J., Saad, M., Mirande, C., Tassin, B., 2016. Synthetic fibers in atmospheric fallout: A source of microplastics in the environment? Marine Pollution Bulletin 104, 290–293. https://doi.org/10.1016/j.marpolbul.2016.01.006

Droppo, I.G., Leppard, G.G., Flannigan, D.T., Liss, S.N., 1997. The Freshwater Floc: A Functional Relationship of Water and Organic and Inorganic Floc Constituents Affecting Suspended Sediment Properties. Water, Air, & Soil Pollution 99, 43–54. https://doi.org/10.1023/A:1018359726978

Duan, J., Bolan, N., Li, Y., Ding, S., Atugoda, T., Vithanage, M., Sarkar, B., Tsang, D.C.W., Kirkham, M.B., 2021. Weathering of microplastics and interaction with other coexisting constituents in terrestrial and aquatic environments. Water Res 196, 117011. https://doi.org/10.1016/j.watres.2021.117011

Eerkes-Medrano, D., Thompson, R.C., Aldridge, D.C., 2015. Microplastics in freshwater systems: A review of the emerging threats, identification of knowledge gaps and prioritisation of research needs. Water Research 75, 63–82. https://doi.org/10.1016/j.watres.2015.02.012

European Chemicals Agency, 2019. Annex XV restriction report proposal for a restriction: intentionally added microplastics. Version 1.2. Proposal 1.2. ECA.

Filella, M., 2006. Colloidal Properties of Submicron Particles in Natural Waters, in: Environmental Colloids and Particles. John Wiley & Sons, Ltd, pp. 17–93. https://doi.org/10.1002/9780470024539.ch2

Foley, C.J., Feiner, Z.S., Malinich, T.D., Höök, T.O., 2018. A meta-analysis of the effects of exposure to microplastics on fish and aquatic invertebrates. Science of The Total Environment 631–632, 550–559. https://doi.org/10.1016/j.scitotenv.2018.03.046

GESAMP, 2015. Sources, fate and effects of microplastics in the marine environment: a global assessment, (Kershaw, P.J., ed.). Rep. Stud. No 90. Joint Group of Experts on the Scientific Aspects of Marine Environmental Protection (GESAMP) http://www.gesamp.org/publications/reports-and-studies-no-90

Gewert, B., Plassmann, M.M., MacLeod, M., 2015. Pathways for degradation of plastic polymers floating in the marine environment. Environ. Sci.: Processes Impacts 17, 1513–1521. https://doi.org/10.1039/C5EM00207A

Geyer, R., 2020. A Brief History of Plastics, in: Streit-Bianchi, M., Cimadevila, M., Trettnak, W. (Eds.), Mare Plasticum - The Plastic Sea: Combatting Plastic Pollution Through Science and Art. Springer International Publishing, Cham, pp. 31–47. https://doi.org/10.1007/978-3-030-38945-1_2

Goodwin, J., 2009. Colloids and interfaces with surfactants and polymers, 2nd Edition. ed. John Wiley & Sons Ltd, West Sussex.

Gregory, M.R., 1977. Plastic pellets on New Zealand beaches. Marine Pollution Bulletin 8, 82–84. https://doi.org/10.1016/0025-326X(77)90193-X

Gu, B., Mehlhorn, T.L., Liang, L., McCarthy, J.F., 1996. Competitive adsorption, displacement, and transport of organic matter on iron oxide: I. Competitive adsorption. Geochimica et Cosmochimica Acta 60, 1943–1950. https://doi.org/10.1016/0016-7037(96)00059-2

Guo, H., Barnard, A., 2013. Naturally occurring iron oxide nanoparticles : morphology, surface chemistry and environmental stability. J. Mater. Chem. A 1, 27–42. https://doi.org/10.1039/C2TA00523A

He, S., Jia, M., Xiang, Y., Song, B., Xiong, W., Cao, J., Peng, H., Yang, Y., Wang, W., Yang, Z., Zeng, G., 2022. Biofilm on microplastics in aqueous environment: Physicochemical properties and environmental implications. Journal of Hazardous Materials 424, 127286. https://doi.org/10.1016/j.jhazmat.2021.127286

Hong, Y., Oh, J., Lee, I., Fan, C., Pan, S.-Y., Jang, M., Park, Y.-K., Kim, H., 2021. Total-organic-carbon-based quantitative estimation of microplastics in sewage. Chemical Engineering Journal 423, 130182. https://doi.org/10.1016/j.cej.2021.130182

Horton, A.A., Walton, A., Spurgeon, D.J., Lahive, E., Svendsen, C., 2017. Microplastics in freshwater and terrestrial environments: Evaluating the current understanding to identify the knowledge gaps and future research priorities. Science of The Total Environment 586, 127–141. https://doi.org/10.1016/j.scitotenv.2017.01.190

Jambor, J.L., Dutrizac, J.E., 1998. Occurrence and Constitution of Natural and Synthetic Ferrihydrite, a Widespread Iron Oxyhydroxide. Chem. Rev. 98, 2549–2586. https://doi.org/10.1021/cr970105t

Joshi, P., Kappler, A., 2020. Iron Oxides, Hydroxides, and Oxyhydroxides, in: Gargaud, M., Irvine, W.M., Amils, R., Claeys, P., Cleaves, H.J., Gerin, M., Rouan, D., Spohn, T., Tirard, S., Viso, M. (Eds.), Encyclopedia of Astrobiology. Springer, Berlin, Heidelberg, pp. 1–4. https://doi.org/10.1007/978-3-642-27833-4_5525-1

Kappler, A., Bryce, C., Mansor, M., Lueder, U., Byrne, J.M., Swanner, E.D., 2021. An evolving view on biogeochemical cycling of iron. Nat Rev Microbiol 19, 360–374. https://doi.org/10.1038/s41579-020-00502-7

Kelly, A., Lannuzel, D., Rodemann, T., Meiners, K.M., Auman, H.J., 2020. Microplastic contamination in east Antarctic sea ice. Marine Pollution Bulletin 154, 111130. https://doi.org/10.1016/j.marpolbul.2020.111130

Knorr, K.-H., 2013. DOC-dynamics in a small headwater catchment as driven by redox fluctuations and hydrological flow paths – are DOC exports mediated by iron reduction/oxidation cycles? Biogeosciences 10, 891–904. https://doi.org/10.5194/bg-10-891-2013

Koelmans, A.A., Redondo-Hasselerharm, P.E., Nor, N.H.M., de Ruijter, V.N., Mintenig, S.M., Kooi, M., 2022. Risk assessment of microplastic particles. Nat Rev Mater 7, 138–152. https://doi.org/10.1038/s41578-021-00411-y

Lagarde, F., Olivier, O., Zanella, M., Daniel, P., Hiard, S., Caruso, A., 2016. Microplastic interactions with freshwater microalgae: Hetero-aggregation and changes in plastic density appear strongly dependent on polymer type. Environmental Pollution 215, 331–339. https://doi.org/10.1016/j.envpol.2016.05.006

Lalonde, K., Mucci, A., Ouellet, A., Gélinas, Y., 2012. Preservation of organic matter in sediments promoted by iron. Nature 483, 198–200. https://doi.org/10.1038/nature10855

Lead, J.R., Davison, W., Hamilton-Taylor, J., Buffle, J., 1997. Characterizing Colloidal Material in Natural Waters. Aquatic Geochemistry 3, 213–232. https://doi.org/10.1023/A:1009695928585

Lead, J.R., Wilkinson, K.J., 2006. Environmental Colloids and Particles: Current Knowledge and Future Developments, in: Environmental Colloids and Particles. John Wiley & Sons, Ltd, pp. 1–15. https://doi.org/10.1002/9780470024539.ch1

Leiser, R., Jongsma, R., Bakenhus, I., Möckel, R., Philipp, B., Neu, T.R., Wendt-Potthoff, K., 2021a. Interaction of cyanobacteria with calcium facilitates the sedimentation of microplastics in a eutrophic reservoir. Water Res 189, 116582. https://doi.org/10.1016/j.watres.2020.116582

Leiser, R., Schumann, M., Dadi, T., Wendt-Potthoff, K., 2021b. Burial of microplastics in freshwater sediments facilitated by iron-organo flocs. Sci Rep 11, 24072. https://doi.org/10.1038/s41598-021-02748-4

Leiser, R., Wu, G.-M., Neu, T.R., Wendt-Potthoff, K., 2020. Biofouling, metal sorption and aggregation are related to sinking of microplastics in a stratified reservoir. Water Research 115748. https://doi.org/10.1016/j.watres.2020.115748

Li, M., He, L., Zhang, M., Liu, X., Tong, M., Kim, H., 2019. Cotransport and Deposition of Iron Oxides with Different-Sized Plastic Particles in Saturated Quartz Sand. Environ. Sci. Technol. 53, 3547–3557. https://doi.org/10.1021/acs.est.8b06904

Li, S., Liu, H., Gao, R., Abdurahman, A., Dai, J., Zeng, F., 2018. Aggregation kinetics of microplastics in aquatic environment: Complex roles of electrolytes, pH, and natural organic matter. Environmental Pollution 237, 126–132. https://doi.org/10.1016/j.envpol.2018.02.042

Li, Y., Wang, X., Fu, W., Xia, X., Liu, C., Min, J., Zhang, W., Crittenden, J.C., 2019. Interactions between nano/micro plastics and suspended sediment in water: Implications on aggregation and settling. Water research 161, 486–495. https://doi.org/10.1016/j.watres.2019.06.018

Liu, Juanjuan, Louie, S.M., Pham, C., Dai, C., Liang, D., Hu, Y., 2019. Aggregation of ferrihydrite nanoparticles: Effects of pH, electrolytes,and organics. Environmental Research 172, 552–560. https://doi.org/10.1016/j.envres.2019.03.008

Liu, Jin, Zhang, T., Tian, L., Liu, X., Qi, Z., Ma, Y., Ji, R., Chen, W., 2019. Aging Significantly Affects Mobility and Contaminant-Mobilizing Ability of Nanoplastics in Saturated Loamy Sand. Environ. Sci. Technol. 53, 5805–5815. https://doi.org/10.1021/acs.est.9b00787

Liu, L., Song, J., Zhang, M., Jiang, W., 2021. Aggregation and Deposition Kinetics of Polystyrene Microplastics and Nanoplastics in Aquatic Environment. Bull Environ Contam Toxicol. https://doi.org/10.1007/s00128-021-03239-y

Liu, Y., Hu, Y., Yang, C., Chen, C., Huang, W., Dang, Z., 2019. Aggregation kinetics of UV irradiated nanoplastics in aquatic environments. Water Research 163, 114870. https://doi.org/10.1016/j.watres.2019.114870

Lo, B., Waite, T.D., 2000. Structure of Hydrous Ferric Oxide Aggregates. Journal of Colloid and Interface Science 222, 83–89. https://doi.org/10.1006/jcis.1999.6599

Long, M., Moriceau, B., Gallinari, M., Lambert, C., Huvet, A., Raffray, J., Soudant, P., 2015. Interactions between microplastics and phytoplankton aggregates: Impact on their respective fates. Marine

Chemistry, Particles in aquatic environments: from invisible exopolymers to sinking aggregates 175, 39–46. https://doi.org/10.1016/j.marchem.2015.04.003

Lu, T., Gilfedder, B.S., Peng, H., Peiffer, S., Papastavrou, G., Ottermann, K., Frei, S., 2021. Relevance of Iron Oxyhydroxide and Pore Water Chemistry on the Mobility of Nanoplastic Particles in Water-Saturated Porous Media Environments. Water Air Soil Pollut 232, 168. https://doi.org/10.1007/s11270-021-05125-z

Meides, N., Menzel, T., Poetzschner, B., Löder, M.G.J., Mansfeld, U., Strohriegl, P., Altstaedt, V., Senker, J., 2021. Reconstructing the Environmental Degradation of Polystyrene by Accelerated Weathering. Environ. Sci. Technol. 55, 7930–7938. https://doi.org/10.1021/acs.est.0c07718

Meijer, L.J.J., van Emmerik, T., van der Ent, R., Schmidt, C., Lebreton, L., 2021. More than 1000 rivers account for 80% of global riverine plastic emissions into the ocean. Science Advances 7, eaaz5803. https://doi.org/10.1126/sciadv.aaz5803

Michels, J., Stippkugel, A., Lenz, M., Wirtz, K., Engel, A., 2018. Rapid aggregation of biofilm-covered microplastics with marine biogenic particles. Proceedings of the Royal Society B 285, 20181203. https://doi.org/10.1098/rspb.2018.1203

Näkki, P., Setälä, O., Lehtiniemi, M., 2019. Seafloor sediments as microplastic sinks in the northern Baltic Sea – Negligible upward transport of buried microplastics by bioturbation. Environmental Pollution 249, 74–81. https://doi.org/10.1016/j.envpol.2019.02.099

Nierop, K.G.J.J., Jansen, B., Verstraten, J.M., 2002. Dissolved organic matter, aluminium and iron interactions: precipitation induced by metal/carbon ratio, pH and competition. Science of The Total Environment 300, 201–211. https://doi.org/10.1016/S0048-9697(02)00254-1

Oncsik, T., Trefalt, G., Csendes, Z., Szilagyi, I., Borkovec, M., 2014. Aggregation of Negatively Charged Colloidal Particles in the Presence of Multivalent Cations. Langmuir 30, 733–741. https://doi.org/10.1021/la4046644

Oriekhova, O., Stoll, S., 2018. Heteroaggregation of nanoplastic particles in the presence of inorganic colloids and natural organic matter. Environ. Sci.: Nano 5, 792–799. https://doi.org/10.1039/C7EN01119A

Peiffer, S., Walton-Day, K., Macalady, D.L., 1999. The Interaction of Natural Organic Matter with Iron in a Wetland (Tennessee Park, Colorado) Receiving Acid Mine Drainage. Aquatic Geochemistry 5, 207–223. https://doi.org/10.1023/A:1009617925959

Pfohl, P., Wagner, M., Meyer, L., Domercq, P., Praetorius, A., Hüffer, T., Hofmann, T., Wohlleben, W., 2022. Environmental Degradation of Microplastics: How to Measure Fragmentation Rates to Secondary Micro- and Nanoplastic Fragments and Dissociation into Dissolved Organics. Environ. Sci. Technol. 56, 11323–11334. https://doi.org/10.1021/acs.est.2c01228

PlasticsEurope, 2022. Plastics - the Facts 2022. Plastics the Facts 2022. https://plasticseurope.org/knowledge-hub/plastics-the-facts-2022/

Pradel, A., Ferreres, S., Veclin, C., El Hadri, H., Gautier, M., Grassl, B., Gigault, J., 2021. Stabilization of Fragmental Polystyrene Nanoplastic by Natural Organic Matter: Insight into Mechanisms. ACS EST Water 1, 1198–1208. https://doi.org/10.1021/acsestwater.0c00283

Praetorius, A., Labille, J., Scheringer, M., Thill, A., Hungerbühler, K., Bottero, J.-Y., 2014. Heteroaggregation of Titanium Dioxide Nanoparticles with Model Natural Colloids under Environmentally Relevant Conditions. Environ. Sci. Technol. 48, 10690–10698. https://doi.org/10.1021/es501655v

Prata, J.C., da Costa, J.P., Duarte, A.C., Rocha-Santos, T., 2019. Methods for sampling and detection of microplastics in water and sediment: A critical review. TrAC Trends in Analytical Chemistry 110, 150–159. https://doi.org/10.1016/j.trac.2018.10.029

Ramsperger, A.F.R.M., Jasinski, J., Völkl, M., Witzmann, T., Meinhart, M., Jérôme, V., Kretschmer, W.P., Freitag, R., Senker, J., Fery, A., Kress, H., Scheibel, T., Laforsch, C., 2022. Supposedly identical microplastic particles substantially differ in their material properties influencing particle-cell interactions and cellular responses. Journal of Hazardous Materials 425, 127961. https://doi.org/10.1016/j.jhazmat.2021.127961

Ren, Z., Gui, X., Xu, X., Zhao, L., Qiu, H., Cao, X., 2021. Microplastics in the soil-groundwater environment: Aging, migration, and co-transport of contaminants – A critical review. Journal of Hazardous Materials 419, 126455. https://doi.org/10.1016/j.jhazmat.2021.126455

Rummel, C.D., Jahnke, A., Gorokhova, E., Kühnel, D., Schmitt-Jansen, M., 2017. Impacts of Biofilm Formation on the Fate and Potential Effects of Microplastic in the Aquatic Environment. Environ. Sci. Technol. Lett. 4, 258–267. https://doi.org/10.1021/acs.estlett.7b00164

SAPEA, 2019. A Scientific Perspective on Microplastics in Nature and Society. SAPEA, Science Advice for Policy by European Academies, Berlin. https://doi.org/10.26356/microplastics

Schefer, R.B., Armanious, A., Mitrano, D.M., 2023. Eco-Corona Formation on Plastics: Adsorption of Dissolved Organic Matter to Pristine and Photochemically Weathered Polymer Surfaces. Environ. Sci. Technol. 57, 14707–14716. https://doi.org/10.1021/acs.est.3c04180

Scheurer, M., Bigalke, M., 2018. Microplastics in Swiss Floodplain Soils. Environ. Sci. Technol. 52, 3591–3598. https://doi.org/10.1021/acs.est.7b06003

Schwertmann, U., Cornell, R.M., 2000. Iron oxides in the laboratory: preparation and characterization. John Wiley & Sons Ltd, Weinheim.

Shah, A.A., Hasan, F., Hameed, A., Ahmed, S., 2008. Biological degradation of plastics: A comprehensive review. Biotechnology Advances 26, 246–265. https://doi.org/10.1016/j.biotechadv.2007.12.005

Sharma, V.K., Ma, X., Guo, B., Zhang, K., 2021. Environmental factors-mediated behavior of microplastics and nanoplastics in water: A review. Chemosphere 271, 129597. https://doi.org/10.1016/j.chemosphere.2021.129597

Sharp, E.L., Jarvis, P., Parsons, S.A., Jefferson, B., 2006. The Impact of Zeta Potential on the Physical Properties of Ferric−NOM Flocs. Environ. Sci. Technol. 40, 3934–3940. https://doi.org/10.1021/es051919r

Singh, B., Sharma, N., 2008. Mechanistic implications of plastic degradation. Polymer Degradation and Stability 93, 561–584. https://doi.org/10.1016/j.polymdegradstab.2007.11.008

Spielman-Sun, E., Boye, K., Dwivedi, D., Engel, M., Thompson, A., Kumar, N., Noël, V., 2024. A Critical Look at Colloid Generation, Stability, and Transport in Redox-Dynamic Environments: Challenges and Perspectives. ACS Earth Space Chem. https://doi.org/10.1021/acsearthspacechem.3c00255

Stumm, W., Morgan, J.J., 2012. Aquatic chemistry: chemical equilibria and rates in natural waters. John Wiley & Sons.

Sun, H., Jiao, R., Wang, D., 2020. The difference of aggregation mechanism between microplastics and nanoplastics: Role of Brownian motion and structural layer force. Environmental Pollution 115942. https://doi.org/10.1016/j.envpol.2020.115942

Tadros, T.F., 2015. Interfacial phenomena and colloid stability: basic principles. Walter de Gruyter GmbH & Co KG, Berkshire.

Turner, S., Horton, A.A., Rose, N.L., Hall, C., 2019. A temporal sediment record of microplastics in an urban lake, London, UK. J Paleolimnol 61, 449–462. https://doi.org/10.1007/s10933-019-00071-7

UN Environment, 2017. Frontiers 2016: Emerging issues of environmental concern [WWW Document]. UNEP - UN Environment Programme. URL http://www.unep.org/resources/frontiers-2016-emerging-issues-environmental-concern (accessed 10.4.23).

van Emmerik, T., Mellink, Y., Hauk, R., Waldschläger, K., Schreyers, L., 2022. Rivers as Plastic Reservoirs. Front. Water 3. https://doi.org/10.3389/frwa.2021.786936

Velzeboer, I., Quik, J.T.K., Meent, D. van de, Koelmans, A.A., 2014. Rapid settling of nanoparticles due to heteroaggregation with suspended sediment. Environmental Toxicology and Chemistry 33, 1766–1773. https://doi.org/10.1002/etc.2611

Volk, C., Wood, L., Johnson, B., Robinson, J., Zhu, H.W., Kaplan, L., 2002. Monitoring dissolved organic carbon in surface and drinking waters. J. Environ. Monit. 4, 43–47. https://doi.org/10.1039/B107768F

Vu, T.T.T., Nguyen, P.H., Pham, T.V., Do, P.Q., Dao, T.T., Nguyen, A.D., Nguyen-Thanh, L., Dinh, V.M., Nguyen, M.N., 2022. Comparative effects of crystalline, poorly crystalline and freshly formed iron oxides on the colloidal properties of polystyrene microplastics. Environmental Pollution 306, 119474. https://doi.org/10.1016/j.envpol.2022.119474

Wagner, M., Lambert, S. (Eds.), 2018. Freshwater Microplastics: Emerging Environmental Contaminants?, The Handbook of Environmental Chemistry. Springer International Publishing, Cham. https://doi.org/10.1007/978-3-319-61615-5

Wang, X., Bolan, N., Tsang, D.C.W., Binoy, S., Bradney, L., Li, Y., 2021. A review of microplastics aggregation in aquatic environment: Influence factors, analytical methods, and environmental implications. Journal of Hazardous Materials 123496. https://doi.org/10.1016/j.jhazmat.2020.123496

Wang, Y., Chen, X., Wang, F., Cheng, N., 2023. Influence of typical clay minerals on aggregation and settling of pristine and aged polyethylene microplastics. Environmental Pollution 316, 120649. https://doi.org/10.1016/j.envpol.2022.120649

Ward, C.P., Armstrong, C.J., Walsh, A.N., Jackson, J.H., Reddy, C.M., 2019. Sunlight Converts Polystyrene to Carbon Dioxide and Dissolved Organic Carbon. Environ. Sci. Technol. Lett. 6, 669–674. https://doi.org/10.1021/acs.estlett.9b00532

Wieland, S., Ramsperger, A.F.R.M., Gross, W., Lehmann, M., Witzmann, T., Caspari, A., Obst, M., Gekle, S., Auernhammer, G.K., Fery, A., Laforsch, C., Kress, H., 2024. Nominally identical microplastic models differ greatly in their particle-cell interactions. Nat Commun 15, 922. https://doi.org/10.1038/s41467-024-45281-4

Yan, X., Yang, X., Tang, Z., Fu, J., Chen, F., Zhao, Y., Ruan, L., Yang, Y., 2020. Downward transport of naturally-aged light microplastics in natural loamy sand and the implication to the dissemination of antibiotic resistance genes. Environmental Pollution 262, 114270. https://doi.org/10.1016/j.envpol.2020.114270

Zhang, K., Hamidian, A.H., Tubić, A., Zhang, Y., Fang, J.K.H., Wu, C., Lam, P.K.S., 2021. Understanding plastic degradation and microplastic formation in the environment: A review. Environmental Pollution 274, 116554. https://doi.org/10.1016/j.envpol.2021.116554

Zhang, Y., Luo, Y., Guo, X., Xia, T., Wang, T., Jia, H., Zhu, L., 2020. Charge mediated interaction of polystyrene nanoplastic (PSNP) with minerals in aqueous phase. Water Research 178, 115861. https://doi.org/10.1016/j.watres.2020.115861

Zhang, Y., Luo, Y., Yu, X., Huang, D., Guo, X., Zhu, L., 2022. Aging significantly increases the interaction between polystyrene nanoplastic and minerals. Water Research 219, 118544. https://doi.org/10.1016/j.watres.2022.118544

Zubris, K.A.V., Richards, B.K., 2005. Synthetic fibers as an indicator of land application of sludge. Environmental Pollution 138, 201–211. https://doi.org/10.1016/j.envpol.2005.04.013

Publications and Manuscripts

Study 1: Heteroaggregation of PS microplastic with ferrihydrite leads to rapid removal of microplastic particles from the water column

Status: Published in *Environmental Science: Processes & Impacts*

Vol. 24 (10), 2022

https://doi.org/10.1039/D2EM00207H

Authors: Johanna Schmidtmann, Hassan Elagami, Benjamin S. Gilfedder, Jan H. Fleckenstein, Georg Papastavrou, Ulrich Mansfeld, Stefan Peiffer

Own Contribution in %:

Study design	80
Laboratory analysis	95
Data processing and analyses	95
Interpretation of the results	90
Preparation of the manuscript	90

JS and SP designed the study. JS planned and conducted the Laboratory experiments. UM conducted SEM and EDX analysis. JS prepared figures. JS and SP discussed and interpreted the results. JS prepared the manuscript with input from all co-authors.

JS is the corresponding author.

Graphical Abstract:

Environmental Science Processes & Impacts

ROYAL SOCIETY OF CHEMISTRY

PAPER

View Article Online
View Journal

Check for updates

Cite this: DOI: 10.1039/d2em00207h

Heteroaggregation of PS microplastic with ferrihydrite leads to rapid removal of microplastic particles from the water column†

Johanna Schmidtmann, *[a] Hassan Elagami,[ab] Bejamin S. Gilfedder,[ab] Jan H. Fleckenstein,[cd] Georg Papastavrou,[e] Ulrich Mansfeld[f] and Stefan Peiffer[a]

Received 10th May 2022
Accepted 11th July 2022

DOI: 10.1039/d2em00207h

rsc.li/espi

Microplastic (MP) particles are ubiquitous in aquatic environments. Therefore, understanding the processes that affect their removal from the water column, such as sedimentation, is critical for evaluating the risk they pose to aquatic ecosystems. We performed sedimentation experiments in which polystyrene (PS) and PS + ferrihydrite, a short-range ordered ferric (oxy)hydroxide, were analyzed in settling columns after 1 day and 1 week of settling time. The presence of ferrihydrite increased sedimentation rates of PS at all pH values studied (pH 3–11). At pH 6 we found that almost all PS particles were removed from the water column after only one day of exposure time. SEM/EDS imaging confirmed heteroaggregation between the PS particles and ferrihydrite. Zeta potential measurements indicated that at acidic pH values the negatively charged PS surface was coated with positively charged ferrihydrite particles leading to charge reversal. Our results demonstrate for the first time that ferric (oxy)hydroxides drive heteroaggregation and subsequent removal of MP from the water column, especially at typical pH values found in natural lake environments. Given their abundance in aquatic systems ferric (oxy)hydroxides need to be regarded as key scavengers of MP.

Environmental significance

The transport and fate of microplastic (MP) particles in the aquatic environment is impacted by interactions of MP with natural particles and colloids. Processes like aggregation or adsorption affect the surface properties of MP particles and their environmental fate and mobility. Here we study the effect of heteroaggregation between MP and ferric(oxy)hydroxide on the sedimentation of MP. Such interactions will be of particular relevance in environmental settings where ferric (oxy)hydroxide particles are abundant, *e.g.* at redox interfaces of aqueous surface and subsurface systems following reoxidation of Fe(II). Such interfaces can arise in groundwater, sediments, wetlands, stratified lakes, and marine environments.

Introduction

Pollution with plastic materials has emerged as one of the most relevant current and future environmental problems.[1–3] Micro- and nanosized particles are of particular concern since they can be taken up by organisms and cells[2,4–6] and may accumulate in the food chain.[7] In the last few years, research focused predominantly on the occurrence and distribution of microplastics (MP) in the environment. Only recently, a more fundamental understanding of microplastic particle behavior in the environment has started to attract attention. Processes like particle aggregation are well known to substantially affect the fate and mobility of particles in the aquatic environment and must therefore be included in modeling transport processes.[1] Heteroaggregation (the aggregation of two or more different colloidal particles) of engineered nanoparticles (ENPs) with natural colloids and suspended solids was shown to strongly affect the aquatic transport and sedimentation of ENPs.[8,9] By contrast, most studies focused on the homoaggregation of MP particles and the influence of pH, electrolytes and natural organic matter (NOM) on this process.[10–18] In the aquatic environment, however, processes triggering heteroaggregation play a much larger role due to the abundance of natural particles and colloids compared to MP particles.[1] Dissolved organic matter has been found to stabilize MP particles

[a]Department of Hydrology, University of Bayreuth, Germany. E-mail: j.schmidtmann@uni-bayreuth.de
[b]Limnological Research Station, University of Bayreuth, Germany
[c]Department of Hydrogeology, Helmholtz-Centre for Environmental Research – UFZ, Germany
[d]Hydrologic Modelling Unit, University of Bayreuth, Bayreuth, Germany
[e]Physical Chemistry II, University of Bayreuth, Germany
[f]Bavarian Polymer Institute (BPI), Keylab Electron and Optical Microscopy, University of Bayreuth, Germany

† Electronic supplementary information (ESI) available. See https://doi.org/10.1039/d2em00207h.

View Article Online
Environmental Science: Processes & Impacts Paper

in the aqueous phase by increasing the electrostatic and steric repulsion and to destabilize MP through bridging effects or surface charge reversal.[11,12,14,16,18] Heteroaggregation between MP and biogenic particles was shown to alter the buoyancy of MP and increase its sedimentation rate.[19–22] Despite the abundance and importance of inorganic colloidal material in aquatic systems,[23] studies about the interaction of MP with metal (oxy) hydroxides are scarce. Oriekhova and Stoll (2018) showed that heteroaggregation of polystyrene (PS) at environmental pH is induced by the presence of inorganic colloids (α-Fe_2O_3) and NOM.[24] Furthermore, inorganic coagulants such as polyaluminium chloride (PACl) and aluminium- and iron-based salts have been applied to induce coagulation of MP in aqueous solutions[25] leading to high removal efficiencies of MP particles from the water column.[26,27] In particular, ferric (oxy) hydroxides are abundant in aqueous systems[23,28] and strongly interact with natural organic matter and other water constituents[29–31] to eventually become deposited in sediments and soils.[28,32] Hence, they are a highly relevant aquatic component in respect to heteroaggregation mechanisms in natural aquatic systems. This was also shown by a recent study investigating the aggregation of MP particles with crystalline, poorly crystalline and freshly formed iron oxides.[33] However, to the best of our knowledge no study has been performed on the aggregation and subsequent sedimentation of MP particles with ferric (oxy) hydroxides.

Here, we have studied the aggregation between PS particles and ferrihydrite, a common naturally occurring ferric (oxy) hydroxide.[34] Ferrihydrite has a large surface area (200–300 m^2 g^{-1})[35] and a pH-dependent surface charge which is usually positively charged in the acidic pH range, negatively charged in the alkaline range and the isoelectric point is typically located at neutral pH.[36] By determining surface properties and aggregate size of PS, ferrihydrite and the formed associates we want to test, if heteroaggregation occurs and how it affects the sedimentation of PS.

Experimental

Selection of polystyrene particles

For the experiments we used spherical PS particles purchased from Microparticles (Berlin, Germany). According to the manufacturer, the particles have a diameter of (1.01 $\pm$ 0.03) μm and a density of 1.05 g cm^{-3}. The size and shape of the particles was checked by scanning electron microscopy (*cf.* below). We used a PS concentration of 10 mg L^{-1} (approx. 1.8 $\times$ 10^{10} particles L^{-1}) for the experiments. Comparing the number of particles per volume to plastic concentrations found in the environment, it seems quite high. However, the concentration of plastic particles in the lower micro-meter range (as used in this study) in aquatic environments is not well studied yet.[37] The used concentration is certainly higher than concentration of microplastics found in natural waters, however we had to select a concentration that was sufficiently high enough for the used measurement techniques. Previous studies investigating microplastic interactions and aggregation used concentrations in a similar or often even higher mass per volume ratio (4–160 mg L^{-1}).[11,12,14–16,24,33,38]

Synthesis and characterization of ferrihydrite

The synthesis of ferrihydrite was performed after Cornell and Schwertmann (2003).[23] Two litres of distilled water were preheated to 75 °C to which 20 g unhydrolyzed crystals of $Fe(NO_3)_3 \times 9H_2O$ were added under rapid stirring. The solution was placed for 10 minutes in an oven at 75 °C. The solution was then removed from the oven and rapidly cooled by plunging into iced water. Approximately 30 min later, the solution was transferred to dialysis bags which were placed in distilled water for multiple days. The water was exchanged several times until its conductivity was less than 5 μS cm^{-1}. The reaction product in the dialysis bags was filled into a storage container as soon as the conductivity was <5 μS cm^{-1}[39] and stored at 4 °C.

The synthesis product was analysed for its mineralogy by X-ray powder diffraction (XRD) using a Philips X'Pert Pro diffractometer. The diffractometer was running in reflection mode with monochromated Co$K\alpha_1$ radiation operated at 40 kV and 40 mA in the 2θ range 15°–90° with a step size of 0.02° and scan speed of 0.66° min^{-1}.

For the experiments we used a ferrihydrite concentration of 10 mg L^{-1} which is in the range of iron concentrations in the environment.[40]

Determination of zeta potential and z-averaged hydrodynamic diameter

The zeta potential and the z-averaged hydrodynamic diameter of the PS particles, the ferrihydrite particles as well as the formed heteroaggregates after a reaction time of 1 week were derived from measurements using ZetaSizer Nano ZS (Malvern Panalytical, Germany) by Laser Doppler Electrophoresis or Dynamic Light Scattering (DLS), respectively. A subsample of approx. 1 mL was analyzed at 25 °C using a folded capillary zeta cell (DTS1070, Malvern Panalytical, Germany). Each sample was measured three times. Results are given as average of the individual measurements with standard deviations. All measurements were performed at a concentration of 10 mg L^{-1} PS and 10 mg L^{-1} ferrihydrite, the pH was adjusted to values between 3 and 11 and ionic strength was set to 10 mM by addition of NaCl. Immediately before the ZetaSizer analysis, the samples were briefly shaken to re-suspend any sedimented aggregates.

Sedimentation experiments

To determine the sedimentation rate of PS in the presence of ferrihydrite, we prepared samples with PS (10 mg L^{-1}) and ferrihydrite (10 mg L^{-1}) under standard conditions. The samples with a total volume of 10 mL were prepared in narrow glass vessels (inner diameter ~16 mm). The pH was adjusted to values between 3 and 11 by adding HCl or NaOH. In each vessel, a constant ionic strength of 10 mM was established by addition of adequate amounts of NaCl. After the addition of all reactants, the samples were shaken and allowed to react, one set for 1 day and a second set for 1 week. After 1 day or 1 week the upper 8 mL

of the samples were transferred to a second sample vial without disturbing any settled particles in the lower 2 mL of the sample using a pipette. In the following, we will refer to the lower 2 mL of the sample as sediment and to the upper 8 mL of the sample as solution. Both phases were diluted with ultrapure water (18.2 MΩ cm) to a volume of 9 mL for TOC analysis.

In addition, we also analyzed the sedimentation of PS in the absence of ferrihydrite. For this, we prepared reference samples under identical conditions (pH 3–11 and ionic strength of 10 mM) and PS concentration but without ferrihydrite. After 1 day or 1 week, we removed the upper 8 mL of the samples and analyzed the PS concentration in the upper fraction (solution) and lower fraction (sediment) of the samples.

To determine the PS concentration, we analyzed the samples by thermocatalytic oxidation using a TOC device (TOC-L-Analyzer, Shimadzu, Kyoto, Japan). The presence of Fe species significantly improved the recovery of the PS particles so that 10 mg L^{-1} ferrihydrite was added to all samples before measurement (ESI Fig. S1†). Approx. 10 minutes before the measurement, the samples were acidified with 2 M HCl to dissolve all larger ferrihydrite-aggregates and pre-treated in an ultrasonic bath for 5 minutes. Instead of using the auto sampler of the instruments, the samples were placed on a magnetic stirrer during analysis to prevent sedimentation of the particles.

The PS concentration in sediment and solution was calculated from the measured non-purgeable organic carbon (NPOC) values against a calibration curve (ESI Fig. S1†). Additionally, the recovery of PS was calculated to verify the quality of the method.

Scanning electron microscopy (SEM) and energy-dispersive X-ray spectroscopy (EDS)

Samples were prepared by (i) dropping 4 μL of solution onto a glow-discharged carbon-supported TEM copper grid (S160 Plano, Germany) and (ii) drying under ambient conditions. The samples were coated with a thin layer of platinum by a Cressington 208 HR sputter coater. SEM images were recorded using secondary electron detectors on a Zeiss ULTRA PLUS (Carl Zeiss Microscopy GmbH, Germany) operating at an acceleration voltage of 2 kV. For EDS mapping, the samples were investigated with a Zeiss LEO 1530 (Carl Zeiss Microscopy GmbH, Germany) operating at 2 kV and equipped with an UltraDry EDS detector using Pathfinder software (Thermo Fisher Scientific, USA). EDS resolution was enhanced by use of a thin layer of carbon as specimen support and a low acceleration voltage.

Furthermore, the samples were analyzed using a light microscope and a high 128 definition digital single lens reflex camera (Zeiss Axioplan microscope and Cannon EOS 5D 129 respectively). The advantage of this method is that the samples do not have to be dried but can be analyzed directly in suspension.

Results and discussion

Colloidal properties of polystyrene particles

SEM images revealed spherical, monodisperse particles with a diameter of 1 μm (ESI Fig. S2†) corresponding to the data provided by the manufacturer. The surface of the PS particles was found to be negatively charged over the entire pH range studied. Zeta potentials varied from (-44.0 ± 0.7) mV at pH 3 to (-82.9 ± 5.6) mV at pH 11 (Fig. 1A). The z-averaged hydrodynamic diameter of the PS particles was (1.70 ± 0.15) μm and did not show a trend or significant variations over the pH range (Fig. 1B). Even though the relatively negative zeta potential indicates a strong electrostatic repulsion some aggregates must have formed during storage. This interpretation is in-line with the presence of a detectable sediment, which we consider in the following as reference value for sedimentation of the bare particles.

Sedimentation analysis of the reference samples shows that the PS concentrations in the sediment were rather constant over the pH range and no trend was observed. Fig. 2 displays the percentage of all PS found in the sediment of a sample after 1 day or 1 week of settling time. After a settling time of 1 day, the mean PS concentration in the sediment (11.27 ± 1.31) mg L^{-1} was slightly higher compared to the solution (8.85 ± 0.56) mg L^{-1}. After 1 week, the concentration in the sediment clearly increased to a mean of (21.20 ± 2.24) mg L^{-1}, whereas the PS concentration in the solution was reduced to (7.17 ± 0.64) mg L^{-1}. In a well-mixed dispersion where no sedimentation would take place, 20% of the total PS in the sample should be found in the sediment (bottom 2 mL). However, after 1 day, between 20.4% and 27.9% of the initially added particles were recovered in the sediment and between 34.4% and 47.8% after 1 week. Hence, although highly negative zeta potentials suggest that the PS particles should be stable in dispersion, the sedimentation study indicates that some PS particles tend to homoaggregate and to sediment under the analyzed conditions (10 mM NaCl). This agrees well with a recent study examining the aggregation of exactly the same 1 μm PS particles using spICP-MS.[41] There it was found that 63% of PS particles did not aggregate, 25% were found in aggregates of two particles and the remaining 12% in aggregates of more than 2 particles. The increase in the fraction of sedimented PS from 1 day to 1 week suggests an unknown kinetic control on the sedimentation process. As no pH dependence for the sedimentation has been observed, we attribute the sedimentation primarily to long-term storage effects.

Colloidal properties of ferrihydrite

The X-ray diffractogram of the synthesized ferric (oxy)hydroxide shows six broadened lines (ESI Fig. S3†) characteristic for 6-line ferrihydrite.[23] The isoelectric point (pH_{IEP}) is located at pH ≈ 8.7 (Fig. 1A) and thus slightly higher than values reported in the literature ($pH_{IEP} \approx 7$).[36,42] At pH values < 6, ferrihydrite particles were in nanometer size range and part of the iron (oxy) hydroxides might even be present as dissolved iron. In these samples, count rates were not sufficient for reliable light scattering measurements. Therefore, the zeta potential and z-averaged hydrodynamic diameter results of ferrihydrite samples at pH < 6 have no quantitative value but provide a reasonable estimate for pH_{IEP}. However, based on previously reported findings, we can safely assume that the zeta potential

View Article Online
Environmental Science: Processes & Impacts Paper

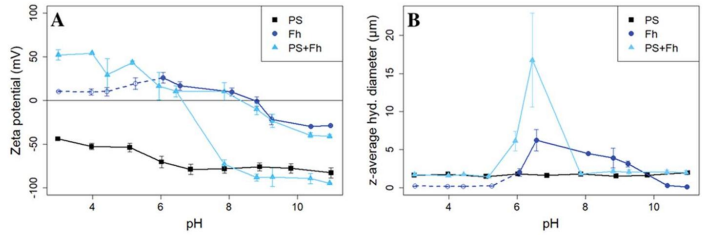

Fig. 1 Zeta potential (A) and z-average hydrodynamic diameter (B) of PS (10 mg L^{-1}, I = 10 mM, black squares), ferrihydrite (Fh, 10 mg L^{-1}, I = 10 mM, darkblue circles), and samples with PS + ferrihydrite (PS + Fh, 10 mg L^{-1} PS, 10 mg L^{-1} Fh, I = 10 mM, lightblue triangles). For ferrihydrite samples with pH < 6, the count rates were not sufficient for reliable light scattering measurements and therefore should be regarded with caution (dashed darkblue line). For samples with PS + ferrihydrite (lightblue) at pH > 7.9 two trajectories of the zeta potential are displayed, because the zeta potential distribution showed not one but two distinct zeta potential peaks (ESI Fig. S4†).

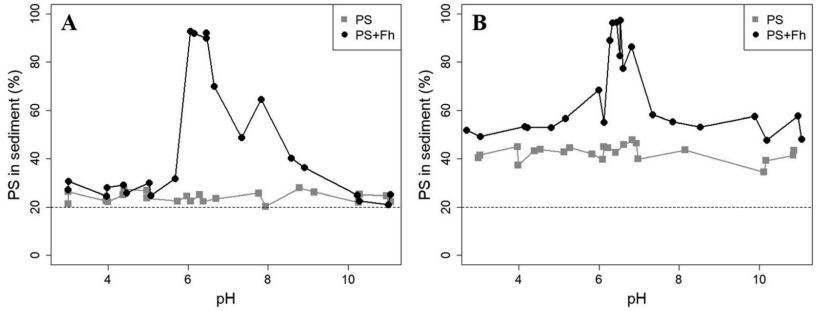

Fig. 2 Percentage of PS found in the sediment of the samples after a settling time of (A) 1 day and (B) 1 week. The grey curve shows the reference samples in which only PS is present, and the black curve shows the samples in which PS and ferrihydrite (PS + Fh) is present. In a well-mixed dispersion where no sedimentation takes place, 20% of the total PS in the sample should be found in the sediment (dashed line).

values of ferrihydrite for pH 3–6 will be positive and increase with decreasing pH.[42]

For pH values between 6 and 9, we notice an increase in the z-averaged hydrodynamic diameter up to a maximum of (6.26 ± 1.42) μm at pH 6.6. The size maximum is not located at the pH_{IEP}. However, the repulsive forces between the particles at the pH of maximum homoaggregation may already be so weak that aggregation takes place. The relatively low zeta potential (Ψ_{zeta} = 16.8 mV) is in line with this interpretation. For samples with a pH > 10, the absolute value of the zeta potential increases again to approx. −30 mV and the z-averaged hydrodynamic diameter is decreasing again to values less than 0.3 μm.

Heteroaggregation and subsequent sedimentation of polystyrene and ferrihydrite

The presence of ferrihydrite leads to substantial increases of the sedimentation rate of PS relative to the rates observed in the reference samples without ferrihydrite, particularly after an exposure time of 1 week (Fig. 2). After 1 day, moderate sedimentation of PS of about 25% of the initially added particles was observed in the acidic (pH < 6) and alkaline range (pH > 9), both in the presence and absence of ferrihydrite. However, at pH values between 6 and 9, the presence of ferrihydrite induced a distinct increase in sedimentation with maximum sedimentation rates between pH 6 and 6.5. In this pH range 90–93% of the PS were found in the sediment after settling. After 1 week, the maximum sedimentation rate (83–97%) of PS particles was found at the same pH range. For all other pH values (pH 3–6 & 7–11), the sedimentation rate of PS in the presence of ferrihydrite increased to 50–60% compared to the sedimentation rate observed after 1 day (with the exception of pH value 7.8). In these pH ranges, sedimentation rates were distinctly higher than those observed in the absence of ferrihydrite. Taken together, these observations point to heteroaggregation between PS particles and ferrihydrite and subsequent sedimentation of these heteroaggregates with a maximum at pH ~6.5.

Interestingly, the characteristic negative surface charge of PS can no longer be identified in the acidic pH range (Fig. 1A). Instead, the zeta potential values are positive with a maximum of (54.1 ± 0.2) mV at pH 4. Therefore, it seems likely that the positively charged ferrihydrite adsorbed to the PS particles which in consequence reversed their negative charge. This is confirmed by EDS mapping of the samples at pH 4 which shows

a surface coating of the PS particles with ferrihydrite (Fig. 3). Similar observations were reported by Li *et al.* (2019) who demonstrated that, depending on the size of the PS particles, iron oxides adsorbed onto the surface of PS or *vice versa*.[43] The smaller sized colloidal objects always adsorbed onto the larger ones. Given the small particle sizes of ferrihydrite colloids observed at acidic pH (Fig. 1B), it therefore seems likely that they adsorbed onto the significantly larger PS particles at these pH conditions. Due to the small size of the ferrihydrite particles compared to the PS, no obvious change in dimensions of the overall particles can be observed (Fig. 2B and 3, ESI Fig. S5A†). The particle size of the heteroaggregates in the acidic pH range is similar to that of the pure PS particles, however with a distinctly different charge. Due to the substantially higher density of ferrihydrite particles (3.9 g cm^{-3})[44] as compared to PS particles (1.05 g cm^{-3}), already very small ferrihydrite particles adsorbed onto the PS surface may lead to the observed increase in sedimentation rate of the PS-ferrihydrite heteroaggregates in the acidic pH range by a factor of 1.3.

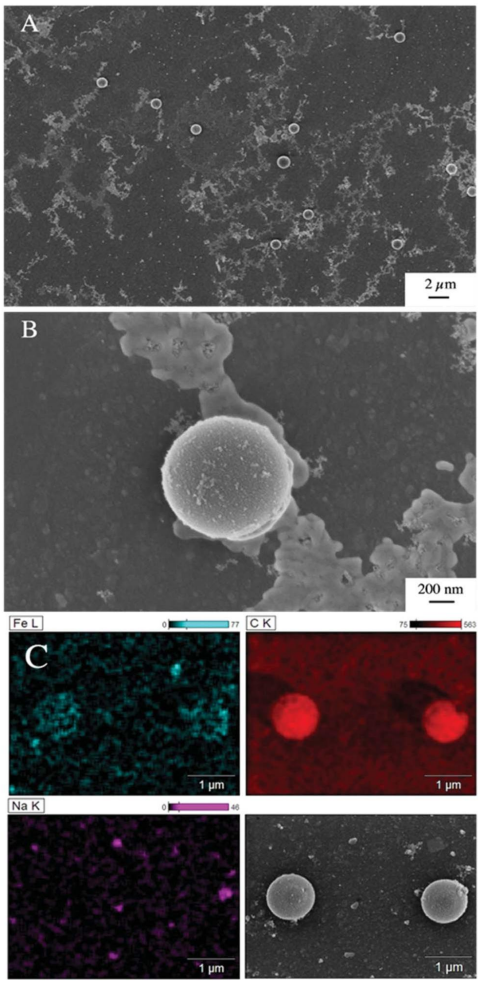

Fig. 3 SEM images of a sample with PS and ferrihydrite at pH 4 showing isolated PS particles and statistically distributed, nano-sized ferrihydrite besides larger agglomerates of dried sodium salt (A). At higher magnification, a coating of the PS particles can be observed (B). EDS analysis indicates a higher iron concentration on the PS particles compared to the carbon background (C).

For samples with pH > 7.9 we identified not one but two distinct peaks in the zeta potential distribution (ESI Fig. S4†). Therefore, two different trajectories of the zeta potential for pH > 7.9 are plotted for the PS-ferrihydrite heteroaggregates (Fig. 1A). One of the trajectories follows the course of the zeta potentials determined for reference PS particles, while the other trajectory matches the zeta potential measurements of unreacted ferrihydrite. We assume that this observation is due to the co-occurrence of PS and ferrihydrite particles that stay separated and that no (major) adsorption and subsequent heteroaggregation takes place in the alkaline range (ESI Fig. S5C†). Since two different types of particles with different sizes are present at this pH range, the results of the z-averaged hydrodynamic diameter are not considered to be very reliable for the alkaline range. Despite their negative charge, sedimentation rates of PS particles in the presence of ferrihydrite are also enhanced at alkaline pH values compared to the sedimentation rates determined in the absence of ferrihydrite. Similar observations were made by Li *et al.* (2019) who were able to demonstrate that the addition of suspended sediment to a suspension of 100 nm PS particles enhances the settling rate of PS at 50 mM NaCl, although both particle types were negatively charged.[38] Aggregation despite apparent electrostatic repulsion has also been described in previous studies and was related to discrete nanoscale surface heterogeneity.[45,46] Therefore, we assume that some particles aggregate despite repulsive forces and therefore cause the amplified sedimentation of PS in presence of ferrihydrite in the alkaline range.

Low, slightly positive zeta potentials (Fig. 1A) were found at circumneutral pH values (between 6 and 8). Such minimum coincides with a very large peak of the z-averaged hydrodynamic diameter of above 15 μm at pH 6.4 (Fig. 1B), which underpins heteroaggregation of several particles. The numerical value of the z-averaged hydrodynamic diameter needs to be regarded as a rough estimate, though. The instrument used here can determine particle diameters only up to a size of 10 μm by DLS. However, SEM and light microscopy show that the aggregate dimensions clearly exceed this limit. Hence, our data indicate that strong heteroaggregation is taking place at pH 6–7 and heteroaggregates with dimensions of more than 10 μm have been formed. Optical microscopy imaging revealed aggregates with sizes ranging from a few micrometers up to 100 μm (ESI Fig. S5B†). Formation of heteroaggregates is further corroborated by SEM images of samples at pH 6.5 (Fig. 4) with EDS analysis clearly showing that ferrihydrite adsorbs on PS particles and connects the PS particles to larger aggregates (Fig. 4C).

View Article Online
Environmental Science: Processes & Impacts Paper

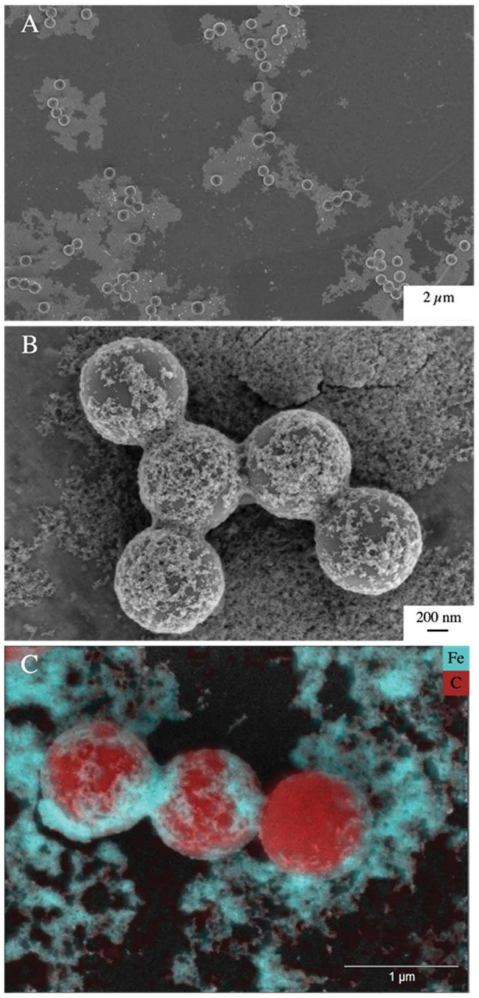

Fig. 4 SEM image of formed heteroaggregates of PS and ferrihydrite at pH 6.5 shows the locally coinciding agglomeration of ferrihydrite and PS particles (A). Higher magnification indicates the ferrihydrite on the surface of and linkages between the PS (B). EDS analysis confirms that the adsorbed/aggregated material on the PS is ferrihydrite (C).

This pH is close to the isoelectric point of ferrihydrite. Similarly, Oriekova and Stoll (2018) observed heteroaggregation of PS nanoplastic with α-Fe_2O_3 particles at pH 8 under varying PS concentrations to occur at PS concentration levels at which the isoelectric point of the mixtures is achieved.[24] Vu *et al.* (2022) observed maximal heteroaggregation of PS and ferrihydrite to occur at pH values at which the surface charge of ferrihydrite is rather low.[33] We therefore propose that the surface charge of MP becomes neutralized upon adsorption of neutral or weakly charged iron colloids leading to an increase of van der Waals attraction forces and subsequent aggregation.[33]

Conclusions

Previous studies have demonstrated heteroaggregation of MP particles and their subsequent removal from the water column with phytoplankton,[20,22] microalgae,[19] suspended sediment[38] or calcite.[47] In this study, we demonstrate for the first time that the presence of ferric iron particles is driving not only heteroaggregation[24,33] but also sedimentation of MP at rates at which almost all PS was found in the sediment already after 1 day of settling. The interactions between PS and ferrihydrite were strongly pH dependent. At acidic pH a coating of the negative PS surface by positively charged ferrihydrite was observed due to strong electrostatic attraction which led to charge reversal. In contrast, no major aggregation took place in the alkaline pH range due to repulsive forces between PS and ferrihydrite. At circumneutral pH, charge neutralization resulted in the formation of large heteroaggregates which subsequently sedimented to the bottom of the sample vial. Irrespective of their idealized shape and their smooth surface, the PS particles analyzed in this study can be regarded as model substances for other MP particles.

Environmental processes, such as UV exposure[48] or the formation of biofilms on the surface will even increase surface reactivity of MP particles[21] so that interactions between ferric (oxy)hydroxides and MP may be even more pronounced. However, removal of MP particles upon interaction with ferric (oxy)hydroxides from the water surface to deeper water compartments at a time scale of days may also reduce the exposure time to UV radiation.

Overall, our research suggests that MP particles will tend to form an environmental corona at their surface consisting of ferric (oxy)hydroxides but also of other constituents[49,50] once entering aqueous systems that affects their environmental behaviour. Removal of MP from the water column following heteroaggregation with ferric (oxy)hydroxides will reduce exposure times of aquatic organisms to MP.[51,52] Inversely it may cause a higher risk for organisms in the benthic zone since lake and river sediments may act as a sink for MP particles.[38,53,54] Moreover, ferric iron induced heteroaggregation of MP particles may be considered an interesting process for MP removal in waste-water treatment systems.

Data availability

The datasets used in this study are published on Zenodo at **https://doi.org/10.5281/zenodo.6855575**.

Conflicts of interest

There are no conflicts to declare.

Acknowledgements

The study was funded by the Deutsche Forschungsgemeinschaft (DFG, German Research Foundation) –

Project Number 391977956 – SFB 1357 Microplastics. The authors would like to thank Martina Heider for taking SEM images at the Bavarian Polymer Institute (BPI), Tiziana Boffa Ballaran for XRD analysis at the Bavarian Research Institute of Experimental Geochemistry and Geophysics (BGI) and Laura Wegner and Jutta Eckert for their help with TOC measurements.

References

1 O. S. Alimi, J. Farner Budarz, L. M. Hernandez and N. Tufenkji, Microplastics and nanoplastics in aquatic environments: aggregation, deposition, and enhanced contaminant transport, *Environ. Sci. Technol.*, 2018, **52**, 1704–1724.
2 K. Duis and A. Coors, Microplastics in the aquatic and terrestrial environment: sources (with a specific focus on personal care products), fate and effects, *Environ. Sci. Eur.*, 2016, **28**, 2.
3 R. C. Thompson, Y. Olsen, R. P. Mitchell, A. Davis, S. J. Rowland, A. W. John, D. McGonigle and A. E. Russell, Lost at sea: where is all the plastic?, *Science*, 2004, **304**, 838.
4 A. F. R. M. Ramsperger, J. Jasinski, M. Völkl, T. Witzmann, M. Meinhart, V. Jérôme, W. P. Kretschmer, R. Freitag, J. Senker, A. Fery, H. Kress, T. Scheibel and C. Laforsch, Supposedly identical microplastic particles substantially differ in their material properties influencing particle-cell interactions and cellular responses, *J. Hazard. Mater.*, 2022, **425**, 127961.
5 J. Rudolph, M. Völkl, V. Jérôme, T. Scheibel and R. Freitag, Noxic effects of polystyrene microparticles on murine macrophages and epithelial cells, *Sci. Rep.*, 2021, **11**, 15702.
6 S. L. Wright, R. C. Thompson and T. S. Galloway, The physical impacts of microplastics on marine organisms: a review, *Environ. Pollut.*, 2013, **178**, 483–492.
7 K. Cverenkárová, M. Valachovičová, T. Mackuľak, L. Žemlička and L. Bírošová, Microplastics in the Food Chain, *Life*, 2021, **11**, 1349.
8 A. Praetorius, J. Labille, M. Scheringer, A. Thill, K. Hungerbühler and J.-Y. Bottero, Heteroaggregation of Titanium Dioxide Nanoparticles with Model Natural Colloids under Environmentally Relevant Conditions, *Environ. Sci. Technol.*, 2014, **48**, 10690–10698.
9 I. Velzeboer, J. T. K. Quik, D. van de Meent and A. A. Koelmans, Rapid settling of nanoparticles due to heteroaggregation with suspended sediment, *Environ. Toxicol. Chem.*, 2014, **33**, 1766–1773.
10 A. Abdurahman, K. Cui, J. Wu, S. Li, R. Gao, J. Dai, W. Liang and F. Zeng, Adsorption of dissolved organic matter (DOM) on polystyrene microplastics in aquatic environments: Kinetic, isotherm and site energy distribution analysis, *Ecotoxicol. Environ. Saf.*, 2020, **198**, 110658.
11 L. Cai, L. Hu, H. Shi, J. Ye, Y. Zhang and H. Kim, Effects of inorganic ions and natural organic matter on the aggregation of nanoplastics, *Chemosphere*, 2018, **197**, 142–151.
12 S. Li, H. Liu, R. Gao, A. Abdurahman, J. Dai and F. Zeng, Aggregation kinetics of microplastics in aquatic environment: Complex roles of electrolytes, pH, and natural organic matter, *Environ. Pollut.*, 2018, **237**, 126–132.
13 T. Oncsik, G. Trefalt, Z. Csendes, I. Szilagyi and M. Borkovec, Aggregation of Negatively Charged Colloidal Particles in the Presence of Multivalent Cations, *Langmuir*, 2014, **30**, 733–741.
14 A. Pradel, S. Ferreres, C. Veclin, H. El Hadri, M. Gautier, B. Grassl and J. Gigault, Stabilization of Fragmental Polystyrene Nanoplastic by Natural Organic Matter: Insight into Mechanisms, *ACS EST Water*, 2021, **1**, 1198–1208.
15 N. Singh, E. Tiwari, N. Khandelwal and G. K. Darbha, Understanding the stability of nanoplastics in aqueous environments: effect of ionic strength, temperature, dissolved organic matter, clay, and heavy metals, *Environ. Sci.: Nano*, 2019, **6**, 2968–2976.
16 J. Wang, X. Zhao, A. Wu, Z. Tang, L. Niu, F. Wu, F. Wang, T. Zhao and Z. Fu, Aggregation and stability of sulfate-modified polystyrene nanoplastics in synthetic and natural waters, *Environ. Pollut.*, 2020, 114240.
17 J. Wu, R. Jiang, W. Lin and G. Ouyang, Effect of salinity and humic acid on the aggregation and toxicity of polystyrene nanoplastics with different functional groups and charges, *Environ. Pollut.*, 2019, **245**, 836–843.
18 S. Yu, M. Shen, S. Li, Y. Fu, D. Zhang, H. Liu and J. Liu, Aggregation kinetics of different surface-modified polystyrene nanoparticles in monovalent and divalent electrolytes, *Environ. Pollut.*, 2019, **255**, 113302.
19 F. Lagarde, O. Olivier, M. Zanella, P. Daniel, S. Hiard and A. Caruso, Microplastic interactions with freshwater microalgae: Hetero-aggregation and changes in plastic density appear strongly dependent on polymer type, *Environ. Pollut.*, 2016, **215**, 331–339.
20 M. Long, B. Moriceau, M. Gallinari, C. Lambert, A. Huvet, J. Raffray and P. Soudant, Interactions between microplastics and phytoplankton aggregates: Impact on their respective fates, *Mar. Chem.*, 2015, **175**, 39–46.
21 J. Michels, A. Stippkugel, M. Lenz, K. Wirtz and A. Engel, Rapid aggregation of biofilm-covered microplastics with marine biogenic particles, *Proc. R. Soc. B*, 2018, **285**, 20181203.
22 P. Möhlenkamp, A. Purser and L. Thomsen, Plastic microbeads from cosmetic products: an experimental study of their hydrodynamic behaviour, vertical transport and resuspension in phytoplankton and sediment aggregates, *Elem. Sci. Anth.*, 2018, **6**, DOI: **10.1525/elementa.317**.
23 R. M. Cornell and U. Schwertmann, *The Iron Oxides: Structure, Properties, Reactions, Occurrences and Uses*, John Wiley & Sons, 2003.
24 O. Oriekhova and S. Stoll, Heteroaggregation of nanoplastic particles in the presence of inorganic colloids and natural organic matter, *Environ. Sci.: Nano*, 2018, **5**, 792–799.
25 W. He, Z. Xie, W. Lu, M. Huang and J. Ma, Comparative analysis on floc growth behaviors during ballasted flocculation by using aluminum sulphate (AS) and polyaluminum chloride (PACl) as coagulants, *Sep. Purif. Technol.*, 2019, **213**, 176–185.

26 Y. Gong, Y. Bai, D. Zhao and Q. Wang, Aggregation of carboxyl-modified polystyrene nanoplastics in water with aluminum chloride: Structural characterization and theoretical calculation, *Water Res.*, 2022, **208**, 117884.
27 G. Zhou, Q. Wang, J. Li, Q. Li, H. Xu, Q. Ye, Y. Wang, S. Shu and J. Zhang, Removal of polystyrene and polyethylene microplastics using PAC and FeCl3 coagulation: Performance and mechanism, *Sci. Total Environ.*, 2020, 141837.
28 B. Lo and T. D. Waite, Structure of Hydrous Ferric Oxide Aggregates, *J. Colloid Interface Sci.*, 2000, **222**, 83–89.
29 H. J. Curtinrich, S. D. Sebestyen, N. A. Griffiths and S. J. Hall, Warming Stimulates Iron-Mediated Carbon and Nutrient Cycling in Mineral-Poor Peatlands, *Ecosystems*, 2022, **25**, 44–60.
30 K. G. J. J. Nierop, B. Jansen and J. M. Verstraten, Dissolved organic matter, aluminium and iron interactions: precipitation induced by metal/carbon ratio, pH and competition, *Sci. Total Environ.*, 2002, **300**, 201–211.
31 S. Peiffer, K. Walton-Day and D. L. Macalady, The Interaction of Natural Organic Matter with Iron in a Wetland (Tennessee Park, Colorado) Receiving Acid Mine Drainage, *Aquat. Geochem.*, 1999, **5**, 207–223.
32 K. Lalonde, A. Mucci, A. Ouellet and Y. Gélinas, Preservation of organic matter in sediments promoted by iron, *Nature*, 2012, **483**, 198–200.
33 T. T. T. Vu, P. H. Nguyen, T. V. Pham, P. Q. Do, T. T. Dao, A. D. Nguyen, L. Nguyen-Thanh, V. M. Dinh and M. N. Nguyen, Comparative effects of crystalline, poorly crystalline and freshly formed iron oxides on the colloidal properties of polystyrene microplastics, *Environ. Pollut.*, 2022, **306**, 119474.
34 E. Jansen, A. Kyek, W. Schäfer and U. Schwertmann, The structure of six-line ferrihydrite, *Appl. Phys. A*, 2002, **74**, 1004–1006.
35 U. Schwertmann and R. M. Cornell, *Iron Oxides in the Laboratory: Preparation and Characterization*, John Wiley & Sons Ltd, Weinheim, 2008.
36 M. Kosmulski, Isoelectric points and points of zero charge of metal (hydr)oxides: 50years after Parks' review, *Adv. Colloid Interface Sci.*, 2016, **238**, 1–61.
37 J. L. Conkle, C. D. Báez Del Valle and J. W. Turner, Are We Underestimating Microplastic Contamination in Aquatic Environments?, *Environ. Manage.*, 2018, **61**, 1–8.
38 Y. Li, X. Wang, W. Fu, X. Xia, C. Liu, J. Min, W. Zhang and J. C. Crittenden, Interactions between nano/micro plastics and suspended sediment in water: Implications on aggregation and settling, *Water Res.*, 2019, **161**, 486–495.
39 L. Gentile, T. Wang, A. Tunlid, U. Olsson and P. Persson, Ferrihydrite Nanoparticle Aggregation Induced by Dissolved Organic Matter, *J. Phys. Chem. A*, 2018, **122**, 7730–7738.
40 A. Kappler, C. Bryce, M. Mansor, U. Lueder, J. M. Byrne and E. D. Swanner, An evolving view on biogeochemical cycling of iron, *Nat. Rev. Microbiol.*, 2021, **19**, 360–374.
41 M. Mansor, S. Drabesch, T. Bayer, A. Van Le, A. Chauhan, J. Schmidtmann, S. Peiffer and A. Kappler, Application of Single-Particle ICP-MS to Determine the Mass Distribution and Number Concentrations of Environmental Nanoparticles and Colloids, *Environ. Sci. Technol. Lett.*, 2021, **8**, 589–595.
42 J. Liu, S. M. Louie, C. Pham, C. Dai, D. Liang and Y. Hu, Aggregation of ferrihydrite nanoparticles: Effects of pH, electrolytes,and organics, *Environ. Res.*, 2019, **172**, 552–560.
43 M. Li, L. He, M. Zhang, X. Liu, M. Tong and H. Kim, Cotransport and Deposition of Iron Oxides with Different-Sized Plastic Particles in Saturated Quartz Sand, *Environ. Sci. Technol.*, 2019, **53**, 3547–3557.
44 T. Hiemstra and W. H. Van Riemsdijk, A surface structural model for ferrihydrite I: Sites related to primary charge, molar mass, and mass density, *Geochim. Cosmochim. Acta*, 2009, **73**, 4423–4436.
45 A. Al Harraq and B. Bharti, Microplastics through the Lens of Colloid Science, *ACS Environ. Au*, 2021, **2**, 3–10, DOI: **10.1021/acsenvironau.1c00016**.
46 I. L. Molnar, W. P. Johnson, J. I. Gerhard, C. S. Willson and D. M. O'Carroll, Predicting colloid transport through saturated porous media: A critical review, *Water Resour. Res.*, 2015, **51**, 6804–6845.
47 R. Leiser, R. Jongsma, I. Bakenhus, R. Möckel, B. Philipp, T. R. Neu and K. Wendt-Potthoff, Interaction of cyanobacteria with calcium facilitates the sedimentation of microplastics in a eutrophic reservoir, *Water Res.*, 2021, **189**, 116582.
48 N. Meides, T. Menzel, B. Poetzschner, M. G. J. Löder, U. Mansfeld, P. Strohriegl, V. Altstaedt and J. Senker, Reconstructing the Environmental Degradation of Polystyrene by Accelerated Weathering, *Environ. Sci. Technol.*, 2021, **55**, 7930–7938.
49 T. S. Galloway, M. Cole and C. Lewis, Interactions of microplastic debris throughout the marine ecosystem, *Nat. Ecol. Evol.*, 2017, **1**, 116.
50 A. F. R. M. Ramsperger, V. K. B. Narayana, W. Gross, J. Mohanraj, M. Thelakkat, A. Greiner, H. Schmalz, H. Kress and C. Laforsch, Environmental exposure enhances the internalization of microplastic particles into cells, *Sci. Adv.*, 2020, **6**, eabd1211.
51 S. Franzellitti, L. Canesi, M. Auguste, R. H. G. R. Wathsala and E. Fabbri, Microplastic exposure and effects in aquatic organisms: A physiological perspective, *Environ. Toxicol. Pharmacol.*, 2019, **68**, 37–51.
52 H. Elagami, P. Ahmadi, J. H. Fleckenstein, S. Frei, M. Obst, S. Agarwal and B. S. Gilfedder, Measurement of microplastic settling velocities and implications for residence times in thermally stratified lakes, *Limnol. Oceanogr.*, 2022, **67**, 934–945.
53 P. Näkki, O. Setälä and M. Lehtiniemi, Seafloor sediments as microplastic sinks in the northern Baltic Sea – Negligible upward transport of buried microplastics by bioturbation, *Environ. Pollut.*, 2019, **249**, 74–81.
54 S. Zhao, J. E. Ward, M. Danley and T. J. Mincer, Field-Based Evidence for Microplastic in Marine Aggregates and Mussels: Implications for Trophic Transfer, *Environ. Sci. Technol.*, 2018, **52**, 11038–11048.

Supporting Information

Heteroaggregation of PS microplastic with ferrihydrite leads to rapid removal of microplastic particles from the water column

Johanna Schmidtmann[a*], Hassan Elagami[a,b], Benjamin S. Gilfedder[a,b], Jan H. Fleckenstein[c,d], Georg Papastavrou[e], Ulrich Mansfeld[f], Stefan Peiffer[a]

[a] Department of Hydrology, University of Bayreuth, Bayreuth Center for Ecology and Environmental Research (BayCEER), Bayreuth, Germany

[b] Limnological Research Station, University of Bayreuth, Bayreuth Center for Ecology and Environmental Research (BayCEER), Bayreuth, Germany

[c] Department of Hydrogeology, Helmholtz-Center for Environmental Research, Leipzig, Germany

[d] Hydrologic Modelling Unit, Bayreuth Center of Ecology and Environmental Research (BayCEER), University of Bayreuth, Bayreuth, Germany

[e] Department of Physical Chemistry II, University of Bayreuth, Bayreuth, Germany

[f] Bavarian Polymer Institute (BPI), Keylab Electron and Optical Microscopy, University of Bayreuth, Bayreuth, Germany

*corresponding author: j.schmidtmann@uni-bayreuth.de

List of Figures

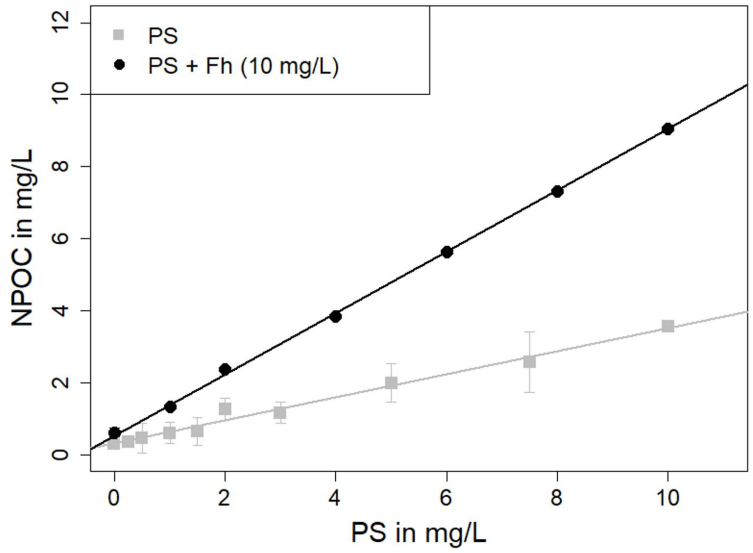

Fig. S1: Calibration curves of 1 µm PS (grey, NPOC[mg/L] = 0.3198*PS[mg/L] + 0.303, R^2 = 0.9851) and 1 µm PS with 10 mg/L ferrihydrite (Fh) (black, NPOC[mg/L] = 0.8522*PS[mg/L] + 0.5355, R^2 = 0.9997) for TOC measurements. On the x-axis, the prepared PS concentrations are plotted and on the y-axis the corresponding non-purgeable organic carbon (NPOC) concentrations measured with the TOC Analyzer. We assume that the presence of ferrihydrite has an unknown catalytic effect on the oxidation of PS. Therefore, the recovery of the PS concentration is significantly enhanced in the presence of ferrihydrite.

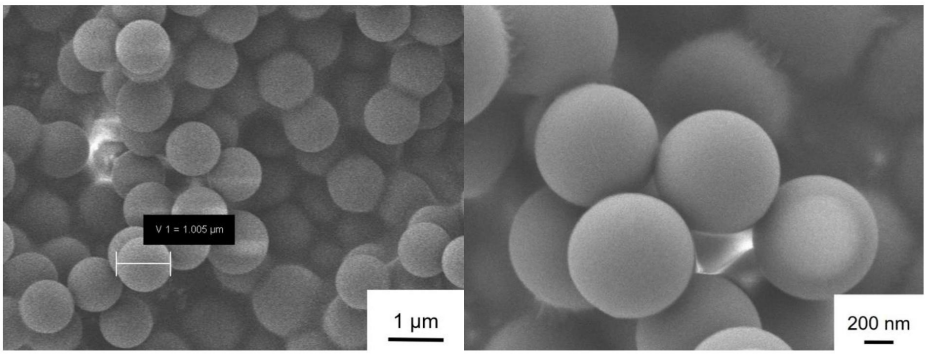

Fig. S2. SEM images of pristine 1 µm PS particles.

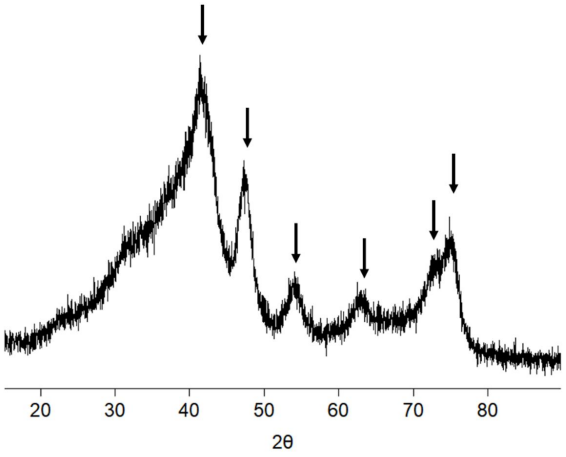

Fig. S3: X-Ray diffractogram (monochromated $CoK\alpha_1$ radiation) of the synthesized ferric oxyhydroxides shows the characteristic six broadened lines of 6-line ferrihydrite.

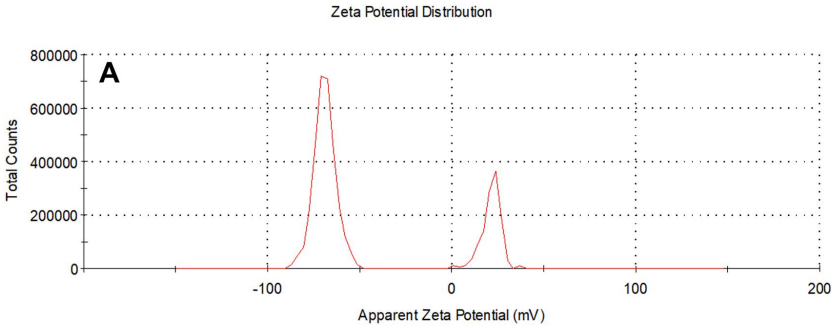

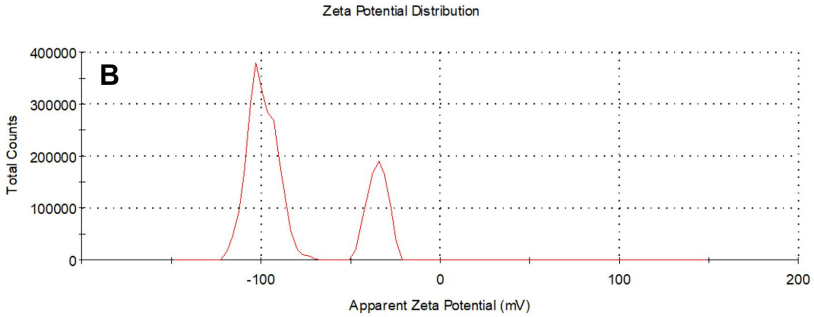

Fig. S4: Zeta Potential distribution of one single measurement of a sample with PS and ferrihydrite as an example for samples in which two zeta potential peaks were measured. A shows one measurement for a sample at pH 7.9 and B one measurement for a sample at pH 9.3. The zeta potential distributions do not show one but two distinct zeta potential peaks and therefore suggests the co-occurrence of PS and ferrihydrite particles that stay separated and that no (major) adsorption or aggregation takes place. The peak at more negative zeta potential values can be attributed to the PS particles and the peak at higher/less negative zeta potential values to the ferrihydrite particles.

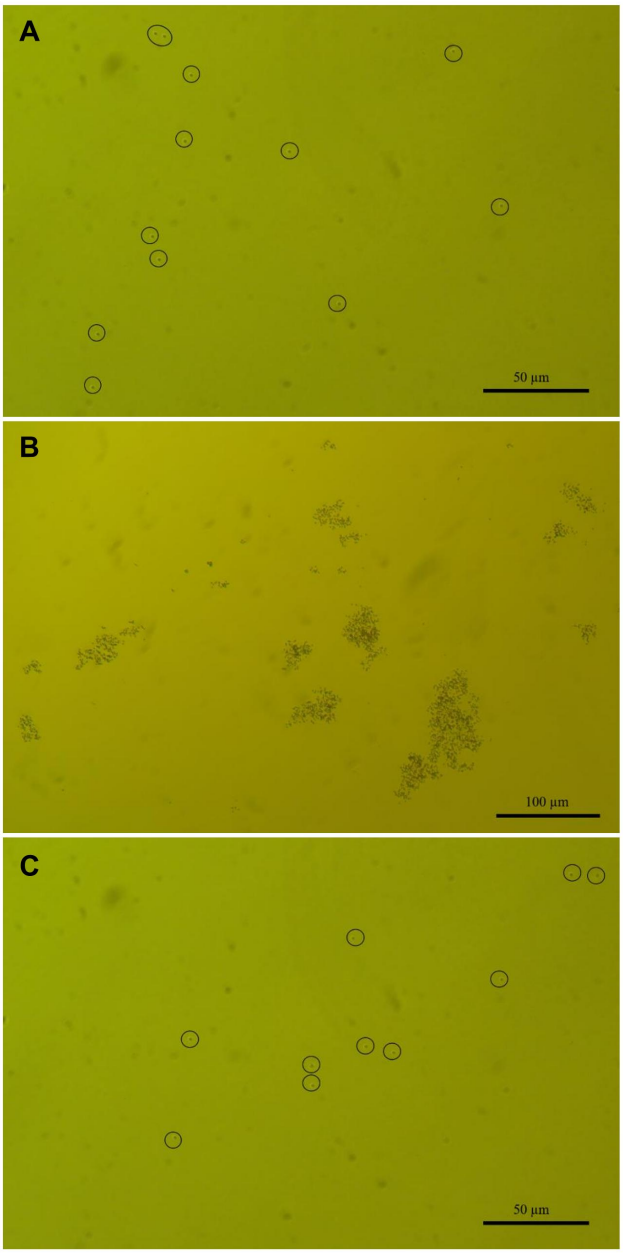

Fig. S5: Microscope image of PS and ferrihydrite after a reaction time of 1 week at pH 4 (A), pH 6.5 (B) and pH 10 (C). At pH values of 4 and 10 only single PS particles were identified (encircled), but no larger aggregates were found as it was the case at pH 6.5 (B). At pH 6.5, heteroaggregates ranging in size from a few micrometers up to 100 µm were observed.

Study 2: UV-weathering affects heteroaggregation and subsequent sedimentation of polystyrene microplastic particles with ferrihydrite

Status: Ready for submission.

Authors: Johanna Schmidtmann, Hannah-Kristin Weishäupl, Luisa Hopp, Nora Meides, Stefan Peiffer

Own Contribution in %:

Study design	90
Laboratory analysis	20
Data processing and analyses	90
Interpretation of the results	90
Preparation of the manuscript	90

JS designed the study with support and consultation of all co-authors. JS and HKW planned the laboratory experiments. HKW and JS conducted the laboratory experiments, whereby HKW performed the largest share. JS prepared the figures, tables and the Graphical Abstract. JS and HKW processed the data. All co-authors interpreted the results. JS prepared the manuscript with input from all co-authors.

JS is the corresponding author.

Graphical Abstract:

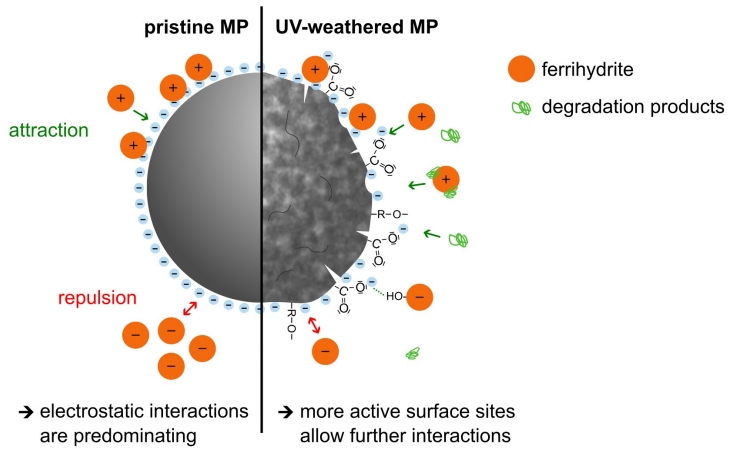

UV-weathering affects heteroaggregation and subsequent sedimentation of polystyrene microplastic particles with ferrihydrite

Johanna Schmidtmann[1], Hannah-Kristin Weishäupl[1], Luisa Hopp[1], Nora Meides[2], Stefan Peiffer[1]*

[1] Department of Hydrology, University of Bayreuth, Bayreuth Center for Ecology and Environmental Research (BayCEER),
[2] Department of Macromolecular Chemistry I, University of Bayreuth

* Corresponding author (j.schmidtmann@uni-bayreuth.de)

Environmental Significance Statement

When microplastic particles enter aquatic environments, they will become exposed to UV-weathering, leading to changes in surface properties, composition and size. Concurrently, such particles will get into contact with natural constituents, driving heteroaggregation and subsequent removal of microplastic particles from the water column upon sedimentation. This work investigates the aggregation and sedimentation of pristine and UV-weathered polystyrene particles with ferrihydrite, a naturally occurring iron(oxy)hydroxide. Our findings suggest that UV-weathering of polystyrene intensifies the interactions with ferrihydrite, potentially reducing the residence time of microplastic particles in the water column and increasing its accumulation in sediments. This knowledge is crucial for understanding the environmental behavior of microplastic, particularly in terms of its distribution in the environment and its long-term ecological effects.

Abstract

Microplastic (MP) particles are ubiquitous in aquatic environments where they become exposed to UV-irradiation with subsequent alteration of surface properties. Such particles will interact with naturally occurring colloids being subject to processes like heteroaggregation that affect both MP surface properties and their removal rates from the water column. In this study, we investigated heteroaggregation and subsequent sedimentation of 1 µm polystyrene (PS, pristine and UV-weathered) with ferrihydrite (Fh), an iron(oxy)hydroxide commonly found in nature. Heteroaggregation of pristine PS with Fh was controlled by electrostatic attraction. At neutral pH values, strong heteroaggregation was observed which led to the sedimentation of almost all PS particles. UV-weathering of PS led to lower negative surface charge, decrease of particle size, and formation of degradation products. Changes in surface properties of PS resulted in a different aggregation behavior with Fh. With increasing weathering time, the isoelectric point (pH_{IEP}) of suspensions with PS and Fh shifted to lower pH values. Furthermore, we observed aggregation and subsequent sedimentation of weathered PS and Fh for a wider pH range (pH 3-7) compared to pristine PS (pH 6.5-7.5). We attribute this observation to increased surface reactivity of PS due to the formation of functional groups on the surface through UV-weathering. In addition, degradation products (e.g. oligomers) formed during weathering might have also interacted with PS and Fh and therefore further affected the surface properties of the particles. Overall, UV-weathering but also interactions of MP particles with environmental particles cause changes of MP surface properties, which influence its environmental behavior in water and might lead to a removal from the water column and accumulation in sediments.

Keywords: degradation, aging, aggregation, settling, transport, colloids

1. Introduction

Microplastic particles (MP, plastic fragments < 5 mm) have been found in nearly every environmental compartment, such as marine and coastal environments[1,2], freshwaters[3,4], soils[5,6], air[7,8], and even at remote places like Antartica[9]. Their widespread distribution has raised concerns about the effect these particles may exert on the functioning of aquatic ecosystems.[10–12] A key requirement for the evaluation of the risk that MP particles pose to the environment and its organisms is a thorough understanding of their transport and fate. In aquatic environments, MP particles are expected to interact with various natural particles and colloids, such as natural organic matter (NOM)[13–15], mineral particles[16–18] or biogenic particles[19–21] which may influence the surface and transport properties of MP particles and eventually lead to heteroaggregation. As an example, coating with NOM, such as humic acids or polysaccharides, may stabilize MP particles in the aqueous phase on the one hand by enhancing electrostatic repulsion and steric hindrance.[22–24] On the other hand, NOM may also lead to destabilization of colloidal MP upon bridging or reversing surface charge.[14,15,22,23,25] Interactions of MP particles with environmental particles appear to be predominantly controlled by electrostatic attraction or repulsion forces and charge neutralization is mainly responsible for heteroaggregation[15,16,18,25] which has been shown to increase the sedimentation rate of MP particles.[16,19–21]

Until now, most studies investigating the interactions of MP particles with environmental particles have been conducted with pristine MP particles.[13,14,16–19] In the environment, however, MP particles are exposed to various weathering processes, including UV-irradiation from the sun. Zhang et al. showed that UV-weathered polystyrene (PS) nanoparticles, unlike the pristine material, interacted with clay minerals and the adsorption of PS nanoparticles onto iron oxides increased with increasing UV-weathering time.[26] UV-induced weathering can lead to changes in chemical composition, surface charge, and mechanical properties of MP particles[27–29], all of which can affect their aggregation behavior. The formation of oxygen-containing functional groups on the MP surface (e.g. carboxyl, peroxy, and keto groups)[27] may increase the number of active surface sites allowing for additional interactions via hydrogen bonding or ion-complexation.[26,30] Overall, these processes increase the hydrophilicity and intensify attractive forces between weathered MP particles and charged environmental particles.[26,30]

Although the importance of UV-weathering of MP particles for interactions with environmental particles and colloids has been demonstrated[26,30], research on the effect of UV-weathering on the heteroaggregation and its effect of sedimentation properties of microplastic particles is still missing.

In this study, we examined the pH-dependent heteroaggregation and subsequent sedimentation of UV-weathered PS particles and ferrihydrite (Fh), a ferric iron (oxy)hydroxide commonly found in the environment.[31–33] In previous work we could show that Fh not only

promotes heteroaggregation but also sedimentation of PS particles.[16] At neutral pH, heteroaggregation between PS and Fh led to almost complete sedimentation of PS particles within just one day.[16] In order to test how heteroaggregation and sedimentation of PS is affected by UV-weathering, we conducted the experiments in this study with PS particles (1 µm), which were pre-weathered in an accelerated UV-chamber for different exposure times. We hypothesize that UV-weathering of PS will render the MP surfaces more reactive and thus intensify the interactions with Fh.

2. Material and Methods

2.1 Material

For the experiments, we used spherical non-functionalized PS particles (diameter 1.01 ± 0.03 µm *microParticles GmbH*, Berlin, Germany). According to the manufacturer, the particles' surfaces contain sulfate from the manufacturing process. The suspension of 10% w/v was diluted to a stock solution of 100 mg L^{-1} with ultrapure water (18.2 MΩ cm). Aggregation and sedimentation experiments were done with a PS concentration of 10 mg L^{-1}. The synthesis of Fh followed the method outlined by Cornell and Schwertmann[34] and previously described in detail by Schmidtmann et al.[16]

2.2 UV-weathering

For UV-weathering experiments of PS particles, we used an UVACUBE 400 irradiation chamber for solar simulation, equipped with a SOL500 lamp (both *Dr. Hönle AG*, Germany). Further information on the weathering chamber can be found in the Supporting Information (Table S1 & S2, Fig. S1). Based on data of the manufacturer, we calculated the acceleration factor of the weathering chamber compared to average irradiation in Germany. The irradiance is 10-fold enhanced (Table S1 & S2). 200 mL of 100 mg L^{-1} PS suspensions were added into 250 mL quartz beakers, closed off with a quartz glass sheet secured with 4 metal clips (Fig. S2) and placed in the chamber for time periods between 0-960 h. For aggregation and sedimentation experiments, PS samples with weathering periods of 0, 48, and 96 h were used. Samples weathered for periods longer than 96 h were only used for the quantification of carbon after each weathering step (see section 2.4.2). To prevent that samples were irradiated with different intensities due to the position in the irradiation chamber, we changed the position of sample beakers in the chamber every 48 h. As the beakers were not sealed gas tight (to allow oxygen supply for the photochemical oxidation) the evaporated amount of water was refilled with ultrapure water every 48 h. After the respective irradiation time was reached, the sample was stored at 4 °C in airtight glass bottles in the dark.

2.3 Sedimentation experiments

Sedimentation experiments were conducted in narrow glass vessels (inner diameter ~ 16 mm). Samples containing either pristine or UV-weathered PS (10 mg L^{-1}) and Fh (10 mg L^{-1}) were prepared under room temperature and ambient pressure. The pH of the samples with a total volume of 10 mL was adjusted to values between 3 and 11 by adding HCl or NaOH. A constant ionic strength of 10 mM was established by addition of adequate amounts of NaCl. Subsequently, the samples were shaken to achieve complete mixing and then allowed to react for one day. This period was chosen as previous work showed that the relevant sedimentation patterns were already observed after one day.[16] Afterwards we carefully removed the upper 8 mL of the samples with a pipette and transferred them to a second sample vial without disturbing any settled particles in the lower 2 mL of the sample. In the following, we will refer to the lower 2 mL of the sample as sediment and to the upper 8 mL of the sample as solution (Fig. S3). The sediment phase was diluted with 6 mL ultrapure water to a volume of 8 mL.
As reference, we analyzed the sedimentation of $PS_{0\text{-}96h}$ in the absence of Fh. Reference samples were prepared under identical conditions (pH 3-11 and ionic strength of 10 mM) and same PS concentration but without Fh.

2.4 TOC analysis

Total organic carbon (TOC) analysis was done to (i) determine the amount of PS that sedimented after reaction with Fh (as described in section 2.3) and (ii) to determine the amount of TOC and dissolved organic carbon (DOC) in PS suspensions after UV-weathering.

2.4.1 Sedimentation

To determine the amount of PS that sedimented in presence or absence of Fh, the carbon content was measured in the sediment as well as in the solution of each sample. A TOC-L-Analyzer (*Shimadzu*, Japan) was used and 10 mg L^{-1} Fh were added to all samples prior measurement as the addition clearly improved the recovery of PS.[35] Approx. 10 minutes prior to analysis, samples were acidified with 2 M HCl and pre-treated in an ultrasonic bath for approx. 5 minutes to dissolve any possible aggregates. To prevent sedimentation of the particles in the sample vial during measurement, the samples were placed on a magnetic stirrer instead of using the auto-sampler of the instrument.

2.4.2 Quantification of TOC and DOC after weathering

To investigate whether or not the PS samples experienced a mass loss during UV-weathering, we conducted TOC-measurements of PS samples after weathering periods of 0-960 h. TOC-analysis was performed in triplets for (i) unfiltered samples and (ii) samples which had been

filtered through 0.45 µm (Chromafil Xtra PA-45/25, *Macherey-Nagel GmbH & Co. KG*, Germany). The unfiltered samples were used to determine the total amount of carbon in each sample. The filtered samples provided information about the quantity of carbon that was present as dissolved substances or fragments < 0.45 µm. As the size fraction of carbon smaller than 0.45 µm is usually termed "DOC", we also use this term in our study. However, please note that even though it contains the word "*dissolved*", it also accounts for fragments, small enough to pass through the 0.45 µm filter. The unfiltered sample at 0 h UV-weathering (PS_{0h}) was set as reference for total carbon concentration (TOC_{0h}) for samples that had been exposed to UV-irradiation. Based on the value of TOC_{0h}, the percentage of TOC and DOC for each weathering period was calculated.

2.5 Determination of zeta potential and hydrodynamic diameter

To investigate surface charge and aggregate size of PS, Fh, and samples containing both particle types, we determined zeta potential and z-averaged hydrodynamic diameter using a ZetaSizer Nano ZS (*Malvern Panalytical*, Germany) by Laser Doppler Electrophoresis or Dynamic Light Scattering (DLS), respectively. A subsample of approximately 1 mL was examined at 25 °C using a folded capillary zeta cell (DTS1070, *Malvern Panalytical*, Germany). Each sample underwent four measurements of electrophoretic mobility, and the results were reported as the average of these measurements with standard deviations. Electrophoretic mobility was converted into zeta potential by use of the Smoluchowski equation as provided by the instrument. All measurements were conducted at a concentration of 10 mg L^{-1} for both PS and Fh, while the pH was adjusted to values ranging from 3 to 11, and the ionic strength was maintained at 10 mM by adding NaCl. Prior to the ZetaSizer analysis, the samples were briefly shaken to re-suspend any sedimented aggregates.

2.6 Scanning Electron Microscopy

SEM analysis was performed to investigate the aggregation of PS and Fh. Sample preparation was the same as described for ZetaSizer measurements. Then, 4 µL of the suspension were dropped onto a glow-discharged carbon-supported TEM copper grid (S160 Plano, Germany) and dried under ambient conditions. The samples were coated with a thin layer of platinum by a Cressington 208 HR sputter coater. SEM images were recorded using secondary electron detectors on a Zeiss ULTRA PLUS (*Carl Zeiss Microscopy GmbH*, Germany).

3. Results and Discussion

3.1 Ferrihydrite characterization

Zeta potential measurements of Fh showed characteristic values for this material (Fig. S4A). The isoelectric point (pH_{IEP}) was located at pH 8, lying in the range of values reported in the literature.[16,36,37] For lower pH values, the zeta potential values were positive and for higher pH values negative. For pH < 5.8, Fh particles exhibited nanometer-scale dimensions (Fig. S4A) and some of the iron (oxy)hydroxide might even have been present as dissolved iron. The count rates for those samples might not be sufficient for reliable light scattering measurements. Consequently, careful consideration should be given to the numerical value of zeta potential and hydrodynamic diameter measurements obtained from Fh samples with pH values < 5.8. Nevertheless, the measurements provided a reasonable estimate for the pH_{IEP}. As expected, maximum homoaggregation of Fh was found at the pH_{IEP}, where repulsive forces between the particles are lowest (Fig. S4B). For samples with pH between 6 and 10, aggregation and sedimentation could be observed as a characteristic red-brown sediment at the bottom of the sample vial.

3.2 Characterization of UV-weathered PS

3.2.1 Formation of surface defects and holes on the surface

UV-weathering had a strong impact on particle size, shape, and surface characteristics. Pristine PS particles were monodisperse and spherically shaped with a smooth surface (Fig. S5). With increasing exposure to UV-weathering, the particle surface became rougher, the particle size decreased and the size distribution between the particles increased (Fig. 1B and additionally Fig. S6 showing SEM images of PS_{48h} - PS_{480h}). Most notably, for weathering times longer than 96 h, we noticed cavities in PS particles (Fig. 1B & Fig. S6D-I). Some particles seemed to become hollow in the center with distinct pierced, or wrinkled surfaces. Similar hollow structures were observed in previous research with spherical 5 µm PS particles[38]. However, to the best of our knowledge, this effect has not yet been observed for plastic particles other than spherical PS beads in the micrometer size range. The mechanism behind the hollowing process remains unclear but may be related to the fabrication process. With increasing weathering time, the heterogeneity of size and shape increased, as we observed varying stages of degradation for the same sample. Some particles showed completely altered surfaces and a crumpled shape, while other particles were smooth and spherical with no visible difference to pristine particles. After 480 h of UV-weathering, no spherical particles were observed anymore. Instead, we found clumps of material, presumably made up of degradation products of the PS particles (Fig. S6K-L).

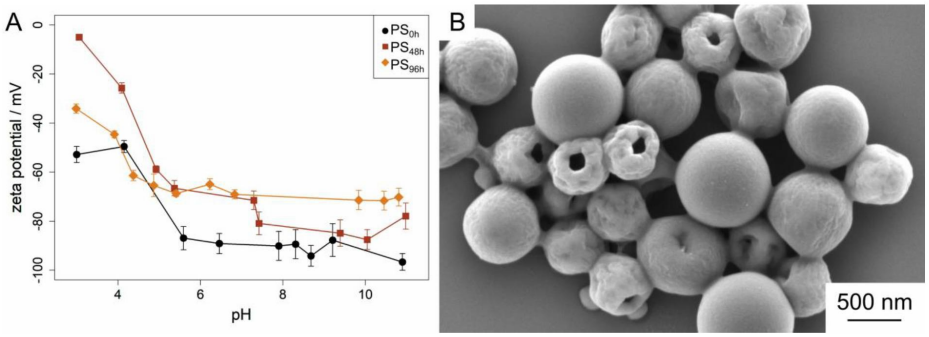

***Fig. 1: A**) Zeta potential values for pristine PS samples (0 h) and PS samples exposed to UV-weathering for 48 and 96 h. **B**) SEM image of PS particles weathered for 144 h.*

3.2.2 UV-weathering results in a decreased negative surface charge

The surface charges of PS particles were negative for all analyzed weathering time steps (0-96 h) over the complete pH range between 3 and 11 (Fig. 1A). The values of pristine particles (PS_{0h}) ranged from -52.9 mV (pH 3) to -96.7 mV (pH 11), indicating strong repulsion between PS particles and therefore a stable dispersion. This was confirmed by sedimentation experiments of PS in the absence of Fh showing only minor sedimentation and no major differences over the tested pH range between 3 and 11 (Fig. S7).

Interestingly, the initial surface charge of the pristine material used in our study was clearly more negative compared to previous studies.[26,39–41] The high negative charge of our PS particles is most likely caused by sulfate groups due to the manufacturing process. With increasing weathering time, PS exhibited less negative zeta potential values in analogy with observations made in UV-weathering studies with 2 µm PS.[42] Most previous studies, however, found increasing negative zeta potential values for UV-weathered PS (diameter between 50 nm and 1 µm)[26,39,40] or polyethylene (PE) particles (diameter 0.4 µm)[41]. The increase in negative surface charge of weathered particles compared to pristine particles was attributed to functional groups formed on the MP surface during UV-weathering, e.g. carboxyl groups[26,39,41]. It is highly probable, that this also happened during our weathering experiments, but became masked by the high initial zeta potential.

Notably, even though the MP particles in previous studies[26,39–41] developed higher negative zeta potentials with UV-weathering, the final values were still less negative than our pristine and UV-weathered PS particles. We therefore propose a combination of two processes taking place for the analyzed 1 µm PS during UV-weathering: (i) cleavage of negatively charged sulfate groups led to a reduction of negative surface charge[39], while (ii) negatively charged

oxygen-containing functional groups were simultanously formed by UV-irradiation. The net effect was a slight shift to a less negative surface charge compared to the initial charge of the pristine particles (Fig. 1A). Unfortunately, we were not able to quantify the amount of leached sulfate in the solution after different weathering periods by use of ion chromatography, with concentrations being below the detection limit (0.1 mg L^{-1}).

3.2.3 UV-weathering converts PS beads to smaller sized fragments

With increasing weathering time, the carbon concentration in the PS suspensions decreased (Fig. 2). Before weathering, the TOC concentration of the unfiltered PS_{0h} sample (100 mg L^{-1}) was 88.0 ± 3.0 mg L^{-1} matching well with the TOC concentration expected based on the carbon content in PS (92.3 mg L^{-1}, PS-monomer: C_8H_8).

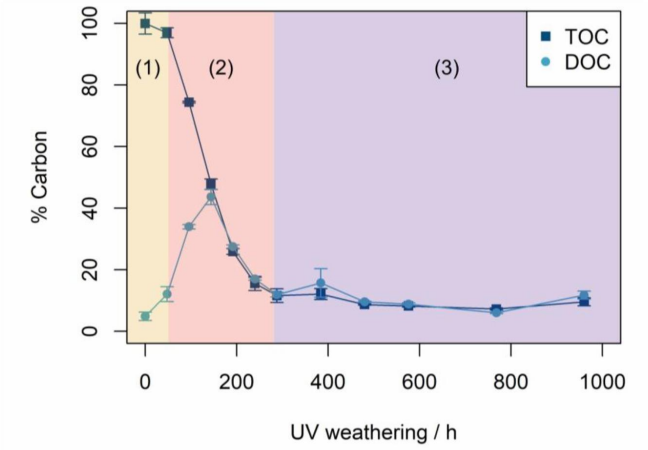

***Fig 2**: Percentage of total (TOC) and dissolved organic carbon (DOC) in PS samples after UV-weathering (0-960 h). DOC accounts for dissolved material and all fragments < 0.45 µm. The percentage was calculated based on the initial carbon concentration in samples before weathering (PS_{0h}). The numbered, colored areas are attributed to the different degradation stages: (1) initiation, (2) propagation, and (3) termination.*

The strongest decrease of TOC was observed between 48-240 h. After 300 h of UV-weathering, only approx. 10% of the initial TOC concentration remained in the samples. This indicates that a substantial portion of carbon (and thus PS) was removed during UV-weathering, likely in gaseous form, as it could not be detected in the solution anymore.
The DOC concentration peaked at 144 h of weathering and decreased again thereafter. The concentrations of TOC and DOC were nearly the same for weathering times larger than 144 h indicating that almost the entire PS particles must have been degraded to fragments smaller

than 0.45 µm or to truly dissolved substances. This was supported by measurements of electrical conductivity (Fig. S8). The initially very low conductivity of 100 mg L^{-1} PS_{0h} suspension (2.7 µS cm^{-1}) increased with UV-weathering to a maximum of 93.8 µS cm^{-1} for PS_{144h}. For longer weathering times, the conductivity decreased again, just as observed for the DOC concentration.

The transformation of 1 µm PS particles to smaller fragments, DOC, and potentially into gas was also visually seen by color and turbidity of the samples. Before UV treatment, the PS suspensions were turbid due to suspended PS particles. With increasing UV-weathering, the suspension cleared out and after 192 h, it visually appeared as a clear solution (Fig. S2).

The stepwise fragmentation of PS including CO_2 formation has previously been reported for UV-weathered PS particles, and was interpreted as degradation of initially formed fragments that are further degraded to water-soluble organics with increasing UV-weathering time.[43,44] Ward et al.[43] measured the DOC concentration in pristine and weathered PS suspensions after filtration. DOC concentrations strongly increased after UV-weathering. They concluded that UV-weathering could partially oxidize PS to DOC and a certain fraction even further to CO_2.[43] The observed loss of mass in carbon and consequently in PS in our experiments might therefore also indicate a transformation of PS into gaseous components like CO_2. Unfortunately, our experimental setup did not allow quantifying those potentially formed gases. The results obtained from Ward et al.[43] cannot directly be compared with those from our experiments as various experimental settings differed. UV chambers and irradiation intensity were different, filter sizes for DOC differed (0.45 µm vs. 0.7 µm[43]) as well as the PS used (1 µm PS beads vs. 192 µm thick PS film[43]). Nevertheless, our observation of temporary increase in DOC and continuous PS mass loss during UV-weathering can be well described with a previously established model for UV based degradation occurring in three stages.[30] In the first *initiation* stage, chain scission of polymer chains occurs accompanied by the formation of radicals (e.g. $R^{\cdot}$, $RO^{\cdot}$, $ROO^{\cdot}$) and reactive oxygen species (ROS), such as hydroxyl ($\cdot OH$) or superoxide ($O_2^{\cdot-}$) radicals takes place.[30] In the following *propagation* stage, highly active radicals promote self-catalyzed reactions[30] and the analyzed PS particles degrade further into smaller particles, dissolved species and gaseous components. Eventually, the *termination* stage is marked by the total mineralization of PS particles.[30] However, for the analyzed 1 µm PS particles, approx. 10% of the initial TOC remained in the sample and were therefore not transformed into gas with the duration of our experiments (Fig. 2).

For UV exposure times of 144 h and longer, almost all PS was recovered in the fraction < 0.45 µm and approx. 50% of the carbon presumably degassed from the sample (Fig. 2). Therefore, we conducted heteroaggregation and sedimentation experiments only for the time steps of 0, 48 and 96 h.

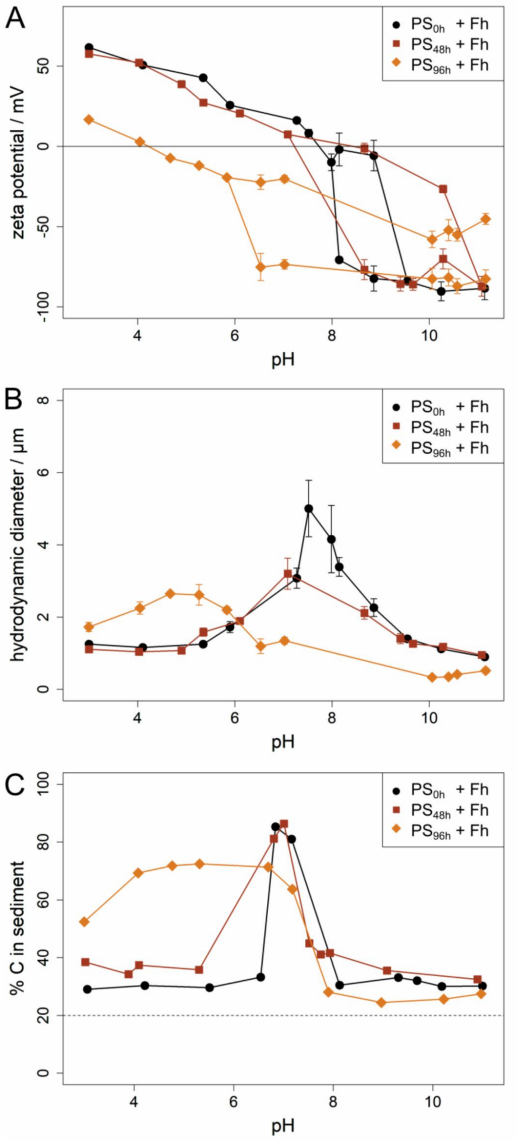

Fig 3. A*) Zeta potential values and* ***B****) hydrodynamic diameter of samples with (UV-weathered) PS and Fh after a reaction time of one day.* ***C****) Sedimentation of (UV-weathered) PS in the presence of Fh: Percentage of carbon (% C) found in the sediment after a settling time of one day. In a well-mixed dispersion, where no sedimentation takes place, 20% of the total PS in the sample (dashed line) should be found in the sediment due to the experimental setup (Fig. S3).*

3.3 Heteroaggregation and subsequent sedimentation of pristine and UV-weathered PS with Fh

3.3.1 Electrostatic interactions control aggregation of pristine and shortly weathered PS with Fh

The observations made for PS_{0h} confirmed results of previous work demonstrating that aggregation of pristine MP particles and iron minerals is controlled by electrostatic attraction.[16,26,41] At acidic pH values, the negatively charged PS particles became coated with positively charged Fh nanoparticles[16], which then led to charge reversal at the PS surfaces from negative to positive (Fig. 3A).[16] Under these conditions, no larger aggregates can be formed, since the coated PS particles tend to repel each other due to the positively charged Fh nanoparticles on their surface (Fig. 3A+B).[16] At neutral pH values, the negatively charged PS particles were also coated with Fh.[16] However, as the surface charge of the heteroaggregates was almost neutral at this pH range, it allowed formation of larger heteroaggregates up to several micrometers (Fig. 3B).[16] At alkaline pH values, both particle types are negatively charged, repel each other, and therefore stay separated in suspension.[16] As a consequence, two peaks in electrophoretic mobility were identified reflecting two distinct zeta potentials (Fig. S9) that refer to two particle fractions. The lower values (~ -80 mV) can be attributed to pristine PS particles while the higher values (~ -10 mV) correspond to values measured for Fh alone (Fig. S10A).[16]

In accordance to previous findings, heteroaggregation resulted in sedimentation of PS particles.[16,19,20,45–48] At neutral pH, where we observed maximum heteroaggregation, we also found maximum sedimentation of PS particles in the presence of Fh (Fig. 3C). Approx. 85% of the initially added amount of PS particles was detected in the sediment at pH 6.8 after one day of settling. Contrary, at pH values at which no increase in aggregate size was observed, also no major sedimentation of PS particles was found (Fig. 3B+C & Fig. S7).

The shortest exposure time to UV-weathering of PS particles (48 h) had minor influence on the heteroaggregation and sedimentation behavior with Fh. Zeta potentials were rather similar to pristine samples and only the maximum aggregate size decreased slightly (Fig. 3A+B). SEM images of those samples showed a similar pattern compared to reaction of pristine samples with Fh[16]: PS_{48h} particles were covered with a thin Fh coating at acidic pH and strong heteroaggregation of PS_{48h} and Fh took place at neutral pH (Fig. 4A-B). Altogether, the observations suggest, that similar to the pristine samples, heteroaggregation of PS_{48h} and Fh was dominated by electrostatic attraction in this initial weathering phase. Furthermore, as in the presence of pristine samples, maximum sedimentation was found at pH 7 with approx. 85% of the carbon being detected in the sediment after one day. At pH values at which no

larger heteroaggregates between PS_{48h} and Fh were formed, no increased sedimentation took place (Fig. 3B+C, Fig. S7).

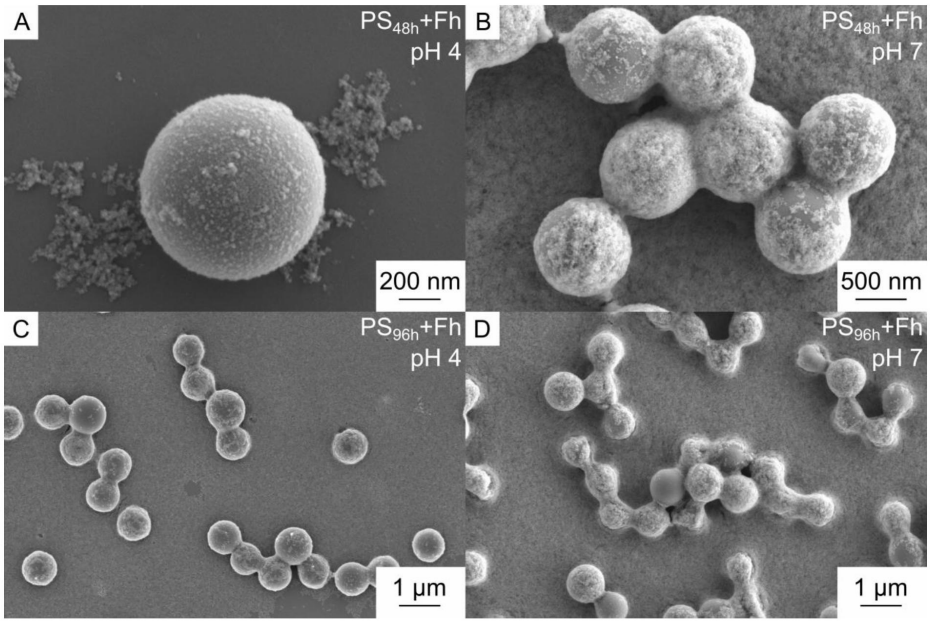

Fig. 4. SEM Images of UV-weathered PS and ferrihydrite (Fh) after one day reaction time. For PS_{48h}, a thin ferrihydrite coating was observed at pH 4 (**A**) and at pH 7 strong heteroaggregation between PS and Fh (**B**). For PS_{96h}, heteroaggregation with Fh was observed at acidic as well as neutral pH values (**C**+**D**).

3.3.2 Contribution of specific interactions to heteroaggregation of PS with Fh after extended UV-weathering time

Compared to the early stage of weathering (0-48 h), exposure of PS particles to an extended weathering period (96 h) led to clearly differing patterns of aggregation with Fh. Similarly to the short weathering period, the tendency of decreasing zeta potential with increasing pH was also observed under these conditions. However, the range of zeta potentials measured over the entire pH range was distinctly smaller for suspensions containing PS particles irradiated for 96 h (+16 to -87 mV) compared to those that experienced a shorter UV exposure time (0-48 h) (+60 to -90 mV) (Fig. 3A). At low pH values, the particle mixture no longer exhibited the highly positive zeta potentials observed in the initial weathering phase but changed to weakly positive

or even negative values close to zero. Also, the pH_{IEP} in suspensions containing PS_{96h} particles and Fh was shifted to a lower, acidic pH value of approx. 4 (Fig. 3A). Thereby, the pH range at which maximum heteroaggregation of PS_{96h} particles and Fh occurred (as indicated by the maximum in hydrodynamic diameter) was also shifted to lower pH values, however, with a lower maximum aggregate size compared to pristine particles (Fig. 3B).

The strong change in the heteroaggregation pattern of PS_{96h} particles with Fh compared to $PS_{0\text{-}48h}$ particles with Fh cannot be explained solely by the observed decrease in negative surface charge of PS particles with increasing weathering time (Fig. 1A). Therefore, we propose that further interaction forces were involved in driving heteroaggregation between PS_{96h} particles and Fh.

Previous research has demonstrated that due to the formation of oxygen-containing functional groups on the MP surface upon weathering, interaction forces other than electrostatic attraction may become active, e.g. hydrogen bonding or ligand exchange.[26,30] As a consequence, UV-weathered (negatively charged) PS nanoparticles were found to be absorbed onto negatively charged minerals despite electrostatic repulsion.[26] Moreover, the formation of degradation products during UV-weathering, which we partly determined as DOC, is indicating a shift in the size spectrum of PS_{96h} particles and the formation of particles with a surface composition containing surface sites in larger quantity and in different quality as compared to $PS_{0\text{-}48h}$ particles. Such properties may have additional effects on the heteroaggregation process. The highest DOC concentrations were determined for PS particles that were exposed to weathering between 96 h and 192 h (Fig. 2). Hence, the complexity of the composition of the sample containing PS_{96h} particles increased compared to that containing $PS_{0\text{-}48h}$ particles. Not only PS particles (with altered properties due to weathering), but additionally, very small (filterable) particles and even dissolved substances formed during weathering may have interacted with Fh, thereby stimulating aggregation.

We therefore propose that the formation of heteroaggregates between PS_{96h} particles and Fh at acidic pH (Fig. 3A+B & Fig. 4C+D) was not simply caused by interactions between negatively charged PS_{96h} particles and positively charged Fh particles alone, but by additional interactions of these particles with degradation products formed during UV-weathering (and partly recovered as DOC fraction). As a consequence, mildly weathered PS_{96h} particles became coated with Fh and further interacted with strongly weathered degradation products, thereby reducing the net surface charge and allowing for aggregation. In parallel, reduction of the net charge of Fh may have been occurred by direct reaction with strongly weathered degradation products to values that still allowed for interactions with PS_{96h} particles, yet reducing their zeta potential.

It appears that these interactions led to a reduction of the repulsive forces of PS_{96h} particles coated with Fh-DOC-particles at acidic pH values so that further aggregation of the particles

took place. Hence, maximum aggregation of PS_{96h} particles and Fh was observed in this pH range. These considerations are underpinned by SEM images showing aggregates of several PS particles (Fig. 4C). Compared to samples with shorter UV exposure times (0-48 h), the maximum heteroaggregate size of PS_{96h} with Fh was smaller (Fig. 3B). We attribute this to two factors: Firstly, the PS particle size decreases with increasing weathering time. Secondly, the particle size of Fh alone differed strongly between the pH values (Fig. S4B). Whereas homoaggregation of Fh was observed at neutral pH, resulting in particle sizes of a few micrometers, the Fh particles at acidic pH range were considerably smaller (Fig. S4B). Hence, the different particle sizes of Fh at different pH ranges probably contributed to the different maximum heteroaggregate sizes observed for heteroaggregation of Fh with $PS_{0\text{-}48h}$ compared to heteroaggregation with PS_{96h}.

As heteroaggregation is driving sedimentation of MP particles[16], the shift in the pH-range in which heteroaggregation was observed also influenced the sedimentation rate of PS_{96h} in the presence of Fh. Instead of a clear maximum at neutral pH (as observed for PS_{0h} and PS_{48h}), we found maximum sedimentation rates over a pH range between 3 and 7 (Fig. 3C). With 70% of the carbon being recovered in the sediment, the maximum sedimentation rate was lower compared to pristine particles. The decrease in maximum sedimentation rate of PS_{96h} in the presence of Fh can on the one hand be explained by the composition of the heteroaggregates and the smaller aggregate size. As explained above, the maximum heteroaggregate size of pristine PS with Fh was clearly larger compared to PS_{96h} with Fh, likely due to the larger particle/aggregate size of Fh at neutral pH range compared to acidic pH values. On the other hand, with increasing weathering, the degradation of PS particles to smaller fragments and dissolved substances is proceeding. Dissolved substances that were not involved in aggregation with PS_{96h} or Fh particles likely remained in the solution and thus did not contribute to the carbon found in the sediment.

However, even though the sedimentation rate slightly decreased, the pH range at which strong sedimentation of PS_{96h} particles in the presence of Fh was observed, was clearly larger (pH 3-7) compared to pristine samples (pH 6.5-7.5). Hence, UV-weathering of PS allowed intensified interactions with Fh, which resulted in sedimentation taking place over a broader pH range.

At neutral and alkaline pH (pH 6-11), a splitting of zeta potentials into two curves was observed for measurements performed after 96 h weathering (Fig. 3A). For PS exposed to a weathering time of 0 and 48 h, the split curves matched very well those curves obtained from samples containing either Fh only or PS only (Fig. S10A+C) indicating the occurrence of two domains of particles with different zeta potentials. However, for the longer UV-weathering period, zeta potential values matched only the lower zeta potential curve for pure PS, while the upper curve was located in between the curves of pure PS and pure Fh (Fig. S10E). This observation suggests that the surface charge of Fh was reduced in the neutral and alkaline pH range,

presumably by adsorption of PS degradation products, which were partly recovered as DOC. On the other hand, some Fh particles might have adsorbed onto PS_{96h}. Even though both particles were negatively charged at alkaline pH, weathering-induced oxygen-containing functional groups on PS surfaces might have promoted interactions via hydrogen bonding.[26] Hence, a partial adsorption of Fh onto PS_{96h} increased the net surface charge and might explain the zeta potential curve with values in-between unreacted Fh and PS.

The occurrence of two classes of particles causing the observed splitting of zeta potentials was corroborated by SEM measurements. At neutral pH, some PS_{96h} particles were strongly coated by Fh and aggregates of several particles occurred (Fig. 4D). At the same time, other PS_{96h} particles remained almost uncoated. Hence, UV-induced changes of PS properties (e.g. size, shape, surface charge, composition) resulted in a more heterogeneous mixture of PS. This led to a greater variety of interactions with Fh (Fig. 5), allowing adsorption and aggregation processes to take place over a broader pH range compared to pristine particles.

Conclusion

In our study, we demonstrated that UV-weathering stimulates heteroaggregation and sedimentation of PS with iron (oxy)hydroxides. UV-weathering led to alteration of PS surface properties, strong fragmentation, and degradation of the particles. The increased reactivity of the PS surface due to UV-weathering, and the formation of degradation products triggered heteroaggregation and subsequent sedimentation over a broad pH range. The different interactions between pristine and UV-weathered MP particles with Fh are displayed in Fig. 5. Hence, our results indicate that UV-weathering further enhances aggregation-facilitated removal of MP particles from the aqueous phase.

In the environment, the resulting degradation products will be quickly distributed in larger water bodies, unlike in our laboratory experiments. Furthermore, the number of naturally occurring particles is by far larger than the one of MP particles[49]. Therefore, considering these two factors, the direct interaction of MP degradation products and MP particles themselves is unlikely in natural settings. Instead, we propose that MP degradation products, measured as DOC fraction, strongly interact with environmental particles either through electrostatic or specific interactions (e.g. hydrogen bonding). Hence, under real environmental conditions, MP degradation products may become part of the natural DOC fraction adsorbing to iron (oxy)hydroxides[50,51] and forming iron-DOC flocs[51,52] which might be transported as environmental colloids affecting the overall fate of MP particles.

In future research, it remains to be tested to what extent the findings made for 1 µm PS beads in our experiments can be generalized for a broad range of MP particles with diverse properties (type of polymer, size, shape, density etc.).

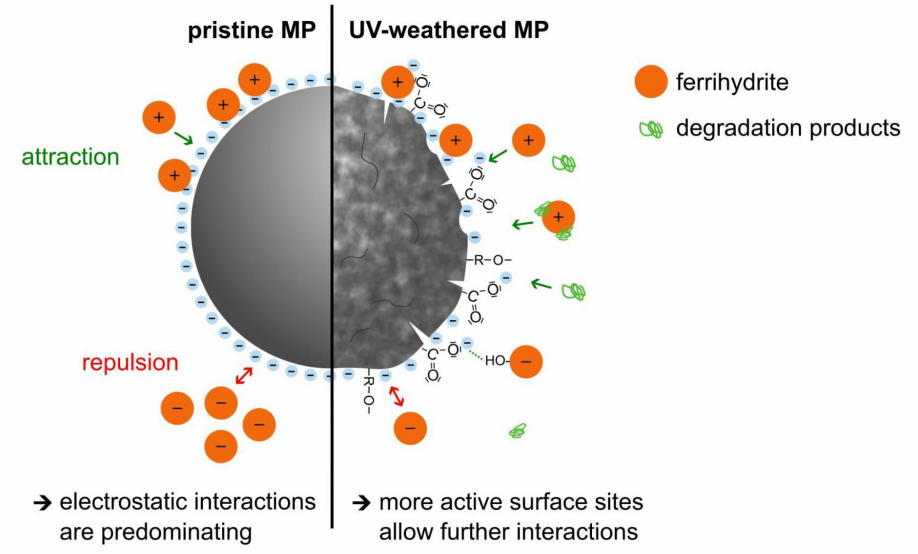

Fig 5. *Conceptual model representing the different interactions of pristine and UV-weathered PS particles with Fh. For pristine MP particles (left), the interactions with Fh are predominated by electrostatic interactions. With increasing UV-weathering (UV-weathered MP, right), not only are there more active surface sites formed on the MP surface, that allow further interactions (e.g. hydrogen bonding) with Fh. Additionally, degradations products might also interact with Fh or the MP particles.*

Conflicts of interest
There are no conflicts to declare.

Acknowledgements

The study was funded by the Deutsche Forschungsgemeinschaft (DFG, German Research Foundation) – Project Number 391977956 – SFB 1357. The authors would like to thank Dr. Ulrich Mansfeld and Martina Heider for taking SEM images at the Bavarian Polymer Institute (BPI).

References

1 M. A. Browne, P. Crump, S. J. Niven, E. Teuten, A. Tonkin, T. Galloway and R. Thompson, Accumulation of microplastic on shorelines woldwide: sources and sinks, *Environmental science & technology*, 2011, **45**, 9175–9179.

2 A. Cózar, F. Echevarría, J. I. González-Gordillo, X. Irigoien, B. Úbeda, S. Hernández-León, Á. T. Palma, S. Navarro, J. García-de-Lomas, A. Ruiz, M. L. Fernández-de-Puelles and C. M. Duarte, Plastic debris in the open ocean, *Proceedings of the National Academy of Sciences*, 2014, **111**, 10239–10244.

3 D. Eerkes-Medrano, R. C. Thompson and D. C. Aldridge, Microplastics in freshwater systems: A review of the emerging threats, identification of knowledge gaps and prioritisation of research needs, *Water Research*, 2015, **75**, 63–82.

4 A. A. Horton, A. Walton, D. J. Spurgeon, E. Lahive and C. Svendsen, Microplastics in freshwater and terrestrial environments: Evaluating the current understanding to identify the knowledge gaps and future research priorities, *Science of The Total Environment*, 2017, **586**, 127–141.

5 M. Scheurer and M. Bigalke, Microplastics in Swiss Floodplain Soils, *Environ. Sci. Technol.*, 2018, **52**, 3591–3598.

6 K. A. V. Zubris and B. K. Richards, Synthetic fibers as an indicator of land application of sludge, *Environmental Pollution*, 2005, **138**, 201–211.

7 R. Dris, J. Gasperi, M. Saad, C. Mirande and B. Tassin, Synthetic fibers in atmospheric fallout: A source of microplastics in the environment?, *Marine Pollution Bulletin*, 2016, **104**, 290–293.

8 L. Cai, J. Wang, J. Peng, Z. Tan, Z. Zhan, X. Tan and Q. Chen, Characteristic of microplastics in the atmospheric fallout from Dongguan city, China: preliminary research and first evidence, *Environ Sci Pollut Res*, 2017, **24**, 24928–24935.

9 A. Kelly, D. Lannuzel, T. Rodemann, K. M. Meiners and H. J. Auman, Microplastic contamination in east Antarctic sea ice, *Marine Pollution Bulletin*, 2020, **154**, 111130.

10 SAPEA, *A Scientific Perspective on Microplastics in Nature and Society*, SAPEA, Science Advice for Policy by European Academies, Berlin, 2019.

11 S. Lambert and M. Wagner, in *Freshwater Microplastics : Emerging Environmental Contaminants?*, eds. M. Wagner and S. Lambert, Springer International Publishing, Cham, 2018, pp. 1–23.

12 L. Persson, B. M. Carney Almroth, C. D. Collins, S. Cornell, C. A. de Wit, M. L. Diamond, P. Fantke, M. Hassellöv, M. MacLeod, M. W. Ryberg, P. Søgaard Jørgensen, P. Villarrubia-Gómez, Z. Wang and M. Z. Hauschild, Outside the Safe Operating Space of the Planetary Boundary for Novel Entities, *Environ. Sci. Technol.*, 2022, **56**, 1510–1521.

13 L. Cai, L. Hu, H. Shi, J. Ye, Y. Zhang and H. Kim, Effects of inorganic ions and natural organic matter on the aggregation of nanoplastics, *Chemosphere*, 2018, **197**, 142–151.

14 S. Li, H. Liu, R. Gao, A. Abdurahman, J. Dai and F. Zeng, Aggregation kinetics of microplastics in aquatic environment: Complex roles of electrolytes, pH, and natural organic matter, *Environmental Pollution*, 2018, **237**, 126–132.

15 A. Pradel, S. Ferreres, C. Veclin, H. El Hadri, M. Gautier, B. Grassl and J. Gigault, Stabilization of Fragmental Polystyrene Nanoplastic by Natural Organic Matter: Insight into Mechanisms, *ACS EST Water*, 2021, **1**, 1198–1208.

16 J. Schmidtmann, H. Elagami, B. S. Gilfedder, J. H. Fleckenstein, G. Papastavrou, U. Mansfeld and S. Peiffer, Heteroaggregation of PS microplastic with ferrihydrite leads to rapid removal of microplastic particles from the water column, *Environ. Sci.: Processes Impacts*, 2022, **24**, 1782–1789.

17 T. T. T. Vu, P. H. Nguyen, T. V. Pham, P. Q. Do, T. T. Dao, A. D. Nguyen, L. Nguyen-Thanh, V. M. Dinh and M. N. Nguyen, Comparative effects of crystalline, poorly crystalline and freshly formed iron oxides on the colloidal properties of polystyrene microplastics, *Environmental Pollution*, 2022, **306**, 119474.

18 O. Oriekhova and S. Stoll, Heteroaggregation of nanoplastic particles in the presence of inorganic colloids and natural organic matter, *Environ. Sci.: Nano*, 2018, **5**, 792–799.

19 F. Lagarde, O. Olivier, M. Zanella, P. Daniel, S. Hiard and A. Caruso, Microplastic interactions with freshwater microalgae: Hetero-aggregation and changes in plastic density appear strongly dependent on polymer type, *Environmental Pollution*, 2016, **215**, 331–339.

20 M. Long, B. Moriceau, M. Gallinari, C. Lambert, A. Huvet, J. Raffray and P. Soudant, Interactions between microplastics and phytoplankton aggregates: Impact on their respective fates, *Marine Chemistry*, 2015, **175**, 39–46.

21 J. Michels, A. Stippkugel, M. Lenz, K. Wirtz and A. Engel, Rapid aggregation of biofilm-covered microplastics with marine biogenic particles, *Proceedings of the Royal Society B*, 2018, **285**, 20181203.

22 Y. Liu, Z. Huang, J. Zhou, J. Tang, C. Yang, C. Chen, W. Huang and Z. Dang, Influence of environmental and biological macromolecules on aggregation kinetics of nanoplastics in aquatic systems, *Water Research*, 2020, **186**, 116316.

23 N. Singh, E. Tiwari, N. Khandelwal and G. K. Darbha, Understanding the stability of nanoplastics in aqueous environments: effect of ionic strength, temperature, dissolved organic matter, clay, and heavy metals, *Environmental Science: Nano*, 2019, **6**, 2968–2976.

24 X. Wang, N. Bolan, D. C. W. Tsang, S. Binoy, L. Bradney and Y. Li, A review of microplastics aggregation in aquatic environment: Influence factors, analytical methods, and environmental implications, *Journal of Hazardous Materials*, 2021, 123496.

25 S. Lu, K. Zhu, W. Song, G. Song, D. Chen, T. Hayat, N. S. Alharbi, C. Chen and Y. Sun, Impact of water chemistry on surface charge and aggregation of polystyrene microspheres suspensions, *Science of The Total Environment*, 2018, **630**, 951–959.

26 Y. Zhang, Y. Luo, X. Yu, D. Huang, X. Guo and L. Zhu, Aging significantly increases the interaction between polystyrene nanoplastic and minerals, *Water Research*, 2022, **219**, 118544.

27 N. Meides, T. Menzel, B. Poetzschner, M. G. J. Löder, U. Mansfeld, P. Strohriegl, V. Altstaedt and J. Senker, Reconstructing the Environmental Degradation of Polystyrene by Accelerated Weathering, *Environ. Sci. Technol.*, 2021, **55**, 7930–7938.

28 T. Menzel, N. Meides, A. Mauel, U. Mansfeld, W. Kretschmer, M. Kuhn, E. M. Herzig, V. Altstädt, P. Strohriegl, J. Senker and H. Ruckdäschel, Degradation of low-density polyethylene to nanoplastic particles by accelerated weathering, *Science of The Total Environment*, 2022, **826**, 154035.

29 N. Meides, A. Mauel, T. Menzel, V. Altstädt, H. Ruckdäschel, J. Senker and P. Strohriegl, Quantifying the fragmentation of polypropylene upon exposure to accelerated weathering, *Microplastics and Nanoplastics*, 2022, **2**, 23.

30 J. Duan, N. Bolan, Y. Li, S. Ding, T. Atugoda, M. Vithanage, B. Sarkar, D. C. W. Tsang and M. B. Kirkham, Weathering of microplastics and interaction with other coexisting constituents in terrestrial and aquatic environments, *Water Res*, 2021, **196**, 117011.

31 P. Joshi and A. Kappler, in *Encyclopedia of Astrobiology*, eds. M. Gargaud, W. M. Irvine, R. Amils, P. Claeys, H. J. Cleaves, M. Gerin, D. Rouan, T. Spohn, S. Tirard and M. Viso, Springer, Berlin, Heidelberg, 2020, pp. 1–4.

32 U. Schwertmann and R. M. Cornell, *Iron oxides in the laboratory: preparation and characterization*, John Wiley & Sons Ltd, Weinheim, 2000.

33 A. Kappler, C. Bryce, M. Mansor, U. Lueder, J. M. Byrne and E. D. Swanner, An evolving view on biogeochemical cycling of iron, *Nat Rev Microbiol*, 2021, **19**, 360–374.

34 R. M. Cornell and U. Schwertmann, *The Iron Oxides: Structure, Properties, Reactions, Occurrences and Uses*, John Wiley & Sons, 2003.

35 J. Schmidtmann and S. Peiffer, A rapid method to quantify sub-micrometer polystyrene particles in aqueous model systems by TOC analysis, *Microplastics and Nanoplastics*, , DOI:10.1186/s43591-024-00080-y.

36 M. Kosmulski, Isoelectric points and points of zero charge of metal (hydr)oxides: 50years after Parks' review, *Advances in Colloid and Interface Science*, 2016, **238**, 1–61.

37 J. Liu, S. M. Louie, C. Pham, C. Dai, D. Liang and Y. Hu, Aggregation of ferrihydrite nanoparticles: Effects of pH, electrolytes,and organics, *Environmental Research*, 2019, **172**, 552–560.

38 Z. Liu, Y. Zhu, S. Lv, Y. Shi, S. Dong, D. Yan, X. Zhu, R. Peng, A. A. Keller and Y. Huang, Quantifying the Dynamics of Polystyrene Microplastics UV-Aging Process, *Environ. Sci. Technol. Lett.*, 2022, **9**, 50–56.

39 Y. Liu, Y. Hu, C. Yang, C. Chen, W. Huang and Z. Dang, Aggregation kinetics of UV irradiated nanoplastics in aquatic environments, *Water Research*, 2019, **163**, 114870.

40 J. Liu, T. Zhang, L. Tian, X. Liu, Z. Qi, Y. Ma, R. Ji and W. Chen, Aging Significantly Affects Mobility and Contaminant-Mobilizing Ability of Nanoplastics in Saturated Loamy Sand, *Environ. Sci. Technol.*, 2019, **53**, 5805–5815.

41 Y. Wang, X. Chen, F. Wang and N. Cheng, Influence of typical clay minerals on aggregation and settling of pristine and aged polyethylene microplastics, *Environmental Pollution*, 2023, **316**, 120649.

42 M. Völkl, V. Jérôme, A. Weig, J. Jasinski, N. Meides, P. Strohriegl, T. Scheibel and R. Freitag, Pristine and artificially-aged polystyrene microplastic particles differ in regard to cellular response, *Journal of Hazardous Materials*, 2022, **435**, 128955.

43 C. P. Ward, C. J. Armstrong, A. N. Walsh, J. H. Jackson and C. M. Reddy, Sunlight Converts Polystyrene to Carbon Dioxide and Dissolved Organic Carbon, *Environ. Sci. Technol. Lett.*, 2019, **6**, 669–674.

44 P. Pfohl, M. Wagner, L. Meyer, P. Domercq, A. Praetorius, T. Hüffer, T. Hofmann and W. Wohlleben, Environmental Degradation of Microplastics: How to Measure Fragmentation Rates to Secondary Micro- and Nanoplastic Fragments and Dissociation into Dissolved Organics, *Environ. Sci. Technol.*, 2022, **56**, 11323–11334.

45 P. Möhlenkamp, A. Purser and L. Thomsen, Plastic microbeads from cosmetic products: an experimental study of their hydrodynamic behaviour, vertical transport and resuspension in phytoplankton and sediment aggregates, *Elementa: Science of the Anthropocene*, , DOI:10.1525/elementa.317.

46 Y. Li, X. Wang, W. Fu, X. Xia, C. Liu, J. Min, W. Zhang and J. C. Crittenden, Interactions between nano/micro plastics and suspended sediment in water: Implications on aggregation and settling, *Water research*, 2019, **161**, 486–495.

47 R. Leiser, G.-M. Wu, T. R. Neu and K. Wendt-Potthoff, Biofouling, metal sorption and aggregation are related to sinking of microplastics in a stratified reservoir, *Water Research*, 2020, 115748.

48 R. Leiser, R. Jongsma, I. Bakenhus, R. Möckel, B. Philipp, T. R. Neu and K. Wendt-Potthoff, Interaction of cyanobacteria with calcium facilitates the sedimentation of microplastics in a eutrophic reservoir, *Water Res*, 2021, **189**, 116582.

49 A. A. Koelmans, P. E. Redondo-Hasselerharm, N. H. M. Nor, V. N. de Ruijter, S. M. Mintenig and M. Kooi, Risk assessment of microplastic particles, *Nat Rev Mater*, 2022, **7**, 138–152.

50 B. Gu, T. L. Mehlhorn, L. Liang and J. F. McCarthy, Competitive adsorption, displacement, and transport of organic matter on iron oxide: I. Competitive adsorption, *Geochimica et Cosmochimica Acta*, 1996, **60**, 1943–1950.

51 E. L. Sharp, P. Jarvis, S. A. Parsons and B. Jefferson, The Impact of Zeta Potential on the Physical Properties of Ferric−NOM Flocs, *Environ. Sci. Technol.*, 2006, **40**, 3934–3940.

52 I. G. Droppo, G. G. Leppard, D. T. Flannigan and S. N. Liss, The Freshwater Floc: A Functional Relationship of Water and Organic and Inorganic Floc Constituents Affecting Suspended Sediment Properties, *Water, Air, & Soil Pollution*, 1997, **99**, 43–54.

Supporting Information

UV-weathering affects heteroaggregation and subsequent sedimentation of polystyrene microplastic particles with ferrihydrite

Johanna Schmidtmann[1*], Hannah-Kristin Weishäupl[1], Luisa Hopp[1], Nora Meides[2], Stefan Peiffer[1]

[1] Department of Hydrology, University of Bayreuth, Bayreuth Center for Ecology and Environmental Research (BayCEER), Bayreuth, Germany

[2] Department of Macromolecular Chemistry I, University of Bayreuth, Bayreuth, Germany

* Corresponding author: j.schmidtmann@uni-bayreuth.de

List of Tables

List of Figures

Table S1. Calculation of the total irradiance of the UV-weathering chamber and the acceleration factor for Germany.

Solar irradiation per year (Germany)	1086	kWh m^{-2}
Hours of solar irradiation per year	8760	h
Average solar irradiation intensity (Germany)	124	W m^{-2}
Irradiation intensity UVACUBE + SOL500	1216.11	W m^{-2}
Acceleration factor	**9.81**	

For the calculation of the total irradiance of the PS particles in the weathering chamber, we used the global radiation in Germany (mean 30-year monthly and annual sums) as reference. For the period 1991-2020, the average radiation per year is 1086 kWh m^{-2}.[1]

Compared to the average irradiation in Germany, the irradiance in the weathering chamber is approx. 10-fold enhanced.

Table S2. Application of the acceleration factor to the UV-weathering periods used in this study.

UV-weathering (hours)	Theoretical weathering time in Germany (days)
48	20
96	39
144	59
192	78
240	98
480	196
960	392

[1] https://www.dwd.de/EN/ourservices/solarenergy/maps_globalradiation_mvs.html;jsessionid=1A740BA78B9C6A53FD423260F80C3EED.live11051?nn=495490, accessed 26.07.2023

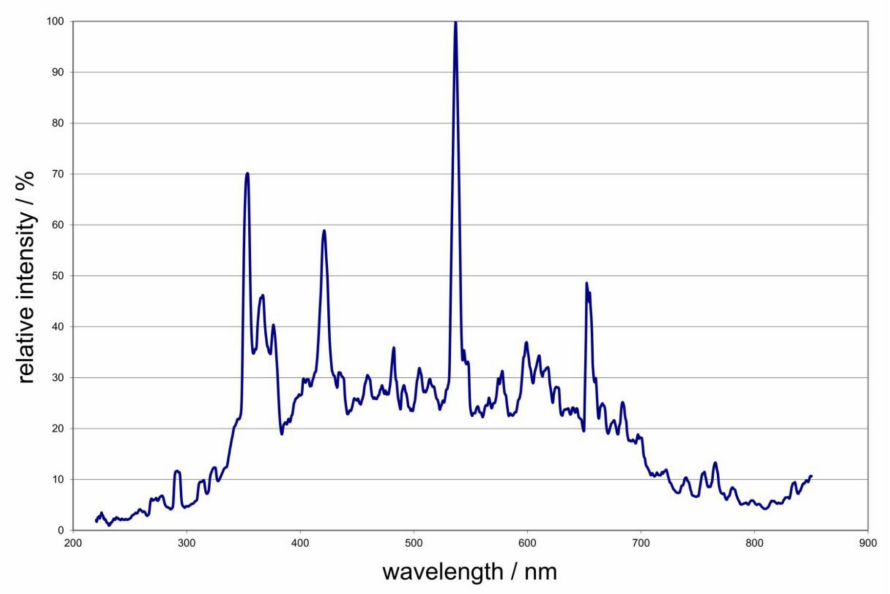

Figure. S1. Wavelength spectrum of a SOL500S lamp (without filterglass). The graph was provided by *Dr. Hönle AG*.

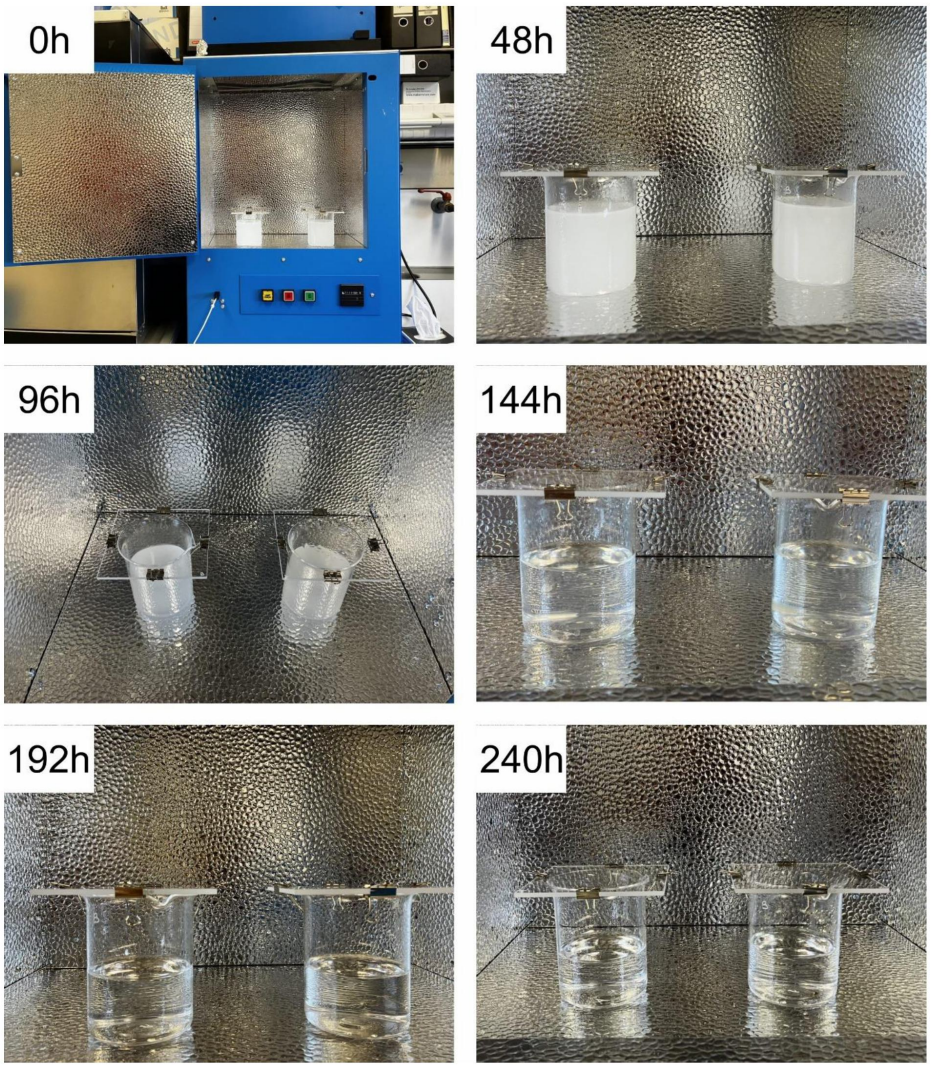

Figure S2. Images of the initial 100 mg L^{-1} PS suspensions after different UV weathering durations in the weathering chamber.

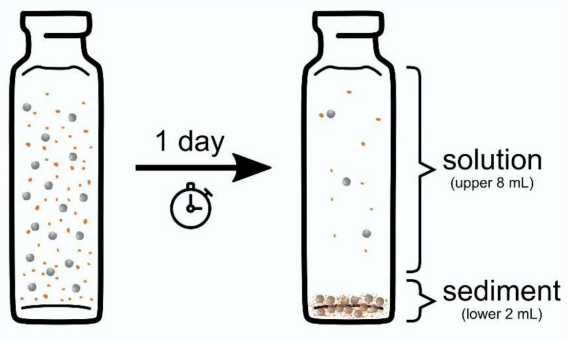

Figure S3. Simplified illustration of the sedimentation experiments with 10 mg L^{-1} PS and 10 mg L^{-1} ferrihydrite.

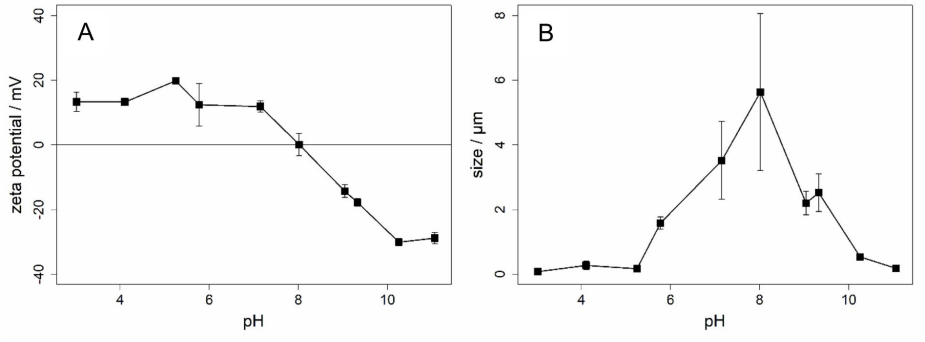

Figure S4. Zeta potential (**A**) and hydrodynamic diameter (**B**) of 10 mg L^{-1} ferrihydrite. At acidic pH values, the particle size of ferrihydrite was only in nanometer size range and some of the material might have been present as dissolved iron. Therefore, the count rates of these samples might have been insufficient for reliable light scattering measurements.[2]

[2] Schmidtmann et al., Environ. Sci.: Processes Impacts, 2022, 24, 1782–1789.

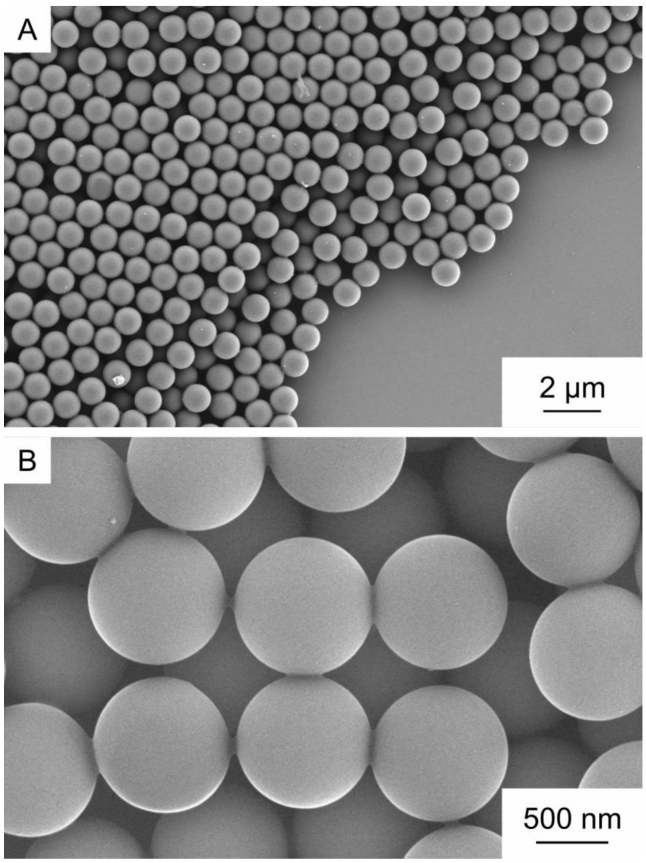

Figure S5. SEM images of pristine PS particles.

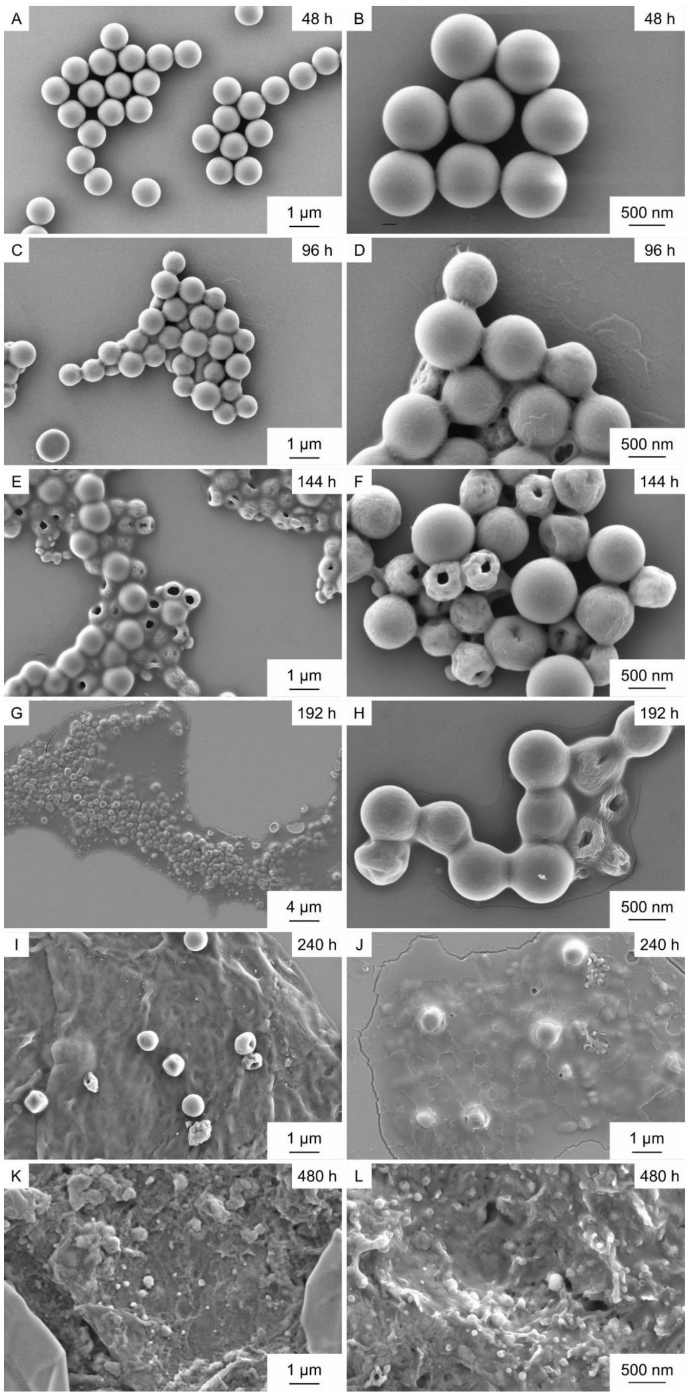

Figure S6. SEM images of UV-weathered PS particles.

9

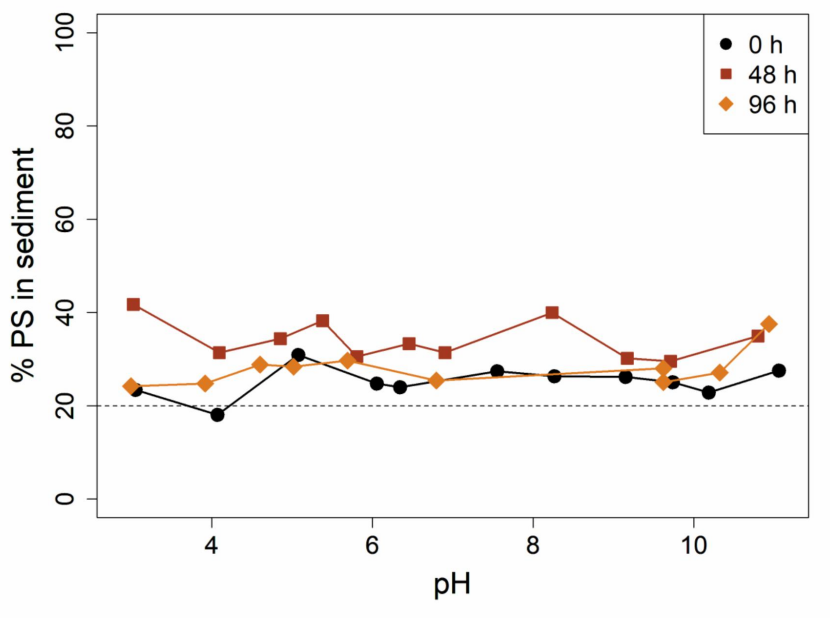

Figure S7. Sedimentation of pristine and UV-weathered PS in absence of ferrihydrite: Percentage of carbon found in the sediment after a settling time of one day. In a well-mixed dispersion where no sedimentation takes place, 20% of the total PS in the sample should be found in the sediment (dashed line).

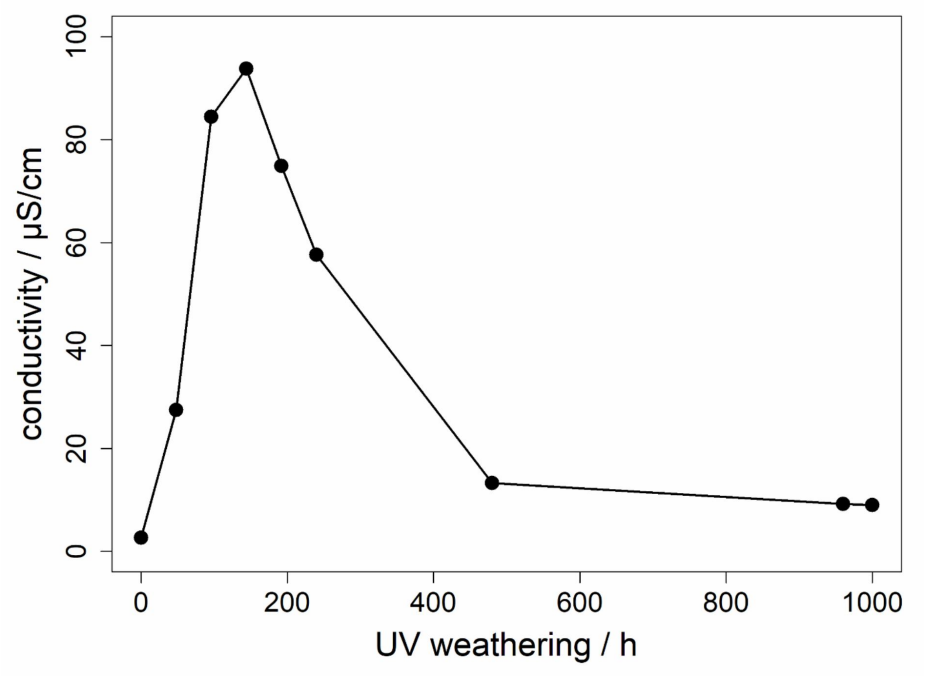

Figure S8. Electrical conductivity of the initial 100 mg L^{-1} PS suspensions after different UV-weathering time steps.

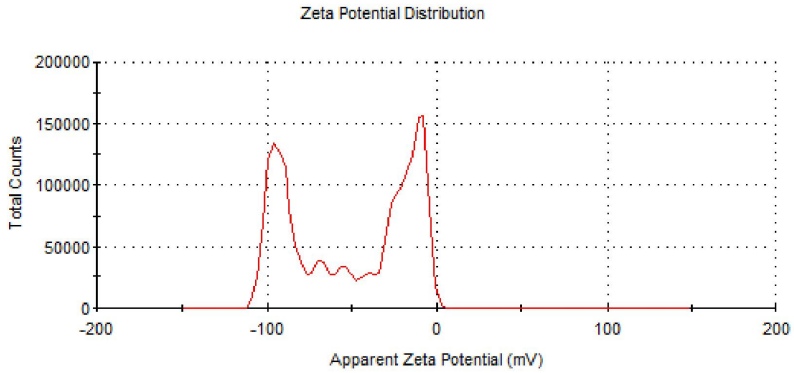

Figure S9. Zeta Potential distribution of one single measurement of a sample with PS and ferrihydrite (pH 8.9) as an example for samples in which two zeta potential peaks were measured. The zeta potential distributions do not show one but two distinct zeta potential peaks and therefore suggest the co-occurrence of PS and ferrihydrite particles that stay separated, and that no (major) aggregation takes place. The peak at -92 mV values can be attributed to the PS particles and the peak at -16 mV to the ferrihydrite particles.

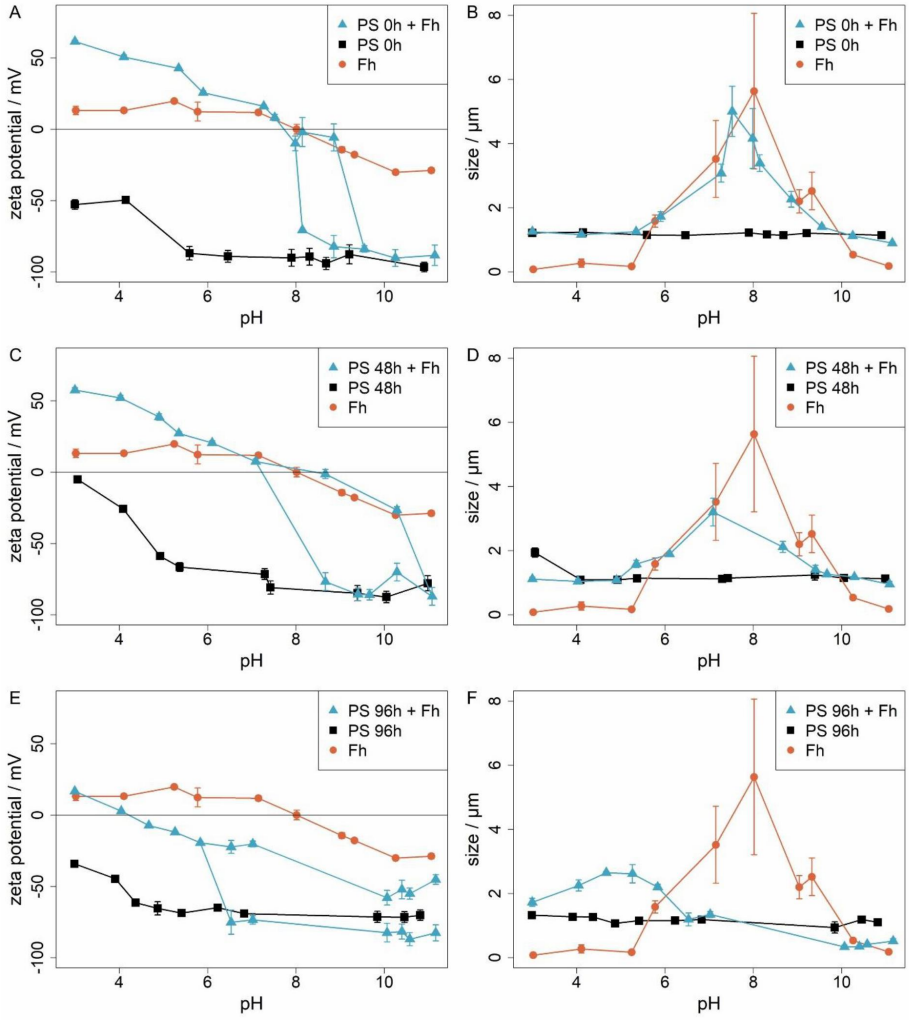

Figure S10. Zeta potential values and hydrodynamic diameter of samples with PS, ferrihydrite (Fh), and PS+Fh compared for each weathering duration (0, 48, and 96 h).

Study 3: Ferrihydrite coating reduces microplastic induced soil water repellency

Status: Published in *Environmental Science: Processes & Impacts*

Vol. 25 (6), 2023

https://doi.org/10.1039/D3EM00077J

Authors: Andreas Cramer, Johanna Schmidtmann, Pascal Bernad, Anders Kaestner, Matthias Engelhardt, Stefan Peiffer, Andrea Carminati

Own Contribution in %:

Study design	40
Laboratory analysis	50
Data processing and analyses	40
Interpretation of the results	50
Preparation of the manuscript	50

AC (Andreas Cramer), JS, SP and ACar (Andrea Carminati) designed the study. AC and JS planned and conducted the laboratory experiments. AC processed the neutron imaging data and JS processed the data of chemical analyses. AC and JS prepared the figures and tables. JS designed the Graphical Abstract. All co-authors interpreted the results. AC and JS prepared the manuscript with input from all co-authors. AC and JS contributed equally.

AC and JS are the corresponding authors.

Graphical Abstract:

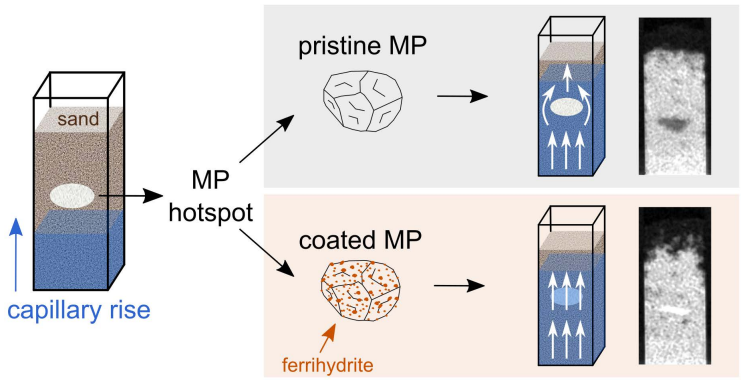

Environmental Science Processes & Impacts

ROYAL SOCIETY OF CHEMISTRY

PAPER

Cite this: *Environ. Sci.: Processes Impacts*, 2023, **25**, 1094

Ferrihydrite coating reduces microplastic induced soil water repellency†

Andreas Cramer, ‡*[a] Johanna Schmidtmann, ‡*[b] Pascal Benard,[a] Anders Kaestner,[c] Matthias Engelhardt,[d] Stefan Peiffer[b] and Andrea Carminati[a]

Received 22nd February 2023
Accepted 2nd May 2023

DOI: 10.1039/d3em00077j

rsc.li/espi

Addition of microplastics (MP) to soil has the potential to increase soil water repellency. However, coating of MP with soil abundant substances *e.g.*, iron compounds, can reduce this effect. Here, we tested if pre-coating or *in situ* coating of MP with ferrihydrite (Fh) reduces soil water repellency. We applied hotspots of pristine and coated MP (20–75 μm, PS and PET) to sand and imaged capillary rise *via* neutron radiography. Capillary rise experiments in wetting–drying cycles were conducted using water and Fh suspension. Pristine MP hotspots were not wettable. Capillary rise of water into coated MP hotspots differed in wettability depending on polymer type. While coated PS was still non-wettable, water imbibed into the coated PET hotspot. Capillary rise of Fh suspensions in wetting and drying cycles also showed varying results depending on polymer type. MP hotspots were still non-wettable and local water content increased only marginally. Our results indicate that Fh coating of MP changes MP surface wettability depending on polymer type and therefore counteracts the hydrophobic properties of pristine MP. However, MP coating is likely to be slowed down by the initial hydrophobicity of pristine MP. Dynamics of MP coating and increasing wettability are key factors for biotic and abiotic degradation processes.

Environmental significance

The contamination of soil with microplastics (MP) is ubiquitous and occurs locally by deposition of larger plastic fragments with hotspots of high MP content leading to a loss of soil wettability. Consequently, locally reduced soil water content and air entrapment may occur, affecting soil functions such as capillary water flow as well as MP degradation. Here, we demonstrated that, depending on polymer type, coating of MP with iron (oxy)hydroxides reduces hydrophobicity of MP and allows for capillary infiltration of water. However, the initial low wettability of MP is likely to slow down the coating of MP. We conclude that the interaction of MP with surface-active environmental particles is important for the fate of MP and its impact on soil wettability.

1. Introduction

Terrestrial ecosystems are confronted with ever increasing amounts of microplastic (MP) particles of different origin, type, shape, size, and state of degradation.[1] The extent of MP contamination depends on anthropogenic activity levels.[2] In floodplains in Swiss nature reserves, concentrations up to 593 particles per kg of MP are reported.[3] Zhou *et al.* (2018) estimated 1.3–14 713 particles per kg in a coastal soil,[4] Vollertsen & Hansen (2017) reported 53 000–528 000 particles per kg in agricultural soils[5] and in industrial soils 0.3–67.5 g kg^{-1} of MP were reported.[6] However, also in remote locations like Antarctica, MP has been found in soils.[7] The global plastic production of 2021 is estimated to 367 Mt.[8] The total accumulated plastic waste generation is estimated to reach over 25 000 Mt by the year 2050 with maximum half of it being either correctly discarded, incinerated or recycled.[9] Polyethylene terephthalate (PET), one of the main polymers used for packaging materials, constitutes a big part of plastic litter.[1,8,10,11] Soil analysis for polymers mainly revealed groups of polyethylene (PE), polypropylene (PP), polyamide (PA) and polystyrene (PS).[1,2]

Hitherto, most studies are focusing on the effect of MP on biological impacts while investigations on soil properties and functions are scarce. Since MP particles are typically hydrophobic, once they are deposited at the soil surface or incorporated into the bulk soil, they are likely to locally increase soil water repellency.[12] Previous experiments showed that pristine

[a]*Department of Environmental Systems Science, ETH Zürich, Physics of Soil and Terrestrial Ecosystems, Zürich, Switzerland. E-mail: andreas.cramer@usys.ethz.ch*

[b]*Department of Hydrology, University of Bayreuth, Bayreuth Center for Ecology and Environmental Research (BayCEER), Bayreuth, Germany. E-mail: j.schmidtmann@uni-bayreuth.de*

[c]*Laboratory for Neutron Scattering and Imaging, Paul Scherrer Institute, Villigen, Switzerland*

[d]*Department of Physical Chemistry II, University of Bayreuth, Bayreuth, Germany*

† Electronic supplementary information (ESI) available: MP size distribution, SEM images of coated MP particles, zeta potential curve of pristine MP particles, neutron images during capillary rise, results of contact angle measurements, BET surface area analysis of pristine MP particles and mean water saturation values of all samples. See DOI: https://doi.org/10.1039/d3em00077j

‡ These authors contributed equally.

MP increases soil water repellency with the effect of inhibiting capillary rise.[12] Water bypasses areas of high MP contents, leading to locally reduced soil water contents by increasing tortuosity and entrapping air.[12] These observations imply that MP in soil is not easily wetted by soil water. Due to the importance of water on soil biotic and abiotic processes, this is expected to impact transport and fate of MP.

In the environment, MP particles may undergo various processes changing their surface properties *e.g.*, weathering by UV-light, hydrolysis, microbial activity and interactions with environmental particles and substances.[13–17] Once incorporated into soil, MP is exposed to a variety of abundant soil and soil water constituents being able to alter MP surfaces[18] and potentially increase their wettability. Such binding agents include inorganic substances such as minerals, metal hydroxides or organic matter.[18–20] Recent studies demonstrated the formation of a surface coating and heteroaggregation of PS particles with ferrihydrite (a ferric iron (oxy)hydroxide) in the aqueous phase.[21] Depending on the pH value, the surface properties of the MP were controlled by the ferric particles.[21] Such iron compounds are not only highly abundant components in aquatic systems but also in soil and soil water (up to 20% (w/w)).[22] MP can get in contact with ferrihydrite (Fh) suspension in unsaturated sand, a situation comparable to and commonly found at the capillary fringe, where anoxic Fe(II) bearing groundwater may come in contact with oxygen with subsequent formation of Fe(II) to Fh.[23] Thus, they are posing important coating agents of MP surfaces in terrestrial environments. First studies showed that MP particles and iron oxides interact in porous media and the relative smaller particles adsorbed onto the surface of the larger ones.[24] The resulting changes in surface properties influence the (co)transport of MP particles.[24] However, studies on the interactions between MP and soil components and the resulting changes of MP surface properties are scarce as most studies focus on the interactions of MP and environmental particles in aquatic systems.[21,25,26]

Here, we tested if Fh coating influences the wettability of MP in soil. To this end, we investigated whether hotspots of pristine and coated MP (20–75 μm, PS and PET) embedded in a porous medium consisting of quartz sand will show differences in wettability during capillary rise (Fig. 1). Such regions of high MP content in soil are relevant since contamination usually occurs locally by deposition of larger plastic fragments, for example, by mulch film residues and their subsequent incorporation into the soil followed by fragmentation.[27–29] The resulting wettability of MP hotspots was visualized and quantified by means of water saturation using neutron imaging and by determination of static contact angles (CA) by use of the sessile drop method (SDM). Neutron imaging is non-destructive to the soil structure and highly sensitive to hydrous material rendering this method optimal for imaging water in porous media.[30–32] The common process of extracting and determining MP in soil, *e.g.*, density separation, is labor intensive and destructive to the soil structure. Neutron imaging allows to determine MP particle properties *in situ* without destroying the soil structure. Furthermore, hydrogen atoms are abundant in polymers allowing neutron imaging to distinguish PET and PS from dry soil material.[12,33]

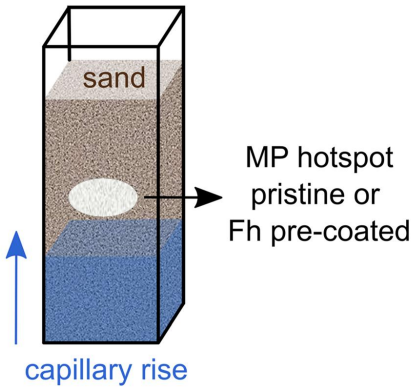

Fig. 1 Schematic setup of a sample container filled with sand and MP hotspot.

Differing material neutron attenuation coefficients can be used to quantify sample constituents in space and time.[32]

We hypothesize that (i) the coating of MP particles with Fh increases their wettability; and (ii) the addition of Fh to water leads to a partial coating of pristine MP particles during capillary rise and hence increases the wettability of MP.

2. Experimental

2.1 Investigated media

We applied MP hotspots to porous media in varying combinations to estimate the effect of pristine MP and coated MP on soil wettability, respectively. As polymers we used PET and PS provided by Veolia Deutschland GmbH. It has been milled by a centrifugal mill (ZM200, Retsch GmbH) and sieved into a 20–75 μm fraction. Particle size analysis (Microtrac, Retsch GmbH) revealed irregularly shaped particles, ranging from near spherical to fibrous, resembling an environmentally relevant mixture of MP shapes. Size distributions and shapes are reported in the ESI (Fig. S1†).

As model soil particles, quartz sand (Raneem, Sand-Schulz GmbH, Berlin) in the size range of 700–1200 μm was used. To exclude effects of organic matter on wettability, the sand was treated with hydrogen peroxide (30%) at 95 °C for 8 h and subsequently washed with deionized water. Additionally, magnetic particles were removed to not obstruct the signals from neutron imaging.

2.2 Characterization of MP

2.2.1 Static contact angle. To evaluate static contact angles (CA) of MP, the sessile drop method (SDM) was applied.[34] MP, pristine and coated, was fixed to a microscopy glass slide by attaching a hydrophobic, double-sided adhesive tape.[34,35] 1 μL droplets of deionized water ($n = 11$) were placed on the MP surface with a syringe. Simultaneously, the drop shapes were

recorded with a camera (device: Drop Shape Analyzer DSA30S, Krüss GmbH).

Each droplet geometry was analyzed with an elliptic shape recognition algorithm and measured at the three-phase contact line of liquid, solid and vapor 500 ms after the droplets detached from the syringe (software: Krüss Advance, Krüss GmbH). CA are the result of the combination of surface tensions of the aforementioned three phases according to eqn (1),[36,37] where CA_e^Y is the equilibrium contact angle, γ is surface tension at the respective interfaces between solid (S), liquid (L) and vapor (V):

$$\cos CA_e^Y = \frac{\gamma_{SV} - \gamma_{SL}}{\gamma_{LV}} \quad (1)$$

Statistical analysis was conducted using the software MATLAB (R2021a). A parametric one-way ANOVA test was applied to the CA data of the MP to disclose a potential significant difference and the post hoc test of Bonferroni was employed to identify significant differences between the variants ($p < 0.001$). The letters A, B and C indicate significant differences.

2.2.2 Streaming potential. The streaming potential measurements have been performed with the electrokinetic analyzer SurPASS 3 (Anton Paar GmbH) and the cylindrical cell. The cell was filled to its maximum capacity with 128.4 ± 7.1 mg PS and 154.3 ± 6.3 mg PET, respectively. The particles were immobilized by polyamide-6,6 filter mats (Pieper Filter GmbH) with nominal pore diameters of 10 μm. The solutions were composed of analytic grade KCl (BioUltra, Merck), HCl, and KOH (Titrisol®, Merck). Titrations were performed from pH 4 to pH 10 at a constant overall ionic strength of 10 mM to neglect influences of surface conductivity. The reported zeta potentials have been calculated by means of the Helmholtz–Smoluchowski approximation.

2.2.3 Coating of MP with ferrihydrite. As shown in previous work, Fh colloids adsorb onto the surface of MP.[21] The coating of MP was achieved by shaking 2 g MP per liter Fh suspension. Fh colloids were synthesized after Cornell & Schwertmann (2003).[38] For the coating process, the stock solution of Fh was diluted with deionized water to 100 mg L^{-1}. Additionally the ionic strength was set to 10 mM by addition of NaCl. After shaking the mixture for 2 h in an overhead shaker (Reax 20/4, Heidolph Instruments GmbH & Co. KG) at 16 rpm, the suspension was filtered through a 10 μm filter (nuclepore polycarbonate hydrophilic membranes, Whatman, Cytiva) to separate the coated MP particles from the remaining Fh colloids. The filter was then dried overnight at 40 °C.

Scanning Electron Microscopy (SEM) was conducted to confirm the coating of MP with Fh. The dried material was mounted onto a standard sample holder and coated with a thin layer of platinum (Cressington 208 HR sputter coater). SEM images were recorded with a Zeiss ULTRA PLUS (Carl Zeiss Microscopy GmbH, Germany). To calculate the amount of Fe adsorbed to the MP surface, the specific surface area of PS and PET was determined by the Brunauer–Emmett–Teller (BET) method. This method measures the surface area by a multi-point surface N_2-adsorption isotherm at a temperature of 77 K (NOVA 2000e, Quantachrome Instruments).

Furthermore, the amount of iron adsorbed to the MP surfaces was determined. Approximately 0.03 g of coated MP were added to 5 mL 1 M HCl. The mixture was placed on an overhead shaker for 24 h to dissolve all ferric particles from the MP surface and afterwards filtered through 10 μm. The iron concentration of the filtrate was determined spectrophotometrically (DR 3800 VIS, Hach) at 512 nm using acetate buffer solution and 1,10-phenanthroline. Prior to the measurement, all ferric iron was reduced to ferrous iron by adding ascorbic acid to the sample. Triplicate samples were prepared.

2.3 Neutron imaging

Time-series neutron radiography of capillary rise into aluminum containers (inner dimensions: 6 × 16 × 60 mm) filled with sand and MP was conducted in wetting–drying cycles at the NEUTRA beamline at the Paul Scherrer Institute in Villigen, Switzerland.[39] The containers were pre-filled half with sand before MP was added *via* a funnel with subsequent addition of the other half sand (Fig. 1). The applied MP hotspots were pristine or coated with Fh. The mass of the MP hotspots was 0.02 g and range in size from height of *ca.* 1.5–2.5 mm and width of *ca.* 5.0–7.0 mm covering the whole depth of the sample container (6 mm). Capillary rise was imaged for a duration of 150 s to eventually estimate the water saturation of the capillary fringe. Differences in water saturation allow conclusions about the wettability of MP hotspots. An open container with in and out flow and a permeable bridge as stand for the sample containers was providing a constant water table for capillary rise. The respective liquid was delivered by a peristaltic pump at constant flow rate. Imbibition of different liquids was recorded for ten and six replicates of different MP polymer types (Table 1) with an acquisition time of 2 s and a pixel size of 53 μm. Three different liquids for capillary rise were used: (i) deionized water with 10 mM NaCl (water), (ii) 10 mg per L Fh suspension with 10 mM NaCl (Fh10) and (iii) 100 mg per L Fh suspension with 10 mM NaCl (Fh100). We conducted one wetting–drying cycle with water and two cycles with Fh10 and Fh100. Before the second wetting, the samples were dried at room temperature until constant weight.

Differing material neutron attenuation coefficients can be used to quantify the distribution of sample constituents.[32] The attenuation coefficients for water and Fh suspensions were derived from step-wedge samples with defined thickness filled with the respective liquid. The coefficients were used to calculate water saturation based on porosity and dimensions of the

Table 1 Capillary rise experiment setups for neutron imaging

MP	Liquid	Repetitions
Pristine PET	Water, Fh10, Fh100	10
Coated PET	Water	6
Pristine PS	Water, Fh10, Fh100	10
Coated PS	Water	6

sample.[40] According to eqn (2), where, in each pixel of the images, Θ is the saturation of the respective liquid, $\text{liquid}_{\text{signal}}$ is the gray value signal after subtracting the dry soil signal, $\text{AC}_{\text{liquid}}$ is the respective attenuation coefficient of a liquid, s is the thickness of the sample material in direction of the neutron beam and n is the porosity of the sample material.[40]

$$\Theta = \frac{\text{liquid}_{\text{signal}}}{\text{AC}_{\text{liquid}}} \Big/ (s \times n) \quad (2)$$

The gray value data of the images were normalized to the open beam signal, spot cleaned, and noise reduced.[31,41] Subtracting gray values of the dry sample references from their wetted counterparts provides the signal of imbibed water.[40] The analyzed subsection of sample was set to 21 (width) × 35 (height) pixel resulting in a region of interest (ROI) of merely the MP hotspot of 0.11 mm (width) and 0.2 mm (height). Statistical analysis was conducted using the software MATLAB (R2021a). The non-parametric Kruskal–Wallis test was applied to the water saturation data to disclose a potential significant difference and the post hoc test of Bonferroni was employed to identify significant differences between the treatments ($p < 0.001$). The letters A, B and C indicate significant differences where the combination of two letters shows similarity between those groups.

3. Results and discussion

3.1 Characterization of pristine and coated MP particles

Contact angles are a measure of polarity and hence allow conclusion about the wettability of particles.[34,35] Typically, CA < 90° are regarded to allow for good wettability, while >90° can be considered hydrophobic.[34,35] In our study, all particles exceed this threshold (Table 2). The analyzed MP surfaces partly indicate significant differences between pristine and coated MP as well as in polymer type (Fig. 2a, Tables 2 and S1†). The lower initial static CA of pristine PET (123.81°) compared to PS (143.71°) is significantly different and indicates a higher surface polarity of pristine PET[42] and therefore, a higher wettability.

Coated PET has an average static CA of 101.67° and is significantly different from the other variants. Coating of PS (127.06°) resulted in static CA merely in the range of pristine PET (123.81°) indicating no significant difference between them and no wettability for both polymers. The coating of both polymer types with Fh significantly decreased the contact angle indicating a change in polarity. Nychka & Gentleman (2010) mention that a moderate CA, besides other important surface properties, facilitates microbial colonization.[43] They differentiate between cell-substrate adhesion, where high wettability (CA = 24°) is favorable and cell–cell cohesion where hydrophobicity (CA = 84°) is of importance. Neither of those CA are observed in our experiment and thus, the used substrates were highly water repellent. Of all MP materials, coated PET showed the most favorable wettability for colonization exhibiting an CA of 101.67°.

In line with CA measurements, the coating of PET with Fh was more effective compared to PS. On the PET surface, 87.4 μmol Fe adsorbed per m^2 surface area of MP. Hence, surface coverage with Fh is more than four times higher compared to PS with 20.31 μmol Fe per m^2 surface area MP (Tables 2 and S2†). This is confirmed by SEM images showing a denser coating of the PET surface with small Fh particles compared to PS (Fig. S2†). The zeta potentials of PS and PET are negative in the analyzed pH range between 4 and 10 and become more negative with increasing pH value. The pH value of the Fh suspension used in the experiments was approximately 5.7. At this pH value, the zeta potential values of both polymer types were similar (Fig. S3† and Table 2) and thus cannot be the reason for the different adsorption behavior of Fh. Therefore, we assume that the presence of polar functional groups of the PET structure enhances the adsorption of Fh compared to PS. This is consistent with previous studies that investigated the adsorption of heavy metals or ciprofloxacin on MP.[44–46] They observed that the adsorption capacity of MP particles increased with increasing UV-weathering. The UV-treatment increased the number of functional groups on the surface of MP particles and therefore provided more adsorption sites.[18] For PET, the polymer backbone contains such functional groups even without weathering and therefore provides more adsorption sites for Fh compared to PS.

3.2 Neutron imaging

3.2.1 Capillary rise of water. In line with results from static contact angle measurements, the analysis of water saturation from neutron imaging shows similar qualitative patterns (Fig. 2b). After imbibition of water, mean water saturation values of pristine PET (0.10) exhibit non-significantly higher water saturation compared to pristine PS (0.04) (Table S3†). Both pristine polymers induce low water saturation and need to be considered non-wettable as water bypassed these hotspots (Fig. 3).

Table 2 Characterization of pristine and coated MP. The letters A, B and C indicate significant differences in contact angles of polymer types

MP type	Mean contact angle (°), $n = 11$	Significance contact angle	μmol Fe per m^2 MP, $n = 3$	Zeta potential (mV) (pH 5.7 ± 0.1), $n = 4$
Pristine PS	143.71 ± 3.29	A	—	−32.7 ± 0.5
Pristine PET	123.81 ± 3.87	B	—	−28.1 ± 0.1
Coated PS	127.06 ± 3.74	B	20.3	—
Coated PET	101.67 ± 4.37	C	87.4	—

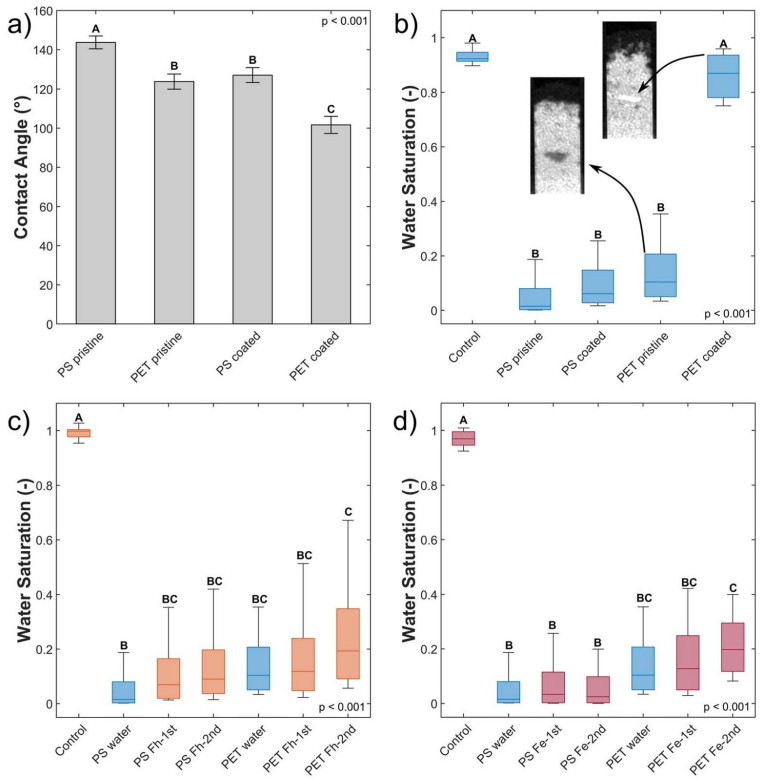

Fig. 2 (a) Contact angle of pristine and coated PS and PET. (b) Water saturation of MP hotspots after capillary rise with water. One wetting cycle for control samples without MP hotspot ($n = 10$), pristine ($n = 10$) and coated MP variants ($n = 6$) are shown. For PET, neutron images after capillary rise are shown. (c) Water saturation of MP hotspots after capillary rise with Fh10 (orange). One wetting cycle for control without MP ($n = 6$) and two wetting–drying cycles for pristine PS and PET variants ($n = 6$) are shown. For comparison, the results of the wetting of pristine PS and PET with water (blue) are shown. (d) Water saturation of MP hotspots after capillary rise with Fh100 (red). One wetting cycle for control samples ($n = 10$) and two wetting cycles for pristine PS and pristine PET variants are shown ($n = 10$). For comparison, the results of the wetting of pristine PS and PET with water (blue) are shown. The letters A, B and C in each graph indicate significant differences whereas the combination of two letters (*e.g.*, AB) shows similarity between those groups.

Coated PET hotspots show a different behavior compared to pristine PET hotspots. The coated PET hotspots are wettable and water flow into the hotspot was observed (Fig. 3). Furthermore, water was even attracted by the hotspot, accelerating towards it and being further distributed from there (Fig. 3). We attribute this observation to a smaller pore geometry of the wettable, coated PET particles resulting in enhanced capillary forces compared to the sand. In the absence of coating, the smaller pore geometry of MP did not affect water flow due to high static CA. The observations are confirmed by water saturation values of the coated PET hotspots comparable to the control but with a broader distribution of values (Fig. 2b).

Other than in the case of PET, only a slight difference in water saturation between pristine and coated PS particles exists. Even though the water saturation of coated PS increased slightly, the wettability of the hotspot did not change, and the hotspot is still considered non-wettable.

The increase in wettability of coated PET compared to coated PS can be explained by the effectiveness of the Fh coating. The amount of Fh adsorbed onto the PET surface was approximately four times higher compared to PS (Table 2). Therefore, we assume that the higher degree of coating of PET enables the formation of capillary water menisci in the pore space facilitating capillary rise. The wettability of hotspots of coated PET appear to contradict the results from static CA measurements with a CA of coated PET above 90° indicating non-polarity (see Section 3.1). Such discrepancy emerges from the methodological differences. Static CA measurements are derived from a quasi-two-dimensional system while capillary rise adheres to effective, dynamic CA of water in a three-dimensional pore

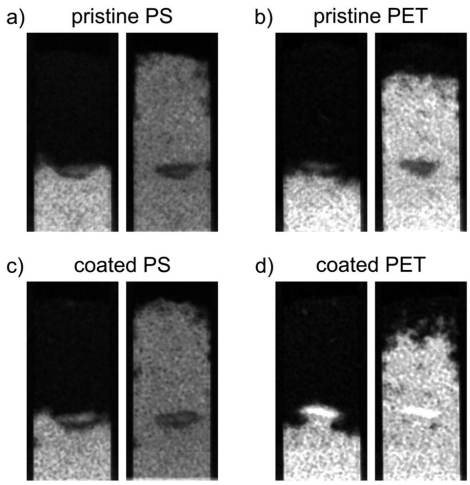

Fig. 3 Neutron images during and at the end of capillary rise of water. The hotspots consist of (a) pristine PS, (b) pristine PET, (c) Fh-coated PS, and (d) Fh-coated PET. For each set, the left image is taken at a time step at which the rising water reaches the hotspot. For coated PET, water flow into the hotspot is observed whereas for the other variants, the water bypasses the hotspot. The right image of each set is taken at the end of capillary rise (150 s).

space. Hence, the static CA derived allow to compare particles and treatments but cannot fully explain the dynamic process of capillary rise into a three-dimensional volume. In case of this study, the solid material consists of irregularly shaped sand grains and MP. The shape of the resultant liquid meniscus, and therefore the CA, is subject to forces based on the geometry of the pore space. In samples mixed with MP, dynamic CA are typically lower compared to static CA.[12] Instead of water not being able to spread beyond low wettability of MP during static CA measurements on a quasi-two-dimensional packing, water, during imbibition into a three-dimensional volume, has the possibility of bypassing into more favorable flow paths for imbibition and enclosing non-wettable locations.[12] Furthermore, forces like inertia of the imbibing liquid can also lead to overcome locations of low wettability. This would explain that the water saturation of coated PET is close to the one of the control but with a wider distribution of values (Fig. 2b).

3.2.2 Capillary rise of ferrihydrite suspensions. In the first part, we showed that a pre-established Fh coating of MP, depending on polymer type, can increase the wettability substantially. In a second experiment, we investigated to what extent coating of pristine MP hotspots can be established *in situ*. To this end, we used ferrihydrite suspensions instead of water and performed capillary rise experiments with a new set of pristine MP hotspots to mimic a situation commonly found at the capillary fringe.[23] To test if there is a dependency between Fh concentration in the soil suspension and increase in water saturation of the MP hotspot, we used two different Fh concentrations (10 and 100 mg L^{-1}).

Slight, but not significant, increases in water saturation relative to uncoated PS and PET were observed upon imbibition of Fh suspensions independent of concentration (Fig. 2c and d). A second wetting cycle did not lead to a change in wettability of the hotspots. Though, increased water saturation with a broader distribution of values show that Fh coating occurred locally during capillary rise. The explanation is that Fh suspensions have limited contact to the MP hotspots due to MP hydrophobicity. The suspensions bypassed the hotspots and only MP particles at the boundaries had contact with the imbibing Fh suspensions. It means that for coating and reducing the wettability of MP, Fh needs first to wet MP, which is a process that is hindered and slowed down by the initial hydrophobicity of MP. An increased number of wetting and drying cycles would likely allow the Fh suspensions to propagate deeper into the hotspots. The fact that larger increases of water saturation were only observed with PET is in line with differences in pre-coating of pristine MP, where PET coating was more profound than PS due to the presence of more functional groups in the PET polymer backbone.

4. Conclusion

We showed that naturally occurring coating agents like ferric (oxy)hydroxide increase the wettability of MP in porous media. This is of importance since MP has been shown to limit capillary flow in soils leading to air entrapments and reduced local water contents.[12]

Depending on polymer type, capillary driven imbibition of water into MP hotspots was facilitated by Fh pre-coating. While coated PS was still non-wettable, coated PET was wettable. We infer, a coating of particles, sufficiently high to render them wettable, depends on the presence of functional groups on the MP surface. Polymers with more functional groups in the polymer backbone like PET can be coated more efficiently compared to less functionalized polymers like PS.

In contrast to Fh pre-coating of MP, *in situ* coating of pristine MP hotspots with Fh suspension did not establish an effective coating regardless of Fh concentrations. The exposed MP hotspots were still non-wettable. Yet, a slight but not significant increase in water saturation and a wider distribution of values was visible. We summarize, that pristine MP, due to its hydrophobic properties, had limited contact to the imbibing Fh suspensions and only MP particles at the hotspot boundaries were exposed to Fh. We speculate, that adsorption of Fh onto MP in soils is a slow process, which requires multiple wetting–drying cycles in order to effectively alter the surfaces of MP in soil and render it wettable.

Translated into a natural process, our capillary rise experiment with wetting–drying cycles mimics fluctuating moisture conditions in the vadose zone. Over time, this process happens numerous times and therefore might allow MP in soil to get in contact with the soil suspension. However, the initial hydrophobicity of MP delays this process. The time frame necessary to overcome MP's inherent hydrophobicity is unclear and strongly depends on polymer type.

Understanding the coating and wetting kinetics of MP is a key factor to predict MP degradation, as the presence of water accelerates biotic and abiotic degradation processes.

Author contributions

The experimental work was performed by A. Cramer and J. Schmidtmann. The manuscript was written by A. Cramer and J. Schmidtmann with contributions of all authors. A. Cramer and J. Schmidtmann contributed equally. All authors have given approval to the final version of the manuscript.

Conflicts of interest

There are no conflicts to declare.

Acknowledgements

This study was funded by the Deutsche Forschungsgemeinschaft (DFG, German Research Foundation) – Project Number 391977956 – SFB 1357. We kindly acknowledge subproject Z01 for providing microplastic particles. This work is based on experiments performed at the Swiss spallation neutron source SINQ, Paul Scherrer Institute, Villigen, Switzerland. The authors would like to thank Jutta Eckert for her support in chemical analysis, Martina Heider for taking SEM images at the Bavarian Polymer Institute (BPI) and Michael Thelen for measuring the BET surface area.

References

1 R. W. Chia, J. Y. Lee, H. Kim and J. Jang, Microplastic pollution in soil and groundwater: a review, *Environ. Chem. Lett.*, 2021, **19**, 4211–4224.
2 B. Xu, F. Liu, Z. Cryder, D. Huang, Z. Lu, Y. He, H. Wang, Z. Lu, P. C. Brookes, C. Tang, J. Gan and J. Xu, Microplastics in the soil environment: Occurrence, risks, interactions and fate–A review, *Crit. Rev. Environ. Sci. Technol.*, 2020, **50**, 2175–2222.
3 M. Scheurer and M. Bigalke, Microplastics in Swiss Floodplain Soils, *Environ. Sci. Technol.*, 2018, **52**, 3591–3598.
4 Q. Zhou, H. Zhang, C. Fu, Y. Zhou, Z. Dai, Y. Li, C. Tu and Y. Luo, The distribution and morphology of microplastics in coastal soils adjacent to the Bohai Sea and the Yellow Sea, *Geoderma*, 2018, **322**, 201–208.
5 J. Vollertsen and A. A. Hansen, *Microplastic in Danish Wastewater: Sources, Occurrences and Fate*, The Danish Environmental Protection Agency, 2017.
6 S. Fuller and A. Gautam, A Procedure for Measuring Microplastics using Pressurized Fluid Extraction, *Environ. Sci. Technol.*, 2016, **50**, 5774–5780.
7 A. Kelly, D. Lannuzel, T. Rodemann, K. M. Meiners and H. J. Auman, Microplastic contamination in east Antarctic sea ice, *Mar. Pollut. Bull.*, 2020, **154**, 111130.
8 Plastics Europe, *Plastics – the Facts 2021: An analysis of European plastics production, demand and waste data*, **https://plasticseurope.org/wp-content/uploads/2021/12/AF-Plastics-the-facts-2021_250122.pdf**.
9 R. Geyer, J. R. Jambeck and K. L. Law, Production, use, and fate of all plastics ever made, *Sci. Adv.*, 2017, **3**, 25–29.
10 M. Padervand, E. Lichtfouse, D. Robert and C. Wang, Removal of microplastics from the environment. A review, *Environ. Chem. Lett.*, 2020, **18**, 807–828.
11 H. Ritchie and M. Roser, *Plastic Pollution, Our World in Data*, published online at **https://OurWorldInData.org**, retrieved from: **https://ourworldindata.org/plastic-pollution**.
12 A. Cramer, P. Benard, M. Zarebanadkouki, A. Kaestner and A. Carminati, Microplastic induces soil water repellency and limits capillary flow, *Vadose Zone J.*, 2022, 1–11.
13 O. S. Alimi, J. Farner Budarz, L. M. Hernandez and N. Tufenkji, Microplastics and Nanoplastics in Aquatic Environments: Aggregation, Deposition, and Enhanced Contaminant Transport, *Environ. Sci. Technol.*, 2018, **52**, 1704–1724.
14 A. L. Andrady, Microplastics in the marine environment, *Mar. Pollut. Bull.*, 2011, **62**, 1596–1605.
15 N. Meides, T. Menzel, B. Poetzschner, M. G. J. Löder, U. Mansfeld, P. Strohriegl, V. Altstaedt and J. Senker, Reconstructing the environmental degradation of polystyrene by accelerated weathering, *Environ. Sci. Technol.*, 2021, **55**, 7930–7938.
16 T. Menzel, N. Meides, A. Mauel, U. Mansfeld, W. Kretschmer, M. Kuhn, E. M. Herzig, V. Altstädt, P. Strohriegl, J. Senker and H. Ruckdäschel, Degradation of low-density polyethylene to nanoplastic particles by accelerated weathering, *Sci. Total Environ.*, 2022, **826**, 154035.
17 A. A. Shah, F. Hasan, A. Hameed and S. Ahmed, Biological degradation of plastics: A comprehensive review, *Biotechnol. Adv.*, 2008, **26**, 246–265.
18 Z. Ren, X. Gui, X. Xu, L. Zhao, H. Qiu and X. Cao, Microplastics in the soil-groundwater environment: Aging, migration, and co-transport of contaminants – A critical review, *J. Hazard. Mater.*, 2021, **419**, 126455.
19 T. Lu, B. S. Gilfedder, H. Peng, S. Peiffer, G. Papastavrou, K. Ottermann and S. Frei, Relevance of Iron Oxyhydroxide and Pore Water Chemistry on the Mobility of Nanoplastic Particles in Water-Saturated Porous Media Environments, *Water, Air, Soil Pollut.*, 2021, **232**, 168.
20 X. Yan, X. Yang, Z. Tang, J. Fu, F. Chen, Y. Zhao, L. Ruan and Y. Yang, Downward transport of naturally-aged light microplastics in natural loamy sand and the implication to the dissemination of antibiotic resistance genes, *Environ. Pollut.*, 2020, **262**, 114270.
21 J. Schmidtmann, H. Elagami, B. S. Gilfedder, J. H. Fleckenstein, G. Papastavrou, U. Mansfeld and S. Peiffer, Heteroaggregation of PS microplastic with ferrihydrite leads to rapid removal of microplastic particles from the water column, *Environ. Sci.: Processes Impacts*, 2022, 1782–1789.
22 W. Amelung, H.-P. Blume, H. Fleige, R. Horn, E. Kandeler, I. Kögel-Knabner, R. Kretzschmar, K. Stahr and

B.-M. Wilke, *Lehrbuch der Bodenkunde*, SpringerVerlag GmbH, 2018.
23 S. Peiffer, A. Kappler, S. B. Haderlein, C. Schmidt, J. M. Byrne, S. Kleindienst, C. Vogt, H. H. Richnow, M. Obst, L. T. Angenent, C. Bryce, C. McCammon and B. Planer-Friedrich, A biogeochemical–hydrological framework for the role of redox-active compounds in aquatic systems, *Nat. Geosci.*, 2021, **14**, 264–272.
24 M. Li, L. He, M. Zhang, X. Liu, M. Tong and H. Kim, Cotransport and Deposition of Iron Oxides with Different-Sized Plastic Particles in Saturated Quartz Sand, *Environ. Sci. Technol.*, 2019, **53**, 3547–3557.
25 O. Oriekhova and S. Stoll, Heteroaggregation of nanoplastic particles in the presence of inorganic colloids and natural organic matter, *Environ. Sci.: Nano*, 2018, **5**, 792–799.
26 T. T. T. Vu, P. H. Nguyen, T. V. Pham, P. Q. Do, T. T. Dao, A. D. Nguyen, L. Nguyen-Thanh, V. M. Dinh and M. N. Nguyen, Comparative effects of crystalline, poorly crystalline and freshly formed iron oxides on the colloidal properties of polystyrene microplastics, *Environ. Pollut.*, 2022, **306**, 119474.
27 D. K. A. Barnes, F. Galgani, R. C. Thompson and M. Barlaz, Accumulation and fragmentation of plastic debris in global environments, *Philos. Trans. R. Soc., B*, 2009, **364**, 1985–1998.
28 M. Bläsing and W. Amelung, Plastics in soil: Analytical methods and possible sources, *Sci. Total Environ.*, 2018, **612**, 422–435.
29 Y. K. Song, S. H. Hong, M. Jang, G. M. Han, S. W. Jung and W. J. Shim, Combined Effects of UV Exposure Duration and Mechanical Abrasion on Microplastic Fragmentation by Polymer Type, *Environ. Sci. Technol.*, 2017, **51**, 4368–4376.
30 R. Hassanein, E. Lehmann and P. Vontobel, Methods of scattering corrections for quantitative neutron radiography, *Nucl. Instrum. Methods Phys. Res., Sect. A*, 2005, **542**, 353–360.
31 A. P. Kaestner and M. Schulz, Processing Neutron Imaging Data - Quo Vadis?, *Phys. Procedia*, 2015, **69**, 336–342.
32 H. Pleinert and E. Lehmann, Determination of hydrogenous distributions by neutron transmission analysis, *Phys. B*, 1997, **234–236**, 1030–1032.
33 C. Tötzke, S. E. Oswald, A. Hilger and N. Kardjilov, Non-invasive detection and localization of microplastic particles in a sandy sediment by complementary neutron and X-ray tomography, *J. Soils Sediments*, 2021, **21**, 1476–1487.
34 J. Bachmann, R. Horton, R. R. van der Ploeg and S. Woche, Modified sessile drop method for assessing initial soil-water contact angle of sandy soil, *Soil Sci. Soc. Am. J.*, 2000, **64**, 564–567.
35 J. Bachmann, S. K. Woche, M. O. Goebel, M. B. Kirkham and R. Horton, Extended methodology for determining wetting properties of porous media, *Water Resour. Res.*, 2003, **39**, 1–14.
36 T. Young, Philos, *Trans. R. Soc. Lon don*, 1805, **95**, 65–97.
37 J. Bachmann and GU. McHale, Eur., *J. Soil Sci.*, 2009, **60**, 420–430.
38 R. M. Cornell and U. Schwertmann, *The Iron Oxides: Structure, Properties, Reactions, Occurrences and Uses*, John Wiley & Sons, 2003.
39 E. H. Lehmann, P. Vontobel and L. Wiezel, Properties of the radiography facility NEUTRA at SINQ and its potential for use as European reference facility, *Nondestr. Test. Eval.*, 2001, **16**, 191–202.
40 A. Carminati, A. Kaestner, R. Hassanein, O. Ippisch, P. Vontobel and H. Flühler, Infiltration through series of soil aggregates: Neutron radiography and modeling, *Adv. Water Resour.*, 2007, **30**, 1168–1178.
41 P. Boillat, C. Carminati, F. Schmid, C. Grünzweig, J. Hovind, A. Kaestner, D. Mannes, M. Morgano, M. Siegwart, P. Trtik, P. Vontobel and E. H. Lehmann, Chasing quantitative biases in neutron imaging with scintillator-camera detectors: a practical method with black body grids, *Opt. Express*, 2018, **26**, 15769.
42 N. Giovambattista, P. G. Debenedetti and P. J. Rossky, Effect of surface polarity on water contact angle and interfacial hydration structure, *J. Phys. Chem. B*, 2007, **111**, 9581–9587.
43 J. A. Nychka and M. M. Gentleman, Implications of wettability in biological materials science, *JOM*, 2010, **62**, 39–48.
44 Y. Wang, X. Wang, Y. Li, J. Li, Y. Liu, S. Xia and J. Zhao, Effects of exposure of polyethylene microplastics to air, water and soil on their adsorption behaviors for copper and tetracycline, *Chem. Eng. J.*, 2021, **404**, 126412.
45 Q. Wang, Y. Zhang, X. Wangjin, Y. Wang, G. Meng and Y. Chen, The adsorption behavior of metals in aqueous solution by microplastics effected by UV radiation, *J. Environ. Sci.*, 2020, **87**, 272–280.
46 P. Liu, L. Qian, H. Wang, X. Zhan, K. Lu, C. Gu and S. Gao, New Insights into the Aging Behavior of Microplastics Accelerated by Advanced Oxidation Processes, *Environ. Sci. Technol.*, 2019, **53**, 3579–3588.

Supporting Information

Ferrihydrite coating reduces microplastic induced soil water repellency

Andreas Cramer[a*‡], Johanna Schmidtmann[b*‡], Pascal Benard[a], Anders Kaestner[c], Matthias Engelhardt[d], Stefan Peiffer[b], Andrea Carminati[a]

a Department of Environmental Systems Science, ETH Zürich, Physics of Soil and Terrestrial Ecosystems, Zürich, Switzerland

b Department of Hydrology, University of Bayreuth, Bayreuth Center for Ecology and Environmental Research (BayCEER), Bayreuth, Germany

c Laboratory for Neutron Scattering and Imaging, Paul Scherrer Institute, Villingen, Switzerland

d Department of Physical Chemistry II, University of Bayreuth, Bayreuth, Germany

*corresponding authors: andreas.cramer@usys.ethz.ch, j.schmidtmann@uni-bayreuth.de

‡These authors contributed equally.

List of Figures

List of Tables

List of Figures

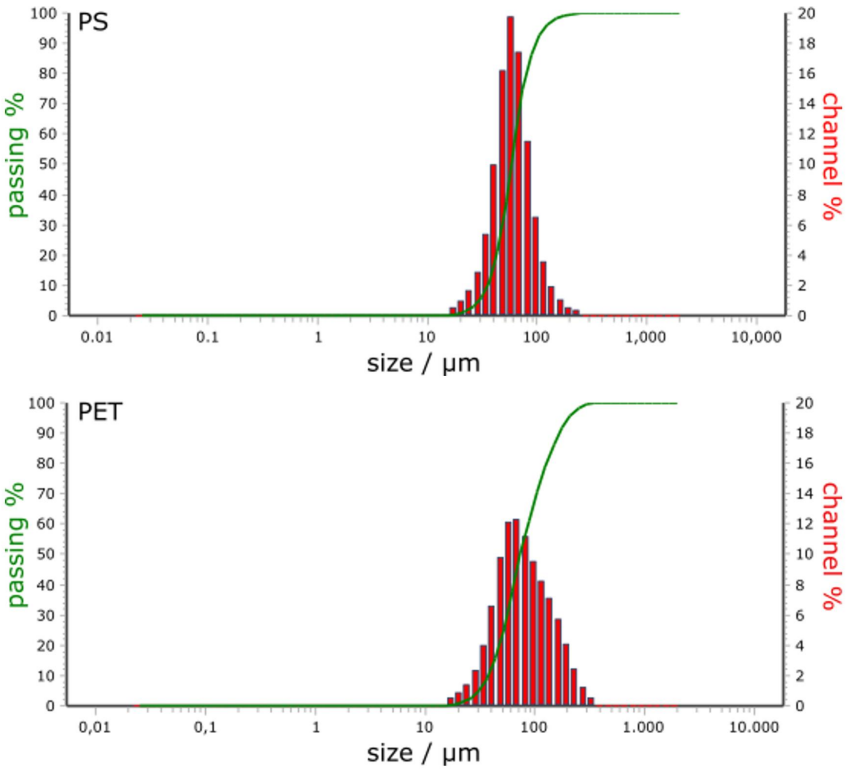

Figure S1. Size distribution of PS and PET particles.

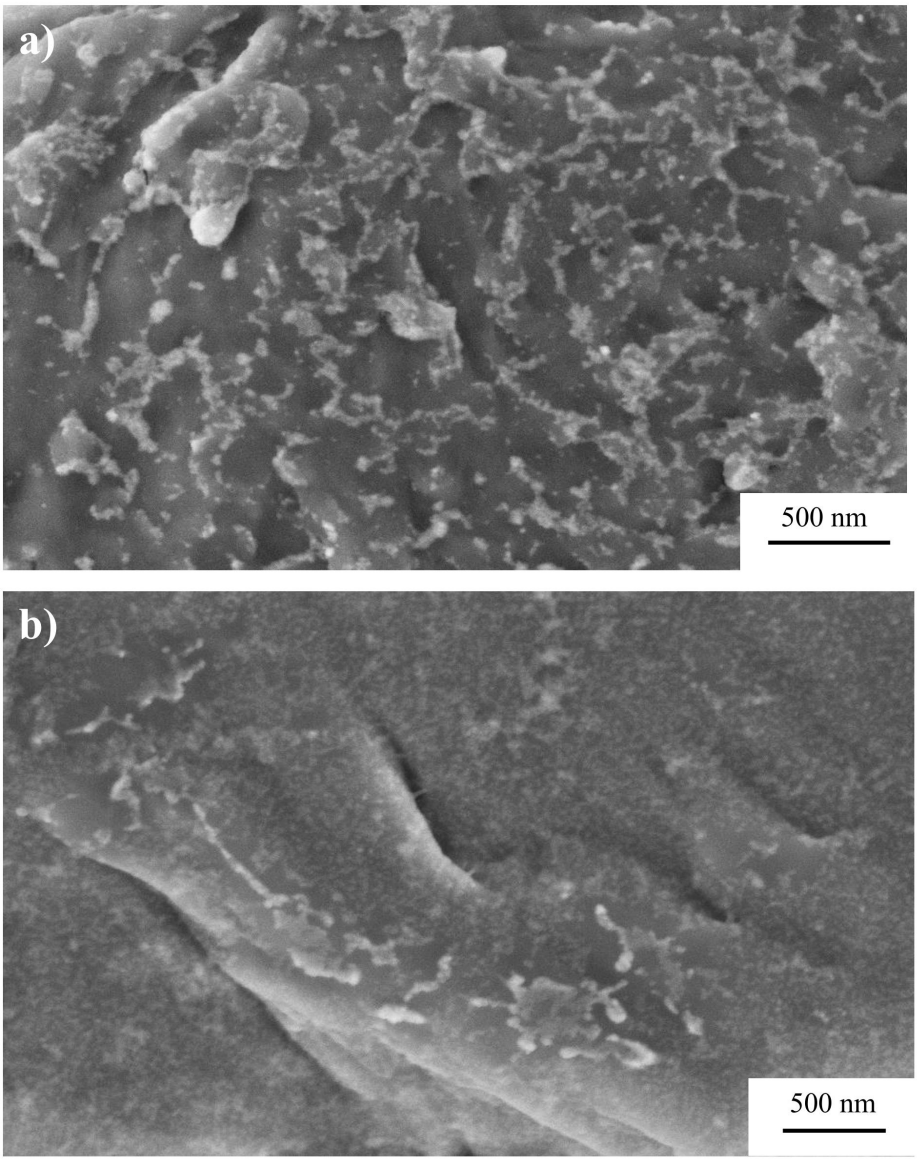

Figure S2. SEM images of coated PS (a) and coated PET (b). Both types of MP have a thin layer of ferrihydrite (light areas) on the surface. For PET the coating of the surface with ferrihydrite seems more evenly distributed compared to PS where larger areas of the PS surface without a coating remain.

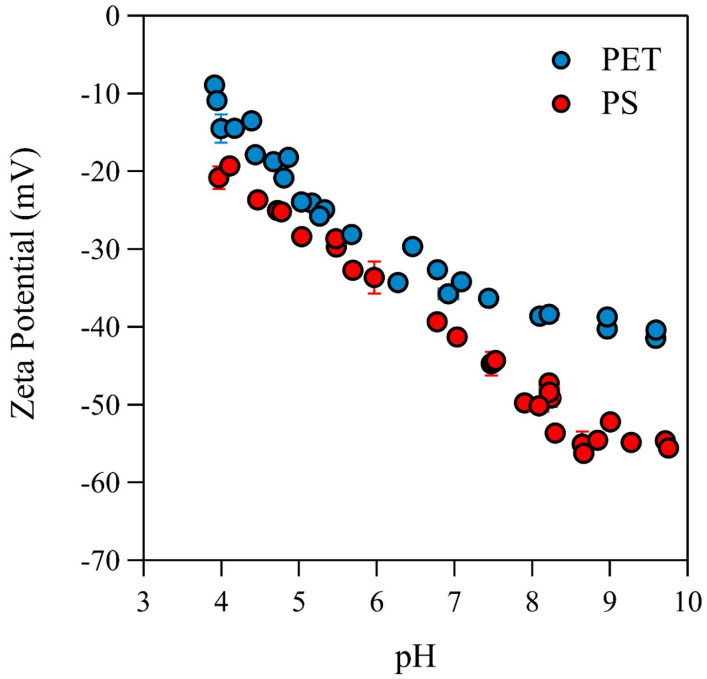

Figure S3. Zeta potentials of PS and PET as functions of the pH value at a constant ionic strength of 10 mM.

List of Tables

Table S1. Results of single drop contact angle (CA) of pristine and coated MP.

	pristine PS	pristine PET	coated PS	coated PET
Single drop CA (°)	138.06	128.44	133.82	101.60
	144.15	126.73	124.82	100.64
	146.03	124.27	133.04	99.36
	143.18	124.28	124.80	100.95
	150.63	115.49	123.36	102.43
	140.86	128.17	124.38	109.94
	146.07	120.27	126.65	103.54
	143.36	123.88	125.66	95.58
	144.84	119.98	123.45	101.96
	141.48	125.66	130.54	95.10
	142.12	124.70	127.16	107.25
mean CA (°)	143.71	123.81	127.06	101.67
STD (°)	3.29	3.87	3.74	4.37
Significance	A	B	B	C

Table S2. BET surface area of pristine PET and PS. The amounts of iron adsorbed on the MP surface per mass MP and per surface area of MP.

		Iron adsorbed on MP surface per mass MP		Iron adsorbed on MP surface per surface area of MP	
	BET surface area (m^2/g)	**Mean (µmol Fe/g MP)**	**STD (µmol Fe/g MP)**	**Mean (µmol Fe/m^2 MP)**	**STD (µmol Fe/m^2 MP)**
PS	1.29	26.25	1.02	20.31	0.79
PET	0.34	29.72	0.64	87.40	1.88

Table S3. Mean water saturation values of all samples.

	Water Saturation (volume water / volume pore space) [-]		
	mean	**STD**	**Significance**
Capillary rise with water			
Control	0.9291	0.0228	A
PS	0.052	0.0712	B
PS coated	0.0906	0.0741	B
PET	0.1342	0.0954	B
PET coated	0.8615	0.0753	A
Capillary rise with Fh10			
Control	0.9925	0.0211	A
PS water	0.052	0.0712	B
PS Fh10 1st	0.1076	0.1057	BC
PS Fh10 2nd	0.1280	0.1128	BC
PET water	0.1342	0.0954	BC
PET Fh10 1st	0.1670	0.15	BC
PET Fh10 2nd	0.2479	0.1868	C
Capillary rise with Fh100			
Control	0.9683	0.028	A
PS water	0.052	0.0712	B
PS Fh100 1st	0.0659	0.0765	B
PS Fh100 2nd	0.0535	0.062	B
PET water	0.1342	0.0954	BC
PET Fh100 1st	0.1579	0.1179	BC
PET Fh100 2nd	0.2112	0.1009	C

Study 4: A rapid method to quantify sub-micrometer polystyrene particles in aqueous model systems by TOC analysis

Status: Published in *Microplastics and Nanoplastics*

Vol. 4 (3), 2024

https://doi.org/10.1186/s43591-024-00080-y

Authors: Johanna Schmidtmann, Stefan Peiffer

Own Contribution in %:

Study design	90
Laboratory analysis	100
Data processing and analyses	90
Interpretation of the results	90
Preparation of the manuscript	90

JS and SP designed the study. JS planned and conducted the laboratory experiments. JS processed and analyzed the data. JS and SP interpreted the results. JS prepared the manuscript with input from SP.

JS is the corresponding author.

Schmidtmann and Peiffer *Microplastics and Nanoplastics* (2024) 4:3
https://doi.org/10.1186/s43591-024-00080-y

Microplastics and Nanoplastics

METHODOLOGY Open Access

A rapid method to quantify sub-micrometer polystyrene particles in aqueous model systems by TOC analysis

Johanna Schmidtmann[1*] and Stefan Peiffer[1]

Abstract

For several laboratory experiments with microplastics, a simple and fast quantification method is advantageous. At the same time, the requirements are often lower compared to microplastic detection from environmental samples. We determined the concentration of non-purgable organic carbon of polystyrene (PS) particles (diameter 0.5, 1, 2, 6 µm) in suspension with known concentrations. Commercially available PS particles were used to test the Total Organic Carbon (TOC) analyzer method for quantifying microplastics in the lower micrometer range under absence of other organic compounds. Addition of iron or aluminum hydroxide to the samples prior to the measurement increased the recovery from 52.9 to 89.7% relative to measurements in the absence of metal hydroxides. With increasing particle size, the recovery in the presence of iron hydroxides decreased from 95.1% at 0.5 µm to 67.1% at 6 µm PS particles and in the presence of aluminum hydroxides from 92.6% at 0.5 µm to 88.9% at 6 µm PS particles. We conclude that metal hydroxides have a catalytic effect on the thermocatalytic oxidation of PS particles and allow a complete conversion to CO_2 for a successful quantification of PS particles using a TOC analyzer. Especially for particles larger than 0.5 µm, in the absence of metal hydroxides, the TOC device is not able to fully oxidize the PS particle to CO_2 and subsequently detect its concentration. Thus, TOC analysis of PS particles in the presence of metal hydroxides provides a cheap and simple alternative for quantifying microplastic particles in the lower micrometer range for laboratory experiments (e.g. sedimentation studies) where no other organic substances are present.

Keywords Microplastic quantification, Catalytic effect, Metal hydroxide, Iron, Aluminum, Thermocatalytic oxidation

Introduction

More than 20 million tons of plastics ended up in the environment in the year 2019 [1]. By now, plastic particles have been found in nearly every environmental compartment [2–4], even at most remote places such as Antarctica and the deep sea [5–7]. Microplastics (MP), plastic particles < 5 mm, are of particular concern as they can be taken up by organisms and cells [8–10]. Quantification of MP particles, especially in the sub-micrometer range, remains a challenge. To estimate the amount of microplastic pollution in the environment, several identification techniques are used, such as Fourier-transform infrared spectroscopy (FTIR), Raman spectroscopy, and gas chromatography - mass spectroscopy (GC-MS) [11]. Each of these techniques has advantages but also limitations (such as detection limit, lower-size limit of detection, complex sample preparation, analysis time,

*Correspondence:
Johanna Schmidtmann
j.schmidtmann@uni-bayreuth.de
[1]Department of Hydrology, Bayreuth Center for Ecology and Environmental Research (BayCEER), University of Bayreuth, Universitätsstraße 30, 95447 Bayreuth, Germany

accuracy, high measurement costs, availability of equipment) [11].

Here, we are presenting a rapid method for quantification of MP in model systems based on the determination of the organic carbon content that allows to generate experimental data within a short time (approx. 10 min per sample with two measurement repetitions). Under well-defined laboratory conditions, the analytical demands for a method are often lower, e.g. if type and size of plastic as well as other substances present in the sample are known. An example of such experiments are sedimentation studies of colloidal MP after interaction with inorganic environmental particles [12]. In samples where MP particles represent the only organic compound, their concentration can be determined by the carbon content of the sample. Total Organic Carbon (TOC) Analyzers are well established for the quantification of dissolved (DOC) and particulate (POC) organic carbon in aquatic samples [14–18]. Yet, application of a TOC Analyzer for quantification of MP particles is rare [12, 19] even though it allows quantification of MP particles in colloidal size range as no lower-size limit exist. Hong et al. [19] used a TOC method with solid sample combustion at 900 °C to quantify MP (45–500 µm) in sewage samples after removing other natural organic matter (NOM) by digestion with Fenton's reagent. The recovery for six different types of plastic particles ranged between 76% and 98% [19]. In contrast, recovery of the determination of 1 µm polystyrene (PS) beads used as a POC source in an interlaboratory study on the determination of POC were unsatisfactory with an average of 43.3% [14].

In a previous work, we used a TOC method (680 °C high temperature catalytic oxidation with Pt catalyst) to determine the PS concentration in aquatic samples from sedimentation experiments [12]. Addition of ferrihydrite, a naturally occurring iron (oxy)hydroxide, enhanced recovery of TOC measurements to 92.7% relative to samples without ferrihydrite with a recovery of 34.7%. These findings suggest that addition of ferrihydrite has an catalytic effect on the conversion of PS to CO_2 [12] and that the poor recoveries observed for PS particles in absence of such a catalytically active metal (oxy)hydroxide [12, 14] reflect incomplete oxidation of PS particles to CO_2 during the TOC measurement.

In this study, we have therefore systematically studied the effect of iron (Fe) and aluminum (Al) hydroxides on the recovery of differently sized PS beads (0.5-6 µm) using a TOC detection method. We selected PS as model polymer material as it is commercially available in many different sizes in the sub-micrometer range.

Methods

Material

For our experiments, we used spherical PS particles with diameters of 0.5, 1, 2, and 6 µm (Polysciences Europe GmbH). For each particle size stock solutions of 100 mg/L were prepared by diluting the original dispersion with ultrapure water (18.2 MΩ cm).

Synthesis of Fe hydroxide (6-line ferrihydrite) was done following the procedure described by Cornell and Schwertmann [20]. Two liters of ultrapure water were heated to 75 °C and 20 g of unhydrolyzed $Fe(NO_3)_3 * 9\ H_2O$ crystals were added while rapidly stirring the solution. The mixture was placed in an oven at 75 °C for 10 min and then quickly cooled by plunging it into ice water. After 30 min, the solution was transferred to dialysis bags and left in distilled water for several days with the water being exchanged multiple times until the conductivity was less than 5 µS/cm. Once the conductivity reached this level, the reaction product in the dialysis bags was transferred to a storage container and kept at 4 °C.

For the synthesis of Al hydroxide, 40 g $AlCl_3 * 6\ H_2O$ were diluted in 0.5 L ultrapure water. By adding 30% NaOH, the initial pH value of 2.6 was adjusted to 6.5. Then the mixture was stirred for 1 h. The pH value was checked during this time, but it remained stable without further addition of NaOH. Afterwards the mixture was transferred to dialysis bags and left in distilled water for several days. Analogous to the synthesis of ferrihydrite, the water was exchanged multiple times until the conductivity was smaller than 5 µS/cm. Once the conductivity reached this level, the reaction product in the dialysis bags was transferred to a storage container and kept at 4 °C.

TOC measurements

To determine the concentration of PS, we analyzed the samples with a TOC-L-Analyzer (Shimadzu). By measuring the non-purgeable organic carbon (NPOC) of each sample, the PS concentration can be calculated. As all carbon (C) in PS is present as organic C and non-purgable, this method is suitable to determine the entire C content of PS.

In brief, during NPOC measurement, the TOC-device and its tubes are firstly washed with the sample solution. Afterwards the actual sample (1 mL) is taken, acidified, and purged with synthetic air (O_2:N_2=20:80) for 1 min at 80 mL/min. Originally this step is done to remove any inorganic C from the sample. In our case however, this is also used to re-suspend the sample directly before 50 µL of the sample are injected to the oven. With the carrier gas (O_2:N_2=20:80), the sample passes through the oven (680 °C) where a Pt/Al_2O_3 catalyst is present to convert all C to CO_2 which is subsequently measured with a CO_2 specific non-dispersive infrared (NDIR) detector. The

entire procedure from sample uptake, purging, and measurement is repeated. In case the relative standard deviation of the first two measurement results is larger than 2%, a third sample is taken.

Sample preparation

The differently sized PS particles were analyzed at varying concentrations between 0 and 15 mg/L in the absence and presence of 10 mg/L Fe or Al hydroxides. The concentration of 10 mg/L Fe or Al hydroxides was chosen based on additional experiments that showed that this concentration is sufficient for successful TOC measurements (Supporting Information). All samples were diluted with ultrapure water (18.2 MΩ cm) to a volume of 10 mL.

Approx. 10 min before the measurement, we acidified the samples with 2 M HCl. Furthermore, the samples were pre-treated in an ultrasonic bath for 5 min to dissolve any formed aggregates (which may form especially in samples containing Fe or Al hydroxides). To make sure that any sedimentation of particles does not affect the measurement, the samples were placed on a magnetic stirrer during analysis instead of using the auto-sampler of the instrument. For all samples, duplicates were prepared and measured.

Data analysis

For each analyzed set of PS samples, a linear regression between initial PS concentration and measured C concentration was calculated and compared to a reference value β_{ref} accounting for the total C concentration to be expected based on the C content of the PS. The mean stoichiometry of PS is $(C_8H_8)_n$ so that β_{ref}=0.923.

Furthermore, the recovery in percent was calculated. This value represents how much of the expected C ($NPOC_{ref}$) of a PS sample was actually measured with the TOC Analyzer ($NPOC_{measured}$). For one specific sample, it was calculated using the equations (1)– (2). The units of NPOC and PS concentrations are mg/L. For one complete dataset (e.g. 1 µm PS particles without addition of metal hydroxide) the total recovery was calculated by dividing the factor of the linear regression (β) of the corresponding dataset by β_{ref}=0.923 (equation (3)).

$$c(NPOC_{ref}) = 0.923 * c(PS) \quad (1)$$

$$recovery\ \% = \frac{c(NPOC_{measured})}{c(NPOC_{ref})} * 100 \quad (2)$$

$$total\ recovery\ \% = \frac{\beta}{\beta_{ref}} * 100 \quad (3)$$

Data was analyzed and figures were created using R 3.6.3 / RStudio 2022.12.0.

Results and discussion

NPOC concentrations of PS samples measured with the TOC Analyzer in the absence of metal hydroxides vary between the differently sized PS particles. For all particle sizes, the measured C concentration is below the expected one for PS concentrations larger than 0.1 mg/L (Fig. 1a). However, depending on the diameter of PS particles, the difference between measured and expected C concentration varies highly. While this difference is rather low for the smallest PS particles (total recovery=89%), it increases as the particle size increases from 0.5 to 6 µm. For 1 and 2 µm PS particles, the total recovery is approx. 50% and for the largest analyzed PS particles (6 µm), only approx. 25% (Fig. 1a+d). Standard deviations of mean NPOC concentrations are very high for particle sizes between 1 and 6 µm (Fig. 1a). This indicates strongly varying and thus unreliable measurement results for these particles. Similar results were observed previously. Aiken et al. reported low recoveries for TOC measurements of different sources of POC. For PS beads the recoveries ranged from 1.4 to 115.8%, for dried bacteria from 9.4 to 132.5%, and for leaf material from 53.6 to 99.8% [14].

Based on the low recovery, we assume that the PS particles are not completely oxidized to CO_2 during the high-temperature catalytic oxidation in the instrument. Interestingly, with increasing concentration the ratio between expected and measured C concentration for one particle size does not increase. This implies that the concentration of PS (at least in the tested range) is not a limiting factor for a complete oxidation of PS particles to CO_2 in the TOC analyzer. Instead, we assume that the particle size is the limiting factor as the recovery decreases with increasing particle size (Fig. 1d). This means that only a certain fraction of each PS particle is converted to CO_2 during the oxidation process of the NPOC measurement and subsequently quantified with the NDIR detector. The remaining, not fully oxidized part of the particle (which increases with particle size) is thus responsible for the low recoveries of NPOC measurements. With increasing particle size, the surface-to-volume ratio of PS particles is decreasing (Fig. 2). The degradation of small plastic particles proceeds faster compared to larger ones due to a higher surface-to-volume ratio [21, 22]. Therefore, we assume that this parameter is also responsible for the more effective oxidation of smaller PS particles because a larger surface area is available for chemical attacks (Fig. 2).

Addition of metal hydroxides to PS samples improves the recovery of the measurement substantially. After addition of 10 mg/L Fe or Al hydroxide to the samples, the recovery of 0.5-2 µm PS particles only slightly deviates from the expected C concentration (Fig. 1b-c). The total recovery increased for all particles sizes and was

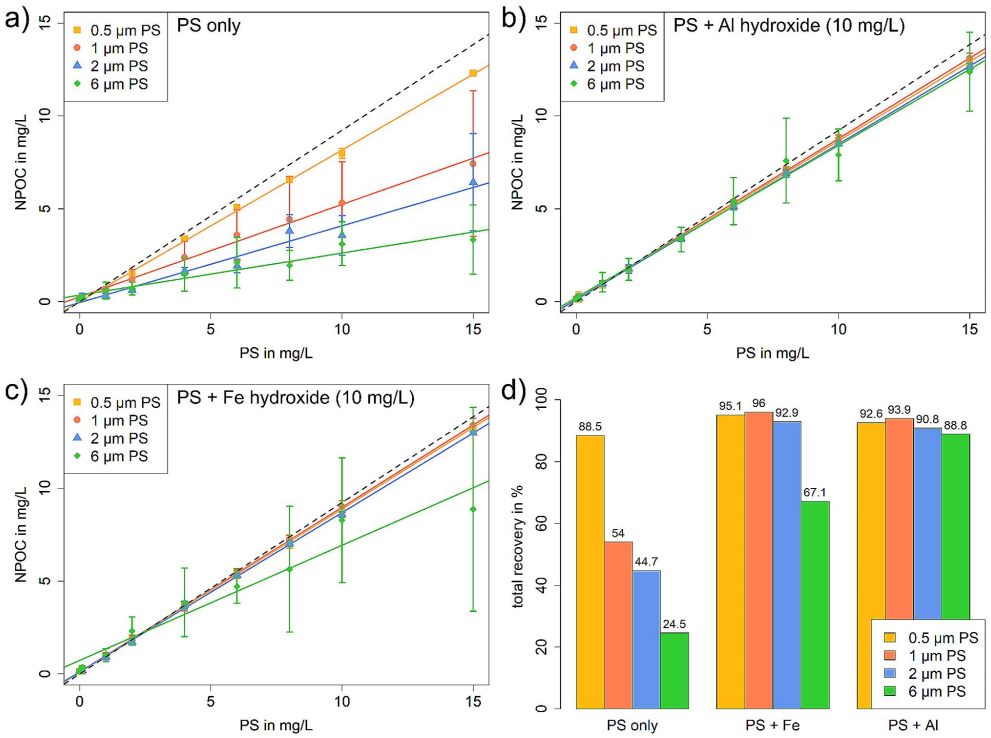

Fig. 1 Mean measured NPOC concentrations of PS samples plotted against the PS concentration: **(a)** in absence of metal hydroxides, **(b)** in presence of 10 mg/L Al hydroxide, and **(c)** in presence of 10 mg/L Fe hydroxide. The error bars represent the standard deviation of the mean. The dashed black line represents the reference NPOC concentration considering the mass percent of C in PS (92.3%). **(d)** Total recovery in percent for each particle size in presence and absence of Fe or Al hydroxide to the PS samples

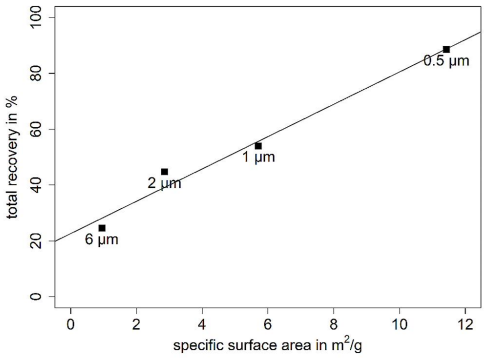

Fig. 2 Recovery of PS particles in absence of metal hydroxides in dependency of the calculated specific surface area (SSA) of PS particles

above 90% for 0.5-2 µm PS particles (Fig. 1d). For the largest particles (6 µm), the total recovery increased to 89% in the presence of Al hydroxide and to 67% in the presence of Fe hydroxide. High standard deviations of mean NPOC concentrations were observed for this particles size, especially for the set of particles that were amended with Fe hydroxide. In contrast, the high standard deviations observed in the samples with 1 and 2 µm PS particles without addition of metal hydroxides, were clearly reduced after addition (Fig. 1a-c). For 1 µm PS, the coefficient of variation was 0.42 without addition of metal hydroxides and was reduced to 0.23 and 0.19 after Fe and Al hydroxide addition, respectively. For 2 µm PS, the coefficient of variation was 0.36. After addition of Fe and Al hydroxides, it had been decreased to 0.18 and 0.21, respectively. These findings indicate that not only the recovery of NPOC measurements increased with addition of metal hydroxides, but also the precision of the measurements. It appears that the presence of metal

hydroxides in the samples catalytically accelerates the combustion to CO_2 and that the catalyst in the TOC device is not sufficient for the conversion of MP particles and other organic particles [14] to CO_2.

In the TOC analyzer used in this study, Pt is used as catalyst, a common noble metal catalyst for the oxidation of organic compounds. However, studies on the thermocatalytic degradation of organic compounds like VOCs found that not only precious or noble metals can act as a catalyst for the oxidation of VOCs but also metal oxide-based catalysts (e.g. Mn, Fe, Al) [23]. The catalytic activity of Pt/Al_2O_3 to oxidize CO at room temperature was enhanced by deposition of Fe-oxide on Pt/Al_2O_3 at room temperature [24]. We therefore conclude that the Fe and Al hydroxides used in this study increase the catalytic activity and allow for fully oxidation of particles and their subsequent TOC measurement. However, an upper limit in particles size seems to exist as indicated by the relatively low recoveries and high standard deviations found for 6 µm particles despite the addition of metal hydroxides.

Conclusions

Without the addition of Fe or Al hydroxides, PS particles were only incompletely oxidized to CO_2 and consequently incompletely quantified using TOC analysis. The presence of metal hydroxides strongly improves the recovery of the determination of PS concentration with TOC analysis. We therefore propose that TOC measurements are a fast, simple, and cheap alternative to commonly used methods for MP quantification in experiments studying the environmental behavior of MP in the sub-micrometer and nanometer range. We recommend the application of this method for samples in which no other organic substances are present, except for MP. It remains to be tested whether in cases where NOM is present, removal of NOM by Fenton reaction may be a useful technique to expand the proposed TOC method also to more complex systems including other organic substances. In this study, we showed the applicability of TOC analysis for PS particles, as they are commercially available in the applied size range. The availability of polymers other than PS in the lower micrometer range is currently very limited. Therefore, it remains to be tested in future studies whether the presented method is also suitable for other types of polymers.

Abbreviations

MP	Microplastic
FTIR	Fourier-transform infrared spectroscopy
GC-MS	Gas chromatography - mass spectroscopy
TOC	Total organic carbon
POC	Particulate organic carbon
DOC	Dissolved organic carbon
NOM	Natural organic matter
PS	Polystyrene
NPOC	Non-purgable organic carbon
NDIR	Non-dispersive infrared
SSA	Specific surface area
VOC	Volatile organic compound

Supplementary Information

The online version contains supplementary material available at https://doi.org/10.1186/s43591-024-00080-y.

Supplementary Material 1

Acknowledgements
The authors would like to thank Martina Rohr and Jutta Eckert for their support with TOC measurements.

Author contributions
JS performed the experiments, analyzed and interpreted the data and was major contributor in writing the manuscript. All authors read and approved the final manuscript.

Funding
This study was funded by the Deutsche Forschungsgemeinschaft (DFG, German Research Foundation)– Project Number 391977956– SFB 1357. We kindly acknowledge subproject Z01 for providing microplastic particles. Open Access funding enabled and organized by Projekt DEAL.

Data availability
The datasets generated and analysed during the current study are available in the zenodo repository: https://doi.org/10.5281/zenodo.10350414.

Declarations

Ethics approval and consent to participate
Not applicable.

Consent for publication
Not applicable.

Competing interests
The authors declare that they have no competing interests.

Received: 5 September 2023 / Accepted: 4 January 2024
Published online: 17 January 2024

References

1. Global Plastics Outlook.: Economic Drivers, Environmental Impacts and Policy Options| READ online. In: oecd-ilibrary.org. https://read.oecd-ilibrary.org/environment/global-plastics-outlook_de747aef-en. Accessed 22 Mar 2023.
2. Duis K, Coors A. Microplastics in the aquatic and terrestrial environment: sources (with a specific focus on personal care products), fate and effects. Environ Sci Eur. 2016;28:2.
3. Barnes DKA, Galgani F, Thompson RC, Barlaz M. Accumulation and fragmentation of plastic debris in global environments. Philos Trans R Soc Lond B Biol Sci. 2009;364:1985–98.
4. Lambert S, Sinclair C, Boxall A. Occurrence, degradation, and Effect of Polymer-based materials in the Environment. In: Whitacre DM, editor. Reviews of Environmental Contamination and Toxicology. Volume 227. Cham: Springer International Publishing; 2014. pp. 1–53.
5. Kelly A, Lannuzel D, Rodemann T, Meiners KM, Auman HJ. Microplastic contamination in East Antarctic Sea Ice. Mar Pollut Bull. 2020;154:111130.
6. Woodall LC, Sanchez-Vidal A, Canals M, Paterson GLJ, Coppock R, Sleight V, Calafat A, Rogers AD, Narayanaswamy BE, Thompson RC. The deep sea is a major sink for microplastic debris. R Soc Open Sci. 2014;1:140317.
7. Van Cauwenberghe L, Vanreusel A, Mees J, Janssen CR. Microplastic pollution in deep-sea sediments. Environ Pollut. 2013;182:495–9.
8. Ramsperger AFRM, Jasinski J, Völkl M, et al. Supposedly identical microplastic particles substantially differ in their material properties

influencing particle-cell interactions and cellular responses. J Hazard Mater. 2022;425:127961.
9. Rudolph J, Völkl M, Jérôme V, Scheibel T, Freitag R. Noxic effects of polystyrene microparticles on murine macrophages and epithelial cells. Sci Rep. 2021;11:15702.
10. Wright SL, Thompson RC, Galloway TS. The physical impacts of microplastics on marine organisms: a review. Environ Pollut. 2013;178:483–92.
11. Prata JC, da Costa JP, Duarte AC, Rocha-Santos T. Methods for sampling and detection of microplastics in water and sediment: a critical review. TRAC Trends Anal Chem. 2019;110:150–9.
12. Schmidtmann J, Elagami H, Gilfedder BS, Fleckenstein JH, Papastavrou G, Mansfeld U, Peiffer S. Heteroaggregation of PS microplastic with ferrihydrite leads to rapid removal of microplastic particles from the water column. Environ Sci: Processes Impacts. 2022;24:1782–9.
13. Ward CP, Armstrong CJ, Walsh AN, Jackson JH, Reddy CM. Sunlight converts polystyrene to Carbon Dioxide and dissolved Organic Carbon. Environ Sci Technol Lett. 2019;6:669–74.
14. Aiken G, Kaplan A, Weishaar L J. Assessment of relative accuracy in the determination of organic matter concentrations in aquatic systems. J Environ Monit. 2002;4:70–4.
15. Volk C, Wood L, Johnson B, Robinson J, Zhu HW, Kaplan L. Monitoring dissolved organic carbon in surface and drinking waters. J Environ Monit. 2002;4:43–7.
16. Blaurock K, Beudert B, Gilfedder BS, Fleckenstein JH, Peiffer S, Hopp L. Low hydrological connectivity after summer drought inhibits DOC export in a forested headwater catchment. Hydrol Earth Syst Sci. 2021;25:5133–51.
17. Blaurock K, Garthen P, da Silva MP, Beudert B, Gilfedder BS, Fleckenstein JH, Peiffer S, Lechtenfeld OJ, Hopp L. (2022) Riparian Microtopography affects event-driven Stream DOC concentrations and DOM Quality in a Forested Headwater Catchment. J Geophys Research: Biogeosciences 127:e2022JG006831.
18. Knorr K-H. DOC-dynamics in a small headwater catchment as driven by redox fluctuations and hydrological flow paths– are DOC exports mediated by iron reduction/oxidation cycles? Biogeosciences. 2013;10:891–904.
19. Hong Y, Oh J, Lee I, Fan C, Pan S-Y, Jang M, Park Y-K, Kim H. Total-organic-carbon-based quantitative estimation of microplastics in sewage. Chem Eng J. 2021;423:130182.
20. Cornell RM, Schwertmann U. The Iron Oxides: structure, Properties, reactions, occurrences and uses. John Wiley & Sons; 2003.
21. Gewert B, Plassmann MM, MacLeod M. Pathways for degradation of plastic polymers floating in the marine environment. Environ Sci: Processes Impacts. 2015;17:1513–21.
22. Booth AM, Kubowicz S, Beegle-Krause C, Skancke J, Nordam T, Landsem E, Throne-Holst M, Jahren S. Microplastic in global and Norwegian marine environments: distributions, degradation mechanisms and transport. Miljødirektoratet M. 2017;–918:1–147.
23. Li X, Niu Y, Su H, Qi Y. Simple thermocatalytic oxidation degradation of VOCs. Catal Lett. 2021. https://doi.org/10.1007/s10562-021-03770-x.
24. Cha BJ, Kim SY, Choi CM, Sung JY, Choi MC, Seo HO, Kim YD. Ultra-low loading of iron oxide on Pt/Al2O3 for enhanced catalytic activity of CO oxidation at room temperature: a simple method for applications. Chem Eng J. 2021;404:126560.

Publisher's Note

Supporting Information

A rapid method to quantify sub-micrometer polystyrene microplastic particles in aqueous model systems by TOC Analysis

Johanna Schmidtmann[*1], Stefan Peiffer[1]

[1] Department of Hydrology, University of Bayreuth, Bayreuth Center for Ecology and Environmental Research (BayCEER), Bayreuth, Germany

*corresponding author: j.schmidtmann@uni-bayreuth.de

Authors

Johanna Schmidtmann, Department of Hydrology, University of Bayreuth, Bayreuth Center for Ecology and Environmental Research (BayCEER), Universitätsstraße 30, 95447 Bayreuth, Germany, j.schmidtmann@uni-bayreuth.de

Stefan Peiffer, Department of Hydrology, University of Bayreuth, Bayreuth Center for Ecology and Environmental Research (BayCEER), Universitätsstraße 30, 95447 Bayreuth, Germany, s.peiffer@uni-bayreuth.de

Determination of the amount of metal hydroxides added to PS samples

In order to analyze how different concentrations of Fe or Al hydroxides affect the NPOC recovery, eight samples with PS concentrations of 10 mg/L were prepared for each particle size. While the PS concentration was constant in all samples, Fe or Al hydroxide were added to samples at different concentrations between 0 and 10 mg/L.

These experiments showed that the recovery of PS-carbon was depended on the amount of Fe and Al hydroxide added to samples (Fig. S1). It was above 90% for small PS particles (0.5-2 µm) at metal hydroxide concentrations larger 2.5 mg/L, whereby the recoveries were increasing with decreasing particle sizes. Hence, a specific amount of Fe or Al hydroxides is needed in the sample to sufficiently catalyze the oxidation of PS particles to CO_2. For small particle sizes, a concentration of 2.5 mg/L is sufficient. For the larger 6 µm PS particles, however, this amount of Fe hydroxide is not yet sufficient (Fig. S1b). Nevertheless, at metal hydroxide concentrations of 10 mg/L, the recovery of TOC measurements increased also for 6 µm PS particles and was therefore selected for the experiments.

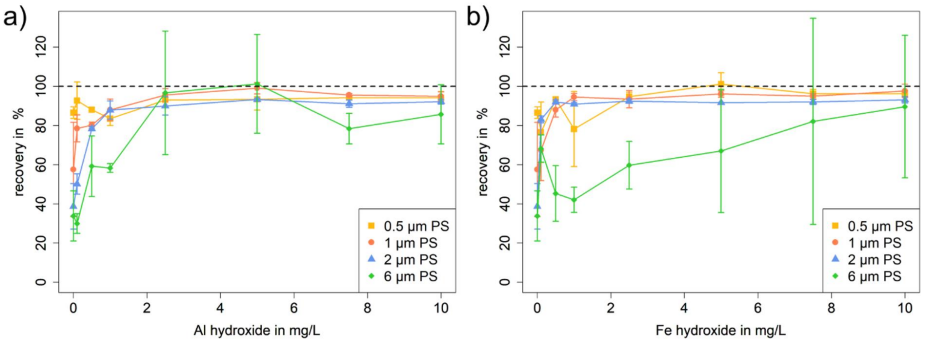

Fig. S1 Recovery of PS particles (0.5-6 µm) depending on the concentration of **a**) Al hydroxide or **b**) Fe hydroxide added to the sample containing 10 mg/L PS.

List of Publications

Published:

Schmidtmann, J., Elagami, H., Gilfedder, B.S., Fleckenstein, J.H., Papastavrou, G., Mansfeld, U. and Peiffer, S. (2022), “Heteroaggregation of PS microplastic with ferrihydrite leads to rapid removal of microplastic particles from the water column”, *Environmental Science: Processes & Impacts*, Vol. 24 No. 10, pp. 1782–1789, doi: 10.1039/D2EM00207H.

Cramer, A., **Schmidtmann, J.**, Benard, P., Kaestner, A., Engelhardt, M., Peiffer, S. and Carminati, A. (2023), “Ferrihydrite coating reduces microplastic induced soil water repellency”, *Environmental Science: Processes & Impacts*, Vol. 25 No. 6, pp. 1094–1101, doi: 10.1039/D3EM00077J.

Schmidtmann, J. and Peiffer, S. (2024), “A rapid method to quantify sub-micrometer polystyrene particles in aqueous model systems by TOC analysis”, *Microplastics and Nanoplastics*, Vol. 4 No. 3, doi: 10.1186/s43591-024-00080-y.

Ready for submission:

Schmidtmann, J., Weishäupl, H.K., Hopp, L., Meides, N. and Peiffer, S., “UV-weathering affects heteroaggregation and subsequent sedimentation of polystyrene microplastic particles with ferrihydrite”.

Additional Publications:

Mansor, M., Drabesch, S., Bayer, T., Van Le, A., Chauhan, A., **Schmidtmann, J.**, Peiffer, S., et al. (2021), “Application of Single-Particle ICP-MS to Determine the Mass Distribution and Number Concentrations of Environmental Nanoparticles and Colloids”, *Environmental Science & Technology Letters*, Vol. 8 No. 7, pp. 589–595, doi: 10.1021/acs.estlett.1c00314.

Opitz, J., Bauer, M., Alte, M., **Schmidtmann, J**. and Peiffer, S. (2022), “Sedimentation Kinetics of Hydrous Ferric Oxides in Ferruginous, Circumneutral Mine Water”, *Environmental Science & Technology,* Vol. 56 No. 10, pp. 6360–6368, doi: 10.1021/acs.est.1c07640.

(Eidesstattliche) Versicherungen und Erklärungen

(§ 9 Satz 2 Nr. 3 PromO BayNAT)
Hiermit versichere ich eidesstattlich, dass ich die Arbeit selbstständig verfasst und keine anderen als die von mir angegebenen Quellen und Hilfsmittel benutzt habe (vgl. Art. 97 Abs. 1 Satz 8 BayHIG).

(§ 9 Satz 2 Nr. 3 PromO BayNAT)
Hiermit erkläre ich, dass ich die Dissertation nicht bereits zur Erlangung eines akademischen Grades eingereicht habe und dass ich nicht bereits diese oder eine gleichartige Doktorprüfung endgültig nicht bestanden habe.

(§ 9 Satz 2 Nr. 4 PromO BayNAT)
Hiermit erkläre ich, dass ich Hilfe von gewerblichen Promotionsberatern bzw. -vermittlern oder ähnlichen Dienstleistern weder bisher in Anspruch genommen habe noch künftig in Anspruch nehmen werde.

(§ 9 Satz 2 Nr. 7 PromO BayNAT)
Hiermit erkläre ich mein Einverständnis, dass die elektronische Fassung meiner Dissertation unter Wahrung meiner Urheberrechte und des Datenschutzes einer gesonderten Überprüfung unterzogen werden kann.

(§ 9 Satz 2 Nr. 8 PromO BayNAT)
Hiermit erkläre ich mein Einverständnis, dass bei Verdacht wissenschaftlichen Fehlverhaltens Ermittlungen durch universitätsinterne Organe der wissenschaftlichen Selbstkontrolle stattfinden können.

Ort, Datum	Johanna Schmidtmann